Molecular Dynamics Simulations and Simulated Diffraction Spectra of Long Chain Fluorinated and Hydrogenated Substances at the Water-Air Interface

Pedro Alexandre Calixto Lourenço

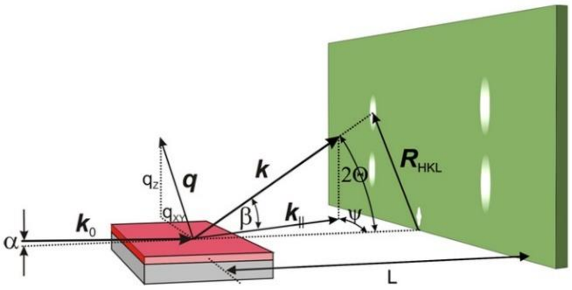

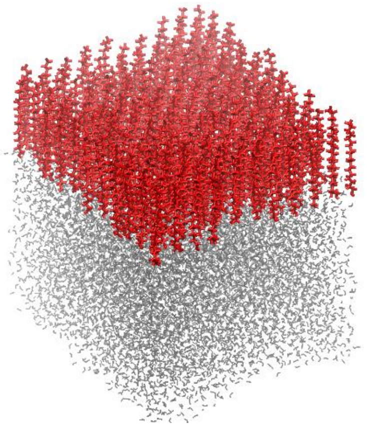

Thesis to obtain the Master of Science Degree in

Chemical Engineering

Supervisors: Doctor Pedro Morgado

Doctor Michel Goldmann

Examination Committee

Chairperson: Doctor Mário Nuno de Matos Sequeira

Supervisor: Doctor Pedro Morgado

Member of the Committee: Doctor José Nuno Lopes

October of 2018

Acknowledgements

First, I would like to show my very great appreciation to Doctor Eduardo Morilla for helping me with academic and personal matters during the course of my thesis and master's degree, which I will forever be thankful for. Early in my master's degree, Professor Eduardo invited me to be a part of his research group where I met Doctor Pedro Morgado and PhD student Gonçalo Silva, whom I appreciate very much for teaching and helping me with the theoretical and computer work of molecular dynamics simulations. The valuable scientific discussions done with this group were crucial for the development of this thesis, while also providing me with very essential groundwork for my future, for which I am also very grateful.

I would also like to offer my thanks to the INSP for offering me an internship and allowing me to live in Paris. I would like to show my appreciation to Doctor Michel Goldmann for his patience in teaching me and discussing with me about x-ray diffraction theory and experiments. The assistance provided by Doctor Bernard Croset on more theoretical parts of this thesis and the assistance given by Doctor Philippe Fontaine were also very valuable.

Even though that little to no experimental work is presented in this thesis I would still like to thank PhD students Helen Ibrahim and Tomás Rego for helping me with AFM and Langmuir trough experiments. I would also like to acknowledge the SIRIUS team at the SOLEIL synchrotron for providing the beamline time and helping in GIXD experiments.

Working with the people mentioned above definitely shaped me academically and individually, and I hope that I was able to demonstrate my appreciation for these people. On a more whimsical note, I would also like to thank my friends and family for bringing me joy when times were stressful. The scientific and unscientific tomfoolery while in the research group was also greatly appreciated.

Resumo

O comportamento dinâmico e a organização estrutural de pequenos agregados de moléculas de cadeia fluorada e hidrogenada à superfície da água foram estudados por simulações de dinâmica molecular.

As simulações de 1H,1H-Perfluoro-1-tetradecanol (F14OH); 1H,1H,-Perfluoro-1-octadecanol (F18OH); 1-Octadecanol (H18OH); 1-tetradecanol (H14OH) e Perfluoroeicosano (F20) à superfície da água a 0 π/m^2 e a 25 ^oC mostram que ambas as moléculas hidrogenadas e fluoradas formam espontaneamente agregados isolados. Os agregados fluorados agrupam de forma muito ordenada e o agregado total apresenta uma periferia poligonal, em contraste com as monocamadas hidrogenadas que formam agregados menos ordenados com uma periferia circular. Estes resultados são confirmados por comparação com dados experimentais de microscopia de força atómica (AFM).

Além disso, um programa que calcula o espectro de difração a partir da informação das simulações foi desenvolvido. Esta ferramenta permite validar ou invalidar a organização estrutural das monocamadas simuladas, por comparação direta com os espectros experimentais obtidos através de difração por incidência de raios-x razantes (GIXD). Foram obtidos os parâmetros das células unitárias cristalinas das simulações de monocamadas de F14OH, F18OH e F20, resultados que são compatíveis com as células unitárias experimentais. O espectro de difração das simulações dos compostos hidrogenados (que usa um forcefield baseado no AA-OPLS) não é compatível com os espectros experimentais de GIXD.

Acrescentando ao projecto, ainda foi calculado o espectro de difração de uma hemi-micela do alcano semi-fluorado F8H16 ($F(CF_2)_8(CH_2)_{16}H$). O espectro produzido está de acordo com o obtido por GIXD, confirmando a estrutura não periódica da hemi-micela e demonstrando que estruturas não periódicas (quasi-cristais) podem produzir picos de difração.

Palavras-Chave: difração de raios x; substâncias fluoradas; simulações de dinâmica molecular; monocamadas de Langmuir; alcanos semi-fluorados

Abstract

The dynamic behaviour and structural organization of small domains of fluorinated and hydrogenated molecules at the surface of water were studied by all-atom molecular dynamics simulations.

The MD simulations of 1H,1H-Perfluoro-1-tetradecanol (F14OH); 1H,1H,-Perfluoro-1-octadecanol (F18OH); 1-Octadecanol (H18OH); 1-tetradecanol (H14OH) and Perfluoroeicosane (F20) at zero surface pressure and 25ºC show that both hydrogenated and fluorinated molecules spontaneously form isolated domains, with the fluorinated aggregates assembling into highly ordered domains with polygonal periphery, while the hydrogenated monolayers are less ordered and present circular domains, with both results confirming atomic force microscopy (AFM) measurements of previous works.

Furthermore, a new tool which calculates the simulated monolayers diffraction spectra was developed. By direct comparison with the experimental spectra, this tool validates or invalidates the structural organizations seen in the MD simulations. Detailed results of the F14OH, F18OH and F20 unit cells are presented and agree with the experimental ones. The diffraction spectra produced by the hydrogenated compounds (which use a forcefield based on the AA-OPLS) is not compatible with the spectra produced from grazing incidence x-ray diffraction (GIXD) experiments.

As a smaller work, the diffraction spectra of a previously simulated perfluoroalkylalkane hemimicelle was calculated which produced diffraction peaks in very good agreement with that obtained through GIXD experiments, fully validating the non-periodic structure of the hemimicelles and demonstrating that non-periodic (quasi-crystal) structures produce well defined diffraction peaks.

Keywords: x-ray diffraction; fluorinated substances; molecular dynamics simulations; Langmuir monolayers; perfluoroalkylalkanes

Acronyms

2D – Two-dimensional/ Two dimensions

3D – Three-dimensional/ Three dimensions

MD – Molecular Dynamics

F14OH - 1H,1H-Perfluoro-1-tetradecanol

F18OH - 1H,1H,-Perfluoro-1-octadecanol

H18OH - 1-Octadecanol

H14OH - 1-tetradecanol

F20 - Perfluoroeicosane

Index

Figures

Tables

1. Introduction

1.1. Motivation

Surface materials science is a very active field and has received much attention from physics and chemistry researchers. Molecular thin films have numerous applications in nanotechnology such as solar cells, transistors for microprocessors or as superconductors. Computer simulations provide researchers with a tool to understand and predict, at the atomic scale, the complex system structures of these nanofilms.

Organic surfactant substances, which self-assemble into molecular thin-films at the water-air interface find various industrial applications. The substitution of the hydrogen atoms for the larger and heavier fluorine atoms results in molecules which form crystals at the water surface with very characteristic patterns and behaviours. However, the dynamic behaviour and growth process of these fluorinated molecules is still not well understood which makes atomistic computer simulations crucial for further research.

The main purpose of this study is to understand the behaviour and characteristics of fluorinated alcohols and the key differences when compared to their more well studied hydrogenated counterparts. As the molecules are insoluble in water forming Langmuir monolayers, grazing incidence x-ray diffraction experiments and molecular dynamics simulations are the means of study to characterize the structure and behaviour of these monolayers.

1.2. Fluorinated Surfactants

Fluorinated surfactants find industrial applications as adjuvant components in fluoropolymer manufacture and processing, aqueous foams for fire extinction, formulations of herbicides, greases and lubricants, paints, polishes and adhesives [1][2]. However, their most exciting applications are in biomedical research and development, for instance, as emulsifiers for blood substitute formulations [3] and inverse emulsions for drug delivery in liquid ventilation context [4] or as components of the walls of microbubbles used for drug delivery and oxygen transport in blood [5]. It is of great importance to develop new models and understand if the current models can provide a good understanding of the unusual properties of these materials.

Insoluble molecular thin films on the surface of a liquid, called Langmuir monolayers, are an excellent model for the study of molecular ordering and structure in two dimensions. Often considered as 2D films, these monolayers are experimentally studied in a Langmuir through where phase transitions occur whenever the surface pressure of the film is changed by compression/decompression at constant temperature. At very low surface pressures (low molecular density) the molecules are very loosely packed and form a gaseous phase above the water surface, while at very high surface pressures the molecules assemble into a crystalline structure, typically in a two-dimensional hexagonal arrangement. Amphiphilic molecules which contain a hydrophilic 'head' group and a hydrophobic 'tail' such as polyfluorinated alcohols are insoluble in water and thus, they are known to self-assemble into Langmuir monolayers at the air-water interface [6]. Its polar head group provides the 'anchoring' to the water surface while its apolar tail is protruding into the air. Long linear perfluoroalkanes which have no amphiphilic character have also been reported to form stable Langmuir monolayers as their bigger van der Waals forces alone are enough to stabilize the monolayer. [7]

Linear fluorinated carbon chains are known to exhibit a helical conformation. The big electrostatic repulsions between its fluorine atoms does not allow for the carbon chain to stay in an all-trans conformation [8], instead, the optimized energy configuration for each C-C-C-C dihedral is with a slight twist angle, giving the carbon chain a helical or cylindrical form, something which is not seen for their hydrogenated analogues.

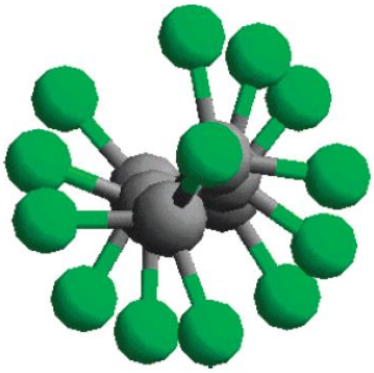

Figure 1 – Representation of the optimized structure of perfluorohexane. The C-C-C-C twist angle produces a helical conformation. (S.S. Jang et al, 2003)

Due to their intrinsic helicity, perfluorinated chains are more rigid than the more flexible hydrogenated chains. Consequently, perfluorinated materials exhibit some peculiar properties that deserve to be more deeply studied.

Experimentally, the crystalline structure of condensed monolayers is studied by grazing incidence x-ray diffraction, where structural information such as; crystalline inter-molecular distance, tilt of molecules and overall organization can be deduced from the measurements. Computer simulations act as a link between microscopic scales and the macroscopic world of the laboratory, showing a new atomic view of the system. In molecular dynamics simulations, the repulsive and attractive forces of atoms are, step-by-step, numerically solved for each atom pair and the dynamic trajectory data obtained can then be used to determine macroscopic and microscopic properties of the molecular system. The recent work put into the development of hydrogenated and fluorinated forcefields allows for molecular dynamics computer simulations of Langmuir monolayers of fluorinated surfactants and perfluoroalkanes.

The key idea of this project is to understand trough molecular dynamics computer simulations the molecular structure and general behaviour of fluorinated films at low surface pressure and highlight the key differences between fluorinated and hydrogenated surfactants. This is complemented by developing a diffraction analysis tool for straightforward structural comparisons with the experimental film's diffraction spectra in order to validate the structures displayed in the simulations.

And thus H18OH, F18OH, F14OH and F20 were chosen for this study as they are known to form very stable Langmuir monolayers and already have experimental x-ray diffraction data and atomic force microscopy data for comparison. Even though there is no experimental data, simulations of H14OH were also performed in order to evaluate the influence of the chain length on the organization of the monolayers. The idea is to assess the tendency of the molecules to aggregate and which phase state they aggregate in.

The diffraction spectra of the simulated monolayers at virtually zero surface pressure was thus inspected and directly compared to the experimental spectra. The dynamics of the aggregates during the simulation were qualitatively analysed and compared to the experimental data.

As a more miscellaneous work, the diffraction pattern of a previously simulated perfluoralkylalkane hemimicelle was also inspected in order to validate or discredit the non-periodic structural organization.

1.3 Molecular Dynamics

Molecular dynamics simulations allow researchers to have a microscopic view and time scales of the atomic or molecular interactions. These interactions are modelled by forcefields which are numerically solved, and predictions of dynamic substance properties or structural organizations are obtained. The recent development of better forcefields and computing power allows one today to simulate complex molecular systems in more macroscopic time scales with ease.

In the standard MD approach, the classical Newton equations of motion (equations (1)) of all atoms in the system of study are numerically solved step-by-step. The force applied in each atom, f_i is the gradient of the interatomic potential energy function, $u(r_i)$, where $r_i = (x, y, z)$ is the set of coordinates representing particle i in space with momentum, p_i and mass, m_i.

$$f_i = \frac{d}{dt} p_i = -\frac{\partial}{\partial r_i} u(r_i) \quad \text{and} \quad \frac{d}{dt} r_i . m_i = p_i \quad (1)$$

This potential energy function, u is the sum of intermolecular (non-bonded potential) and intramolecular (bonded potentials) interactions of the molecules in the system.

The non-bonded interactions represent the repulsive and attractive forces between the molecules/atoms, where the main focus is on the calculation of every atom-pair potential while 3-body and higher order potentials are usually neglected. Due to their simplicity and computational expediency, Coulomb and Lennard-Jones (electrostatic and van der Walls forces, respectively) pair potential terms (equations(2)) are the most used to model these interactions. The parameters used in these equations such as atomic partial charge Q_i , inter-particle distance where the attractive and repulsive forces cancel each other, σ_{ij}, and well depth, ε_{ij} ,are determined experimentally or obtained via Monte Carlo simulations.[9] r_{ij} is the distance between the particles.

$$u_{Lennard-Jones}(r_{ij}) = 4\varepsilon_{ij}\left[\left(\frac{\sigma_{ij}}{r_{ij}}\right)^{12} - \left(\frac{\sigma_{ij}}{r_{ij}}\right)^{6}\right] \quad \text{and} \quad u_{Coulomb}(r_{ij}) = \frac{Q_i Q_j}{4\pi\varepsilon_0 r_{ij}} \quad (2)$$

However, due to the size of these systems, it is most often too computationally intensive to calculate all pair potentials of every atom in the simulation. To avoid these expensive calculations the interactions are assumed to be short-range and only the atoms within a cut-off range, $r_{ij} < r_{cut-off}$ are considered for force calculations.

For molecular systems the bonded interactions must also be considered in the total potential energy function. The potential energies from harmonic atomic bond stretches, harmonic angle bends and dihedral torsions (2-body, 3-body and 4-body interactions, respectively) are represented by equation (3). The dihedral potential usually involves periodic expansions of order m=1,2,. . .,.

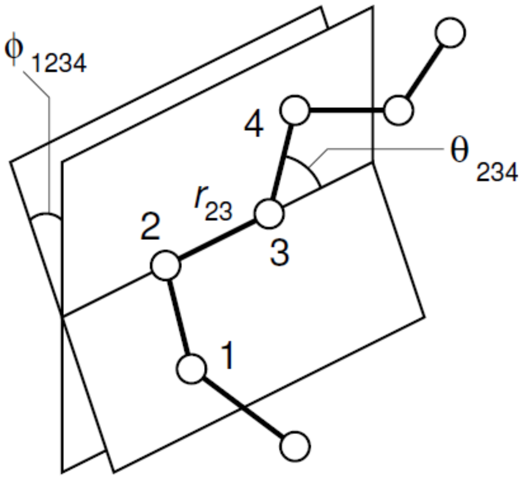

Figure 2 – Geometry of a simple linear molecule, with example interatomic distance r_{23}, bend angle θ_{234} and proper dihedral angle ϕ_{1234}.

$$u_{intramolecular} = \frac{1}{2}\sum_{bonds} k_{ij}^{b}\left(r_{ij} - r_{equilibrium}\right)^2 + \frac{1}{2}\sum_{bonds} k_{ijk}^{\theta}\left(\theta_{ijk} - \theta_{equilibrium}\right)^2 + \frac{1}{2}\sum_{\substack{torsion\\angles}}\sum_{m} k_{ijkl}^{\phi,m}\left(1 + \cos\left(m\phi_{ijkl} - \phi_{equilibrium}\right)\right) \quad (3)$$

With the potential energy function now defined, the Newton equations are step-by-step numerically solved. An example algorithm is shown below.

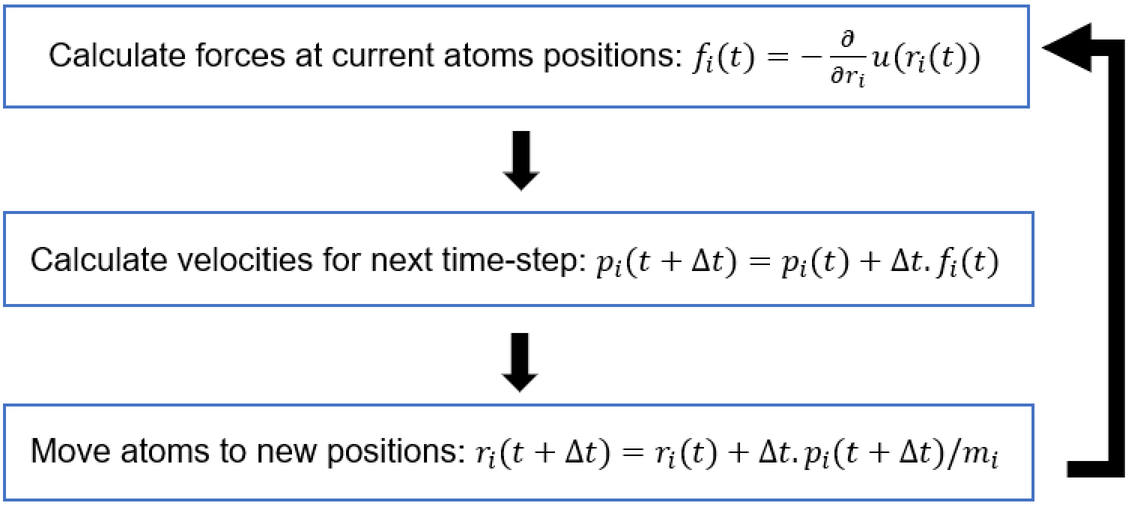
Calculate forces at current atoms positions: $f_i(t) = -\frac{\partial}{\partial r_i}u(r_i(t))$

Calculate velocities for next time-step: $p_i(t+\Delta t) = p_i(t) + \Delta t . f_i(t)$

Move atoms to new positions: $r_i(t+\Delta t) = r_i(t) + \Delta t . p_i(t+\Delta t)/m_i$

Figure 3 – Basis of a MD algorithm.

Periodic boundary conditions are most often used in MD simulations to minimize the surface effects of a finite system. To solve this problem, the simulation box is surrounded by periodic translated copies of itself, thus acting as an infinite system. Whenever an atom passes through one side of the simulation box, another atom re-appears on the opposite side with the same velocity as can be seen in fig.(4). The image particles which are inside the cut-off range are still considered for the force evaluation.

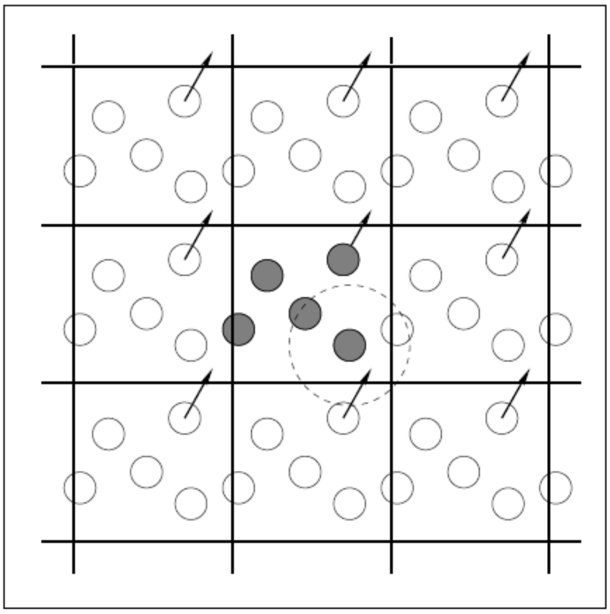

Figure 4 – Illustration of a simulation box (gray particles) in the centre surrounded by image replicas of itself (white particles). Dotted circle is an illustration of the cut-off distance.

Ultimately, direct comparisons of the simulation results with experimental measurements might be main goal of the simulations, in which case a good model of molecular interactions is essential. The continual comparison of the MD results with thermophysical and structural properties measured experimentally are thus invaluable for further force-field development and refinement.

1.4. Crystals, 2D Powders and Bravais Lattices.

Crystals are defined by the periodic translational repetition of an atomic pattern, usually in three dimensions with the smallest possible repeating pattern being the unit cell, which is described by the vectors $\vec{a}$, $\vec{b}$ and $\vec{c}$, in the so-called direct space. However, concerning the monolayers of surfactants studied in this thesis, a 2D lattice with vectors $\vec{a}$ and $\vec{b}$ is enough to characterize the unit cell of these films.

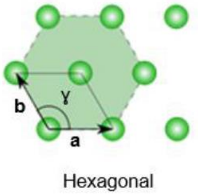

Figure 5 – Example of a two-dimensional hexagonal unit cell, a and b are the lattice distances and γ is the unit cell angle.

Crystallography diffraction experiments are the method to determine the film's unit cell. The main goal is to deduce from the angular information of the diffraction pattern an arrangement. This arrangement, called the reciprocal unit cell bears a simple reciprocal relationship with the unit cell of the direct space.

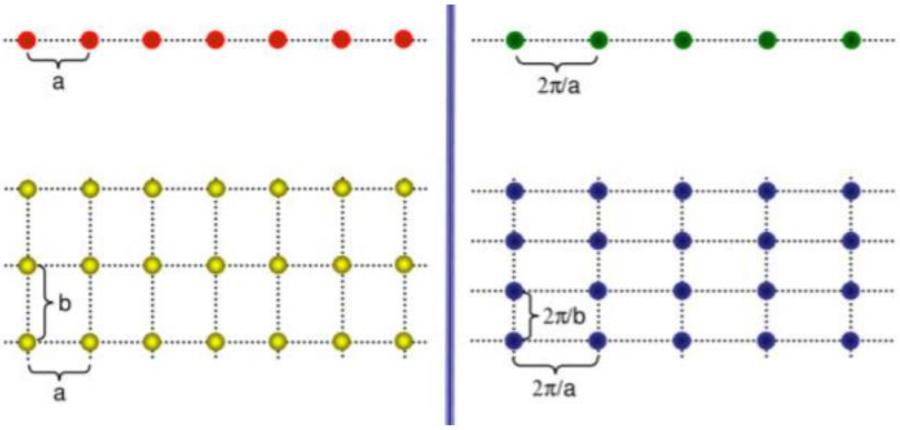

Figure 6 – Representation of a real Bravais lattice, on the left, and a reciprocal lattice, on the right. (Als-Nielsen, J., 2001)

For every direct lattice, there is an equivalent reciprocal lattice. The smaller the distances between points on the Bravais lattice, the higher the distance between points in the reciprocal lattice and vice-versa. In 2D, the equivalent reciprocal lattice is defined by the two reciprocal vectors a* and b* and the angle between them. Thus, to fully characterize the direct space unit cell, one must first measure the diffraction peaks and find the length of a* and b*, along with the angle γ, in the reciprocal space.

Each point of the reciprocal lattice (diffraction peak) can be labelled with a Miller index (h,k) which corresponds to the lines (or planes) of atoms from which diffraction occurs.

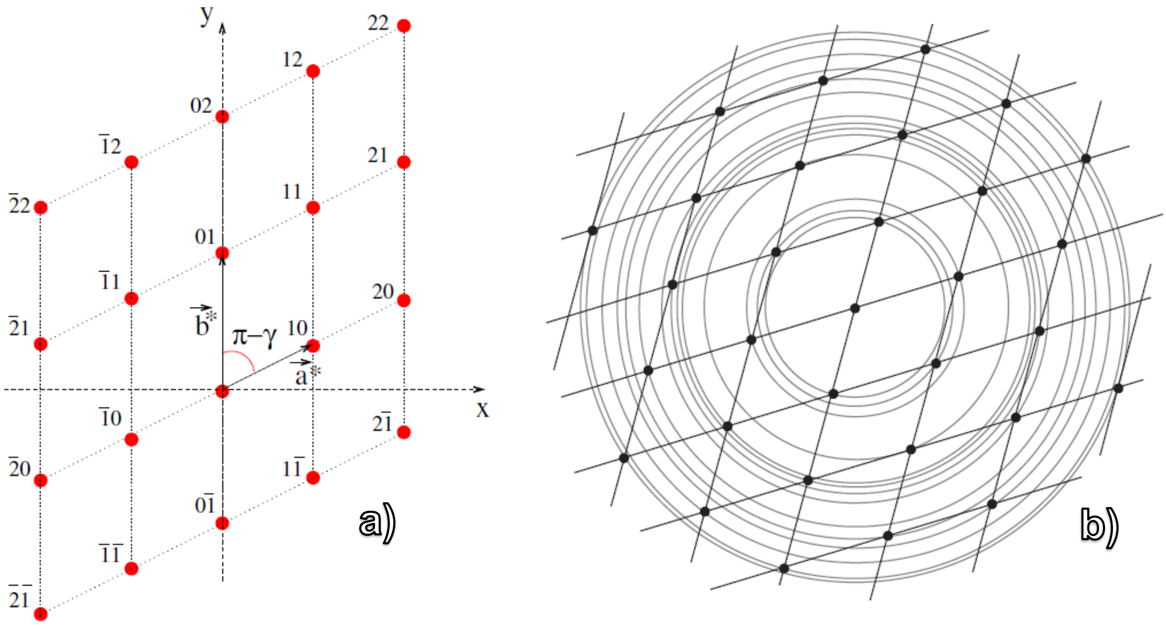

Figure 7 – a) Reciprocal space lattice and its miller indexes corresponding to each diffraction peak of a single perfect crystal. b) Diagram showing the rotation of the reciprocal lattice generating a series of rings as seen in powder diffraction experiments.

Experimentally however, the monolayers are composed of multiple crystallites with various orientations (powder diffraction), which means that the diffraction pattern will be the superposition of the diffraction due to all crystallite, often taking the form of diffraction rings as seen in fig(4b). Thus, the measurement of diffraction rings corresponding to miller indices [01] and [10] allows one to define the length of a* and b* parameters while the measurement of the diffraction ring corresponding to the miller indice [11] assigns the value of γ. [10]

1.5. Radiation Scattering.

To more deeply understand x-ray diffraction, one must first understand the phenomena of scattering.

If one thinks in classical electromagnetism waves, whenever a charged particle absorbs light, the electric and magnetic components of the wave exert a force on the particle causing it to oscillate. A charged particle in periodic motion emits electromagnetic radiation, thus acting as a scattering point for the incident radiation.[11]

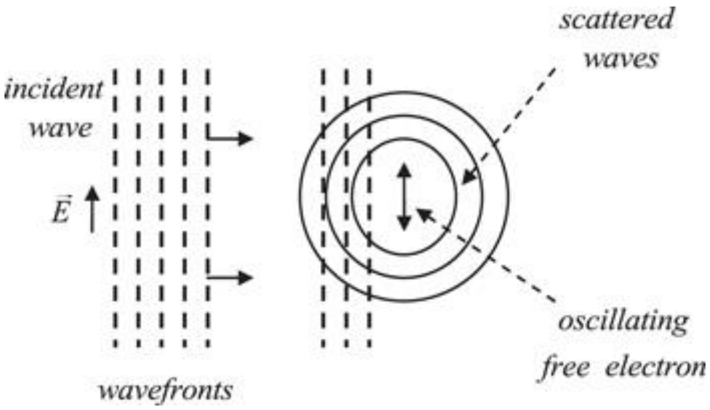

Figure 8 – Schematic illustration of the Thomson scattering process.

The electric field produced due to scattering of radiation with energy E_0, by a particle of charge q and mass m_q is given by Thompson's formula (1). Where $\vec{k}_s$ is the wavevector representative of the scattered waves:

$$E_s(\vec{R}) = \frac{q^2}{m_q c^2} \frac{1}{R} E_0 \sin(\theta)\, e^{i(\omega t - \vec{k}_s \vec{R})} \quad (4)$$

From equation (1) it is known that the scattered intensity is inversely proportional to the mass of the particle. When radiation is scattered by an atom, it can be approximated that it's scattering properties arise only from its electrons rather than the nucleus, because of the former's much smaller mass.

Electrons in different positions will cause the scattered waves to be phase shifted. The crystal structure of the atoms in the solid will determine what directions will yield constructive or destructive interference. The constructive interference of the scattered radiation is what is called diffraction.

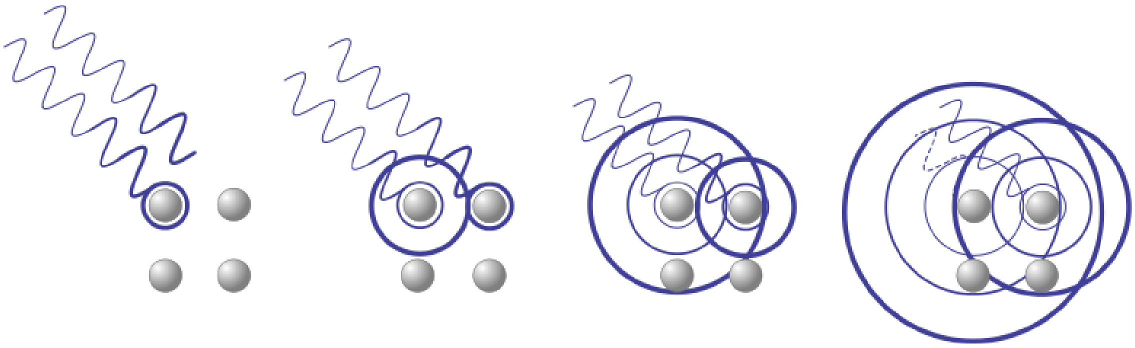

Figure 9 – Schematic of radiation scattering in a solid. The blue circles represent the wave front, where they intersect is where the constructive interference occurs.

In diffraction experiments, the detector moves around the sample and measures the constructive interference as a function of the detector's angle to the incident beam, which is defined as, 2θ.

1.6. Grazing Incidence X-ray Diffraction (GIXD)

X-ray diffraction techniques hold a leading role as a tool for material structure analysis. In diffraction experiments, an intense X-ray beam strikes the material and is scattered by the electrons in the material, the intensity of the scattered waves is then measured by the detector. For some detector angles constructive interference occurs and thus if the wavelength of the x-ray is known, characteristic atomic distances of the crystal are also known.

The penetration depth of the X-rays goes from a few micrometers to a few milimeters, depending on the studied material's absorbance[11]. This poses a problem for the study of thin films, where the scattering resulting from the substrate/water molecules might conceal the diffraction resulting from the 2D film. One then needs to decrease the contribution from the substrate as much as possible.

Thus, to characterize the molecular structure of Langmuir monolayers, the incident x-ray beam must reach the surface of water at grazing incidence α_{inc}, smaller than the critical angle of the air/water interface, conditions for total external reflection to occur. However, some photons do still penetrate in the condensed material (monolayer and substrate) forming the so-called evanescent wave. Such wave propagates parallel to the interface, with its intensity decreasing exponentially in the direction perpendicular to the interface, reducing the penetration depth of the x-ray at the vapor-liquid interface of water to only a few nanometers[13]. And thus, the interaction of the x-ray with the water molecules is greatly reduced, and thus the monolayer is what scatters most of the radiation, improving the signal to noise ratio of the diffraction peaks. [14] [15]

A schematic of the geometric configuration of the GIXD technique is shown below in fig. (10). Diffraction patterns produced by the film at an angle 2θ from the incident beam are collected with a 2D detector.

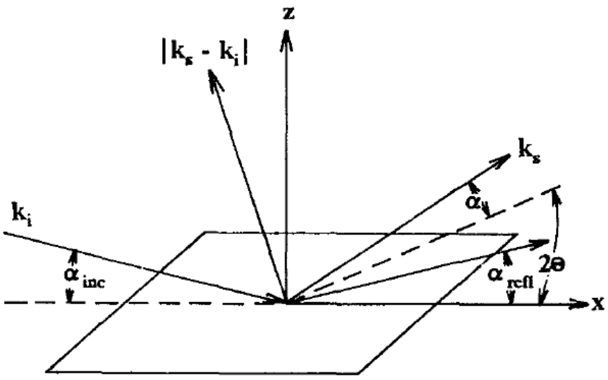

Figure 10 - Typical surface scattering geometry.

The angles that produce diffraction peaks are, as will be shown in section (1.7), dependent on the wavelength of the x-ray, and so, for comparison purposes, this angle is often converted into the scattering vector $\vec{Q}$ which is independent of the wavelength used in the experiment. The in-plane component of $\vec{Q}$ is $Q_{xy} = 4\pi\, sin(\theta)\,/\lambda$ (for small α) and the out of plane component is $Q_z = 2\pi\, sin(\alpha)\,/\lambda$ [16].

Synchrotron radiation facilities around the world provide high energy and monochromatic radiation for diffraction measurements. Moreover, the low divergence of the ranging in microradians allows for defining the angle of incidence satisfactorily.

All GIXD diffraction spectra presented in this work were measured at the SIRIUS beamline of the SOLEIL synchrotron in Orsay, with $\lambda = 0.155\ nm$.

1.7. X-ray Diffraction: How a monochromatic plane wave performs Fourier analysis on the electron density distribution.

Thompsons formula (4) gives the electric field produced by a single point charge, if one considers a volume element dV of a charge density $\rho(\vec{r})$ at $\vec{r}$, then the electromagnetic field of the wave diffused by dV at a distance R’ is given by:

$$dE_s(\vec{R}) = \frac{e^2\rho(\vec{r}).dV}{m_q c^2}\frac{1}{R}\left(E_0 e^{-i\vec{k}_i.\vec{r}}\right)\sin(\theta)\, e^{i(\omega t-\vec{k}_s\vec{R}\prime)} \quad (5)$$

Where e is the charge of an electron and $E_0 e^{-i\vec{k}_i.\vec{r}}$ is the amplitude of the incident wave.

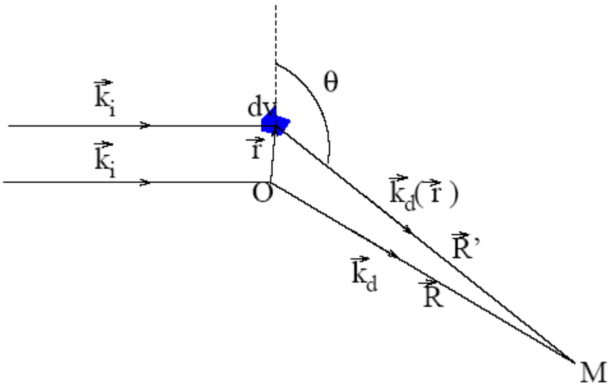

Figure 11 - Scattering of x-rays by a volume element dV of a charge density $\rho(\vec{r})$.

Since $\vec{R} = \vec{r} + \vec{R}'$, and $r \ll R \text{ and } R'$,

$$dE_s(\vec{R}) = \left\{\frac{e^2 dV}{m_q c^2}\frac{1}{R}E_0 \sin(\theta)\, e^{i(\omega t-\vec{k}_s\vec{R}\prime)}\right\}\rho(\vec{r})e^{i\vec{r}\vec{Q}} \quad (6)$$

Where $\vec{Q} = \vec{k}_s - \vec{k}_i$ represents the scattering vector, or momentum transfer vector. The integral of the above expression is then:

$$E_s(\vec{R}) = \left\{\frac{e^2}{m_q c^2}\frac{1}{R}E_0 \sin(\theta)\, e^{i(\omega t-\vec{k}_s\vec{R}\prime)}\right\}\int_V \rho(\vec{r})e^{i\vec{r}\vec{Q}}\, dV \quad (7)$$

The term between brackets is the field scattered by a single electron, E_e, and the integral represents the Fourier transform of the charge density FT(ρ). This fourier transform called the structure factor, $F(\vec{Q})$, represents the effect of the entire crystal structure on the diffracted waves. Put simply, the waves scattered by two electrons with distance $\vec{r}$ will differ by a phase factor of $e^{i\vec{r}\vec{Q}}$. If $\rho(\vec{r})$ is the electron density of a crystal, the effect of the entire crystal on the diffracted waves will amount to:

$$\int_V \rho(\vec{r})e^{i\vec{r}\vec{Q}}\,dV = F(\vec{Q}) \quad (8)$$

The diffraction intensity I, which will be measured by the detector in the beamline as a function of $\vec{Q}$, is given by the modulus of the scattered wave:

$$I = E_s {E_s}^* = |E_e|^2 * \left|F(\vec{Q})\right|^2 \quad (9)$$

And thus:

$$I \propto \left|F(\vec{Q})\right|^2 \quad (10)$$

2. Simulated Structure Factor Calculations and Simulation setup in Gromacs.

2.1. Molecular Dynamics Simulations

All-atom MD simulations were performed in order to have a nanoscopic view of the dynamics and equilibrium state of H18OH, H14OH, F18OH, F14OH and F20 Langmuir films.

All simulations were performed using the GROMACS package [16] [17]. The data was analysed either through Gromacs' integrated programs or the newly developed structure factor program. The VMD software was used for the visualization of trajectories.

The systems studied in this work are modelled using an all-atom force field based on the optimized potentials for liquids simulations (OPLS-AA) [18]. This force-field models each atom as an interaction site and the potential energy is written as the sum of contributions due to bond stretching, bond angle bending, dihedral angle torsion and non-bonded interactions (van der Waals plus electrostatic interactions). For non-bonded interactions of sites in the same molecule, only sites separated by three or more bonds are calculated. The interactions from intra-molecular sites separated by three bonds are multiplied by a 0.5 constant. The non-bonded interaction between sites of different atom types were computed using geometrical rules:

$$\epsilon_{ij} = \sqrt{\epsilon_{ii}\epsilon_{jj}} \quad \text{and } \sigma_{ij} = \sqrt{\sigma_{ii}\sigma_{jj}}$$

The long chain fluorinated alcohols and perfluoro-n-eicosane were modelled using the parameters for perfluoroalkanes proposed by Watkins (perfluoroalkyl moieties) and Jorgensen (alcohol moieties), [19] while the hydrogenated alcohols were modelled with the L-OPLS force field for alkanes [20], with the -CH_2OH moieties modelled by the OPLS-AA. Water was modelled with the three site spc-e rigid body model.

All systems were simulated at 298.15K, using periodic boundary conditions in all directions, under NVT ensemble conditions and using the Berendsen thermostat with a time constant of 0.5 ps. The equations of motion were solved using the leap-frog algorithm with time-steps of 2 fs.

To construct the simulation systems, initial simulation boxes of 10000, 17500 and 40000 water molecules were set. The geometry of the simulation boxes (9.1x9.1x15 nm; 13x13x15 nm and 18.2x18.2x20 respectively) was chosen with a larger z dimension in order to generate a water slab 3.5 nm thick with two liquid-vapour interfaces. These water boxes were simulated for 3 ns in the NVT ensemble. The surfactant and F20 molecules were generated individually, and their energy minimized. Each molecule was then replicated using packmol [21] to assemble the initial starting configurations of 100, 200 or 400 residue molecules aligned in the z direction. Amphiphiles were assembled with the OH groups pointing into the water direction. The water boxes were merged with the vertically aligned molecules and the simulations were started. The very tight initial configuration was used to speed up the equilibration process of the system.

A representation of the initial configuration of the simulations is shown below in fig. (12).

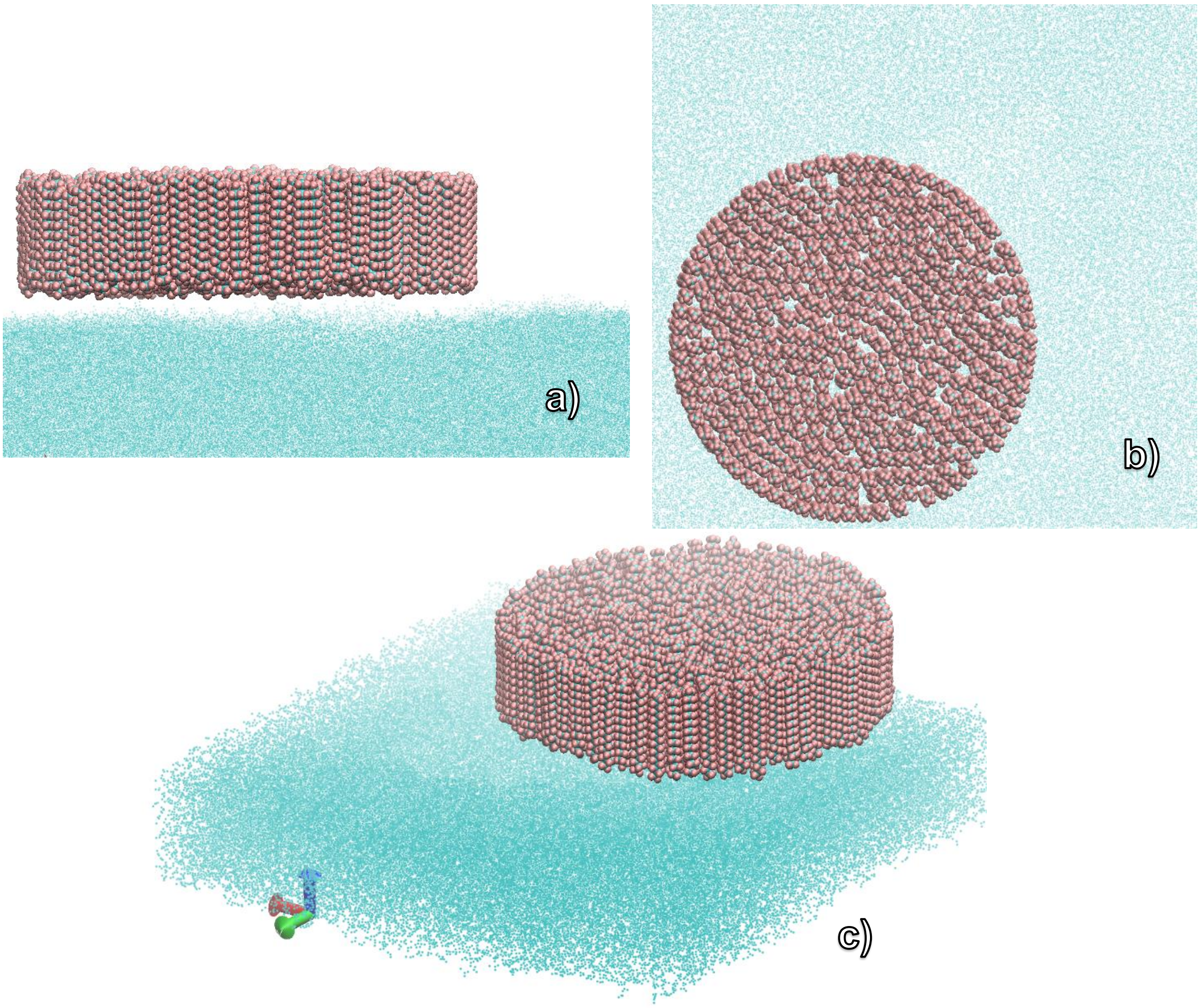

Figure 12 – a) Side view, b) top view and c) isotropic view of the initial starting configuration of the simulation box.

2.2. Diffraction Spectra in Molecular Dynamics.

In crystallography measurements it is common to compute the reverse Fourier transform of the diffraction pattern and obtain the electron density of the crystal for a better understanding of the molecular structure. This is useful to comprehend and characterize monolayer's unit cell, or for protein crystal analysis. [22]

However, in the case of MD simulations, the opposite is true, the molecular structure is known and the diffraction pattern is not. In fact, if one approximates that all the electrons are at the centre of each atom[1], it is possible to calculate which values of $\vec{Q}$ will yield diffraction by direct computation of the simulation data into the discretized structure factor function below.

$$I \propto \left| \sum_{Qz=Qzi}^{Qzf} \sum_{Qy=Qyi}^{Qyf} \sum_{Qx=Qxi}^{Qxf} \sum_{n}^{n_{atoms}} N(n) e^{ix_n Q_x} . e^{iy_n Q_y} . e^{iz_n Q_z} \right|^2 \quad (11)$$

Where N(n) is the number of electrons corresponding to the n^th atom in the data; x_n, y_n, z_n are the cartesian coordinates of the n^th atom; and Q_x, Q_y, Q_z are the cartesian components of the diffraction vector, which iterate from a starting desired value Q_{xi}, Q_{yi}, Q_{zi} until a final desired value Q_{xf}, Q_{yf}, Q_{zf}.

And so, a Fortran program was developed to read the atoms' coordinate data from the Gromac's simulation and calculate the structure factor of the monolayer for each value of $\vec{Q}$. In order to mimic GIXD spectra, two types of scans are made, in-plane scans ($q_{||\ (hk)}$) and rod scans ($q_{z\ (hk)}$), where the subscript (h,k) represents the miller indices; The in-plane scans, are produced by computing only the x and y coordinates of the atoms and iterating the diffraction vectors Q_x, Q_y, Q_z, these scans are intended to determine the amount of ordered phase and unit cell. The rod scans, are produced by iterating trough all desired Q_z, but only iterating trough the values of Q_x and Q_y which satisfy the equality $Q_{xy} = (Q_x)^2 + (Q_x)^2$, with the Q_{xy} representing the center of the peak in the in-plane scan. The Fortran code is shown in the supplementary information.

---

[1] It's worth noting that it is a valid approximation to say that all electrons are positioned in the centre of each atom as the distance of an electron to the atom's centre is much smaller than the distance between molecules, which is what is being measured by GIXD experiments.

2.2.1. Diffraction Satellites

If one imagines a perfect, infinite sized one-dimensional crystal with lattice length ***a***, such as in fig. (13), the Fourier transform of the electron density of such crystal (diffraction pattern) would correspond to Dirac delta functions whenever $q = \frac{2\pi}{a}$. [23] [24]. In this case, the Fourier transform simplifies to equation (12):

$$\sqrt{I} \propto \sum_{n=-\infty}^{\infty} e^{inqa} \quad (12)$$

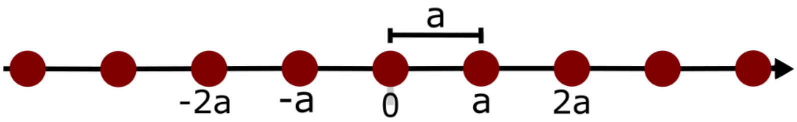

Figure 13 – Interpretation of a one-dimensional and infinite perfect crystal. If X-rays were to strike such material, the well-defined position of atoms would produce diffraction peaks at very well-defined positions.

However, if that same monocrystal is finite with 2N atoms, then all its Bragg peaks are decorated by relative maxima called satellites. This is known in mathematics as the Dirichlet Kernel function (13). The interference of the satellite peaks on the Bragg peak is shown below in fig. (14):

$$\sqrt{I} \propto \sum_{n=-N}^{N} e^{inqa} = \frac{\sin\left(qa\left(N+\frac{1}{2}\right)\right)}{\sin\left(\frac{qa}{2}\right)} \quad (13)$$

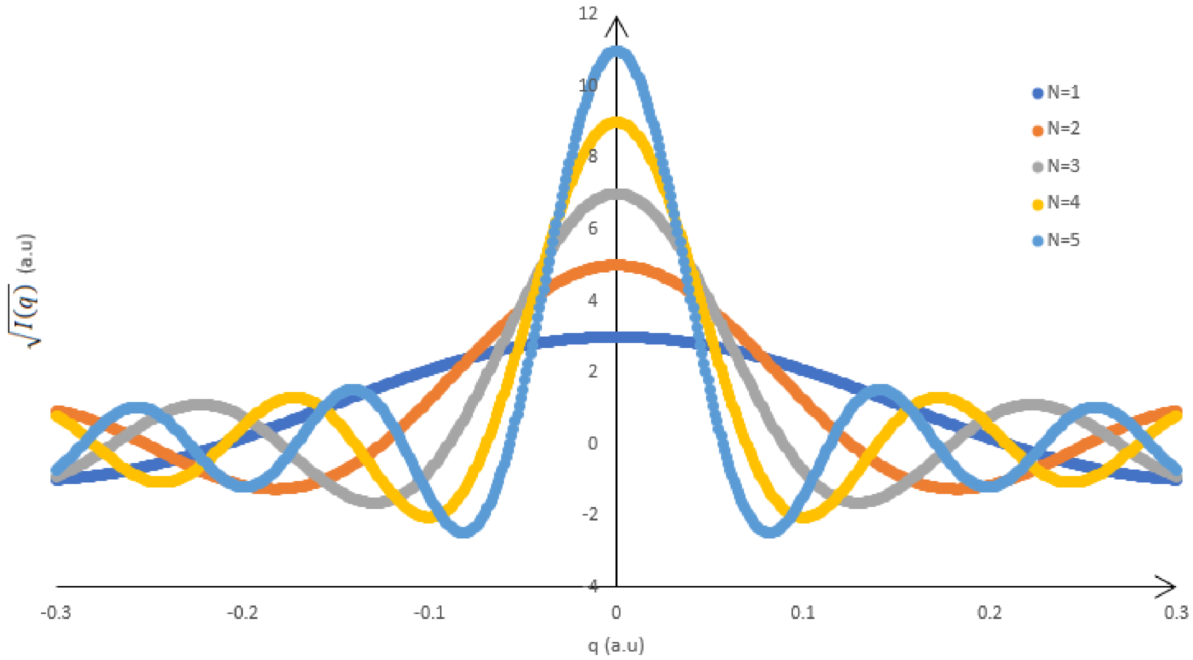

Figure 14 - Graph of Dirichlet-Kernel function representative of theoretical 1D perfect crystals with number of atoms N.

And so, when the number of atoms, *N*, in the crystal increases, the Bragg peak also increases in intensity while decreasing in width, along with distance from the satellites to the main peak being smaller. In fact, the crystal's coherence length L , *(the average length of the crystal where there is no noticeable difference in the unit cell)* is related to the diffraction peak's width at half height, $\boldsymbol{w}$ by $\boldsymbol{w} = \frac{2\pi}{L}$. For $N = \infty$ the function approaches the Dirac function. [24]

Bragg peaks are expected whenever the denominator of equation (13) has a singularity, $\sin\left(\frac{qa}{2}\right) = 0$. As for the satellite peaks, the term $\sin\left(qa\left(N + \frac{1}{2}\right)\right)$ is responsible for the satellites position, which has minima whenever:

$$q = \frac{k\pi + \frac{\pi}{2}}{a\left(N + \frac{1}{2}\right)} \ ,k \ \in N \quad (14)$$

Thus, the q difference between satellites, Δq is given by

$$\Delta q = q_x - q_{x+1} = \frac{\pi}{a\left(N + \frac{1}{2}\right)} = \frac{2\pi}{2a\left(N + \frac{1}{2}\right)} \approx \frac{2\pi}{L} \quad (15)$$

The full width at half height of the Bragg peaks, $\boldsymbol{w}$, is therefore equal to the distance between the satellite peaks, $\Delta \boldsymbol{q}$. This result will be useful in the diffraction results chapter (section 3.2) in which the differences between simulated spectra and experimental spectra from the GIXD are highlighted.

3. Simulation Results

3.1. Molecular Dynamics Results

Langmuirs films with 100, 200 and 400 molecules of F18OH, F14OH, H18OH, H14OH and F20 were simulated at 293.15K, with a large enough water box for it to be analogous to a monolayer with low surface coverage at 0 mN/m of surface pressure. The systems have a water surface to residue molecule ratio of approximately $0.8\ nm^2/molecule$. The 200-molecule and 400-molecule simulations ran for 10 ns or more, with most of the monolayers reaching an equilibrium after just 2.5 ns. The simulations of 100 molecules ran for 5 ns. Only the simulations of 400 molecules are presented in this section, as the simulations of 100 and 200 molecules show very similar results and are presented in the supplementary information or in section (3.1.1). Snapshots of 400 molecule films are shown at 10ns simulation time in fig. (15) to fig. (18).

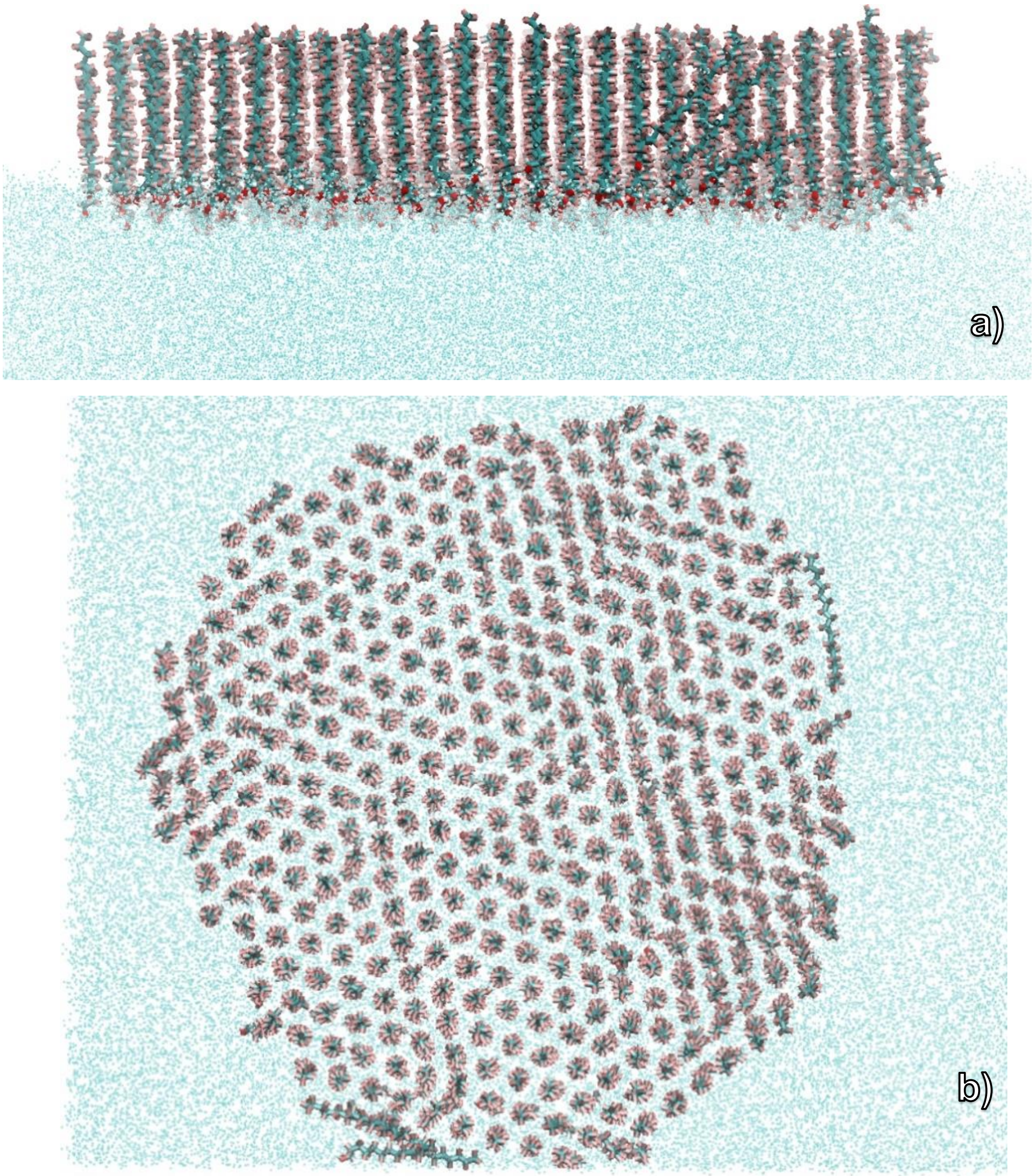

Figure 15 – a) Side and b) top view of 400 molecule aggregate of F18OH at 10 ns simulation time.

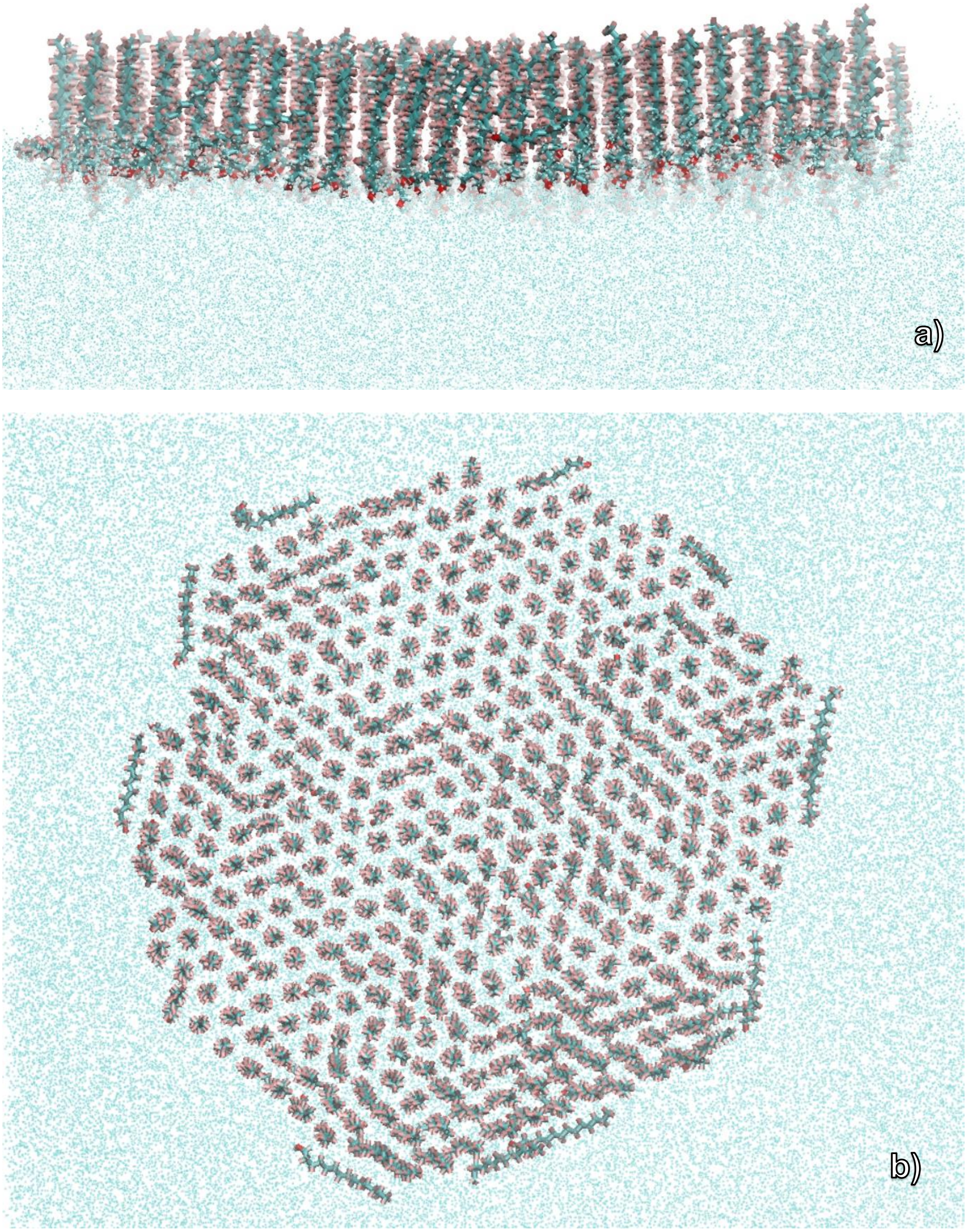

Figure 16 – a) Side and b) top view of 400 molecule aggregate of F14OH at 10 ns simulation time.

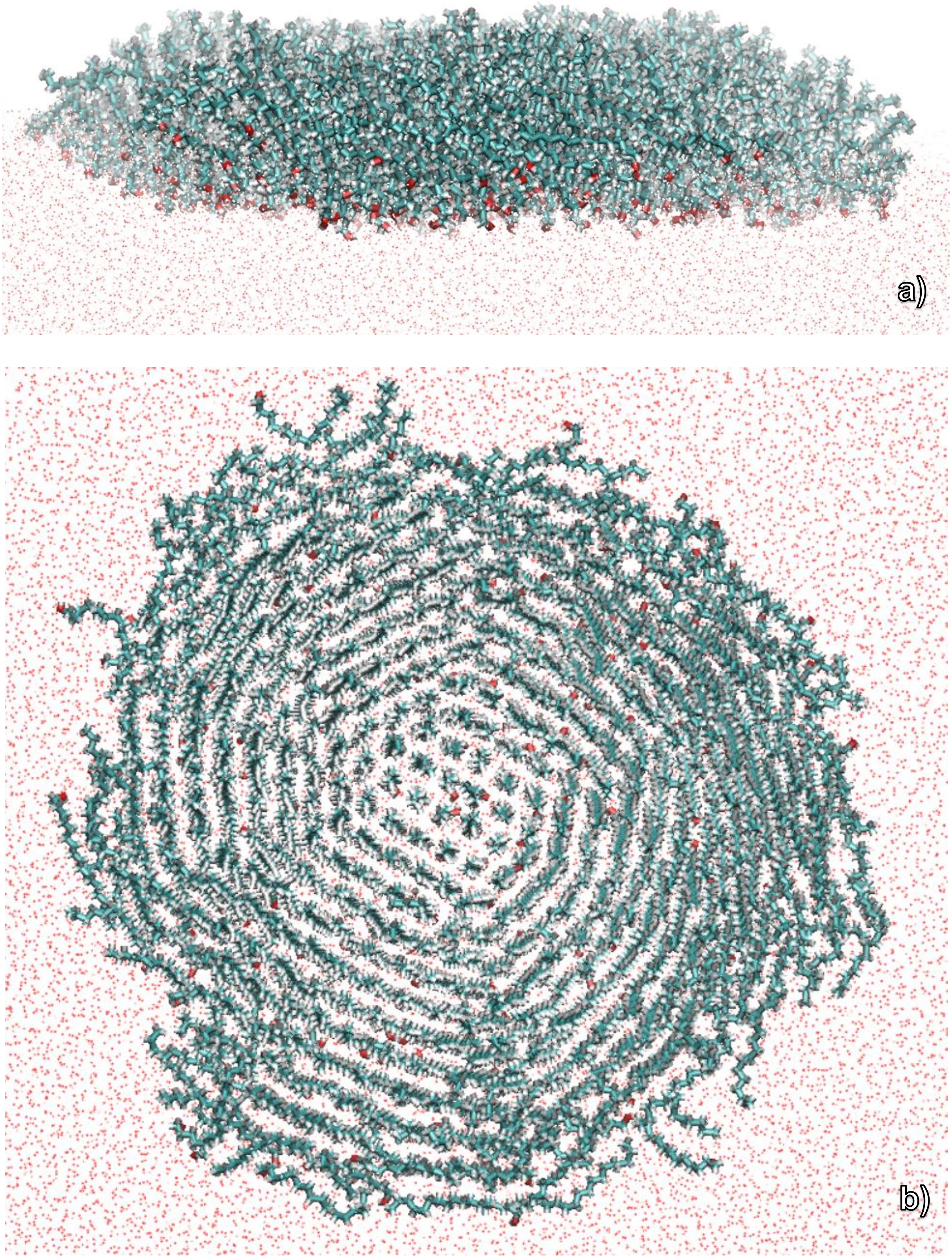

Figure 17 – a) Side and b) top view of 400 molecule aggregate of H18OH at 10 ns simulation time.

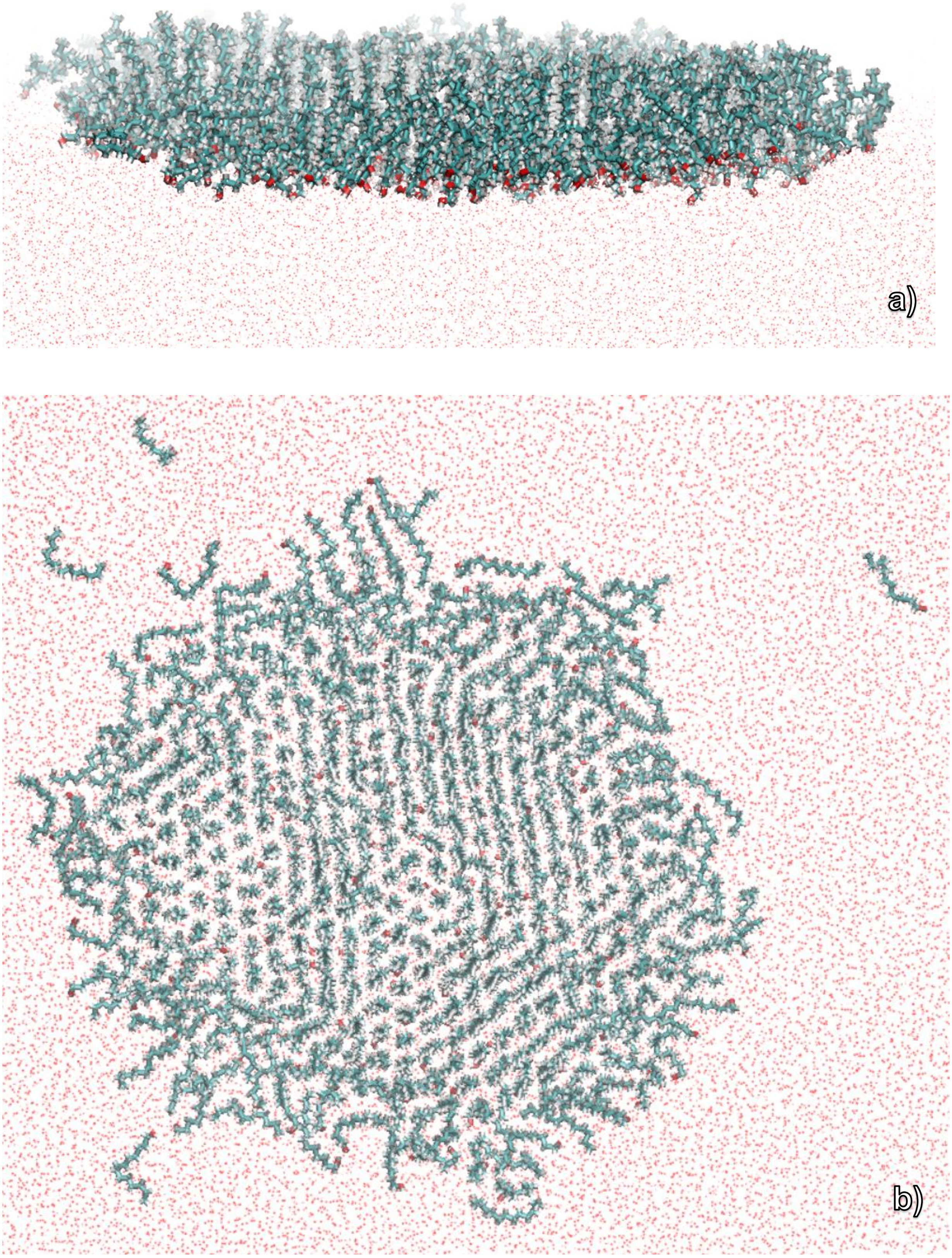

Figure 18 – a) Side and b) top view of 400 molecule aggregate of H14OH at 10 ns simulation time.

At the start of the simulations, both hydrogenated and fluorinated surfactant molecules spontaneously aggregate into isolated domains, evidently forming a condensed phase. During the next two nanoseconds of simulation, the surfactant molecules structurally re-organize themselves until an equilibrium in the aggregate is reached.

The fluorinated molecules clearly form a highly ordered structure with most molecules standing perpendicular to the surface of water. After starting the simulation, the fluorinated domains quickly take the form of a polygonal shape, with its molecules also packed in what appears to be a two-dimensional hexagonal lattice. The F14OH presents a hexagonal domain shape while the shape of the F18OH domain is more polygonal, however the rigidity and inertia of 400 F18OH molecules explains this behaviour since the simulations with 100 and 200 F18OH molecules exhibited the hexagonal domain shape (fig.(25) and fig.(26)). Periodically, a very low number of molecules on the outer edge of the domain will spontaneously lie down on the water surface along the rim of the aggregate. This occurs more regularly for the F14OH than for the F18OH which suggests that the longer chain provides more aggregate stability and ordering.

The hydrogenated surfactants on the other hand are clearly less organized and present a more amorphous structure. The molecules in the centre of the domain stand vertically and packed more orderly, however, as one approaches the rim of the aggregate the molecules become progressively more tilted and disordered with the molecules at the periphery of the aggregate lying fully down on the water surface in various orientations giving the hydrogenated aggregates a circular and smoother shape. The H14OH monolayer, appears to be quite unstable, as the molecules on the outer layer seem to be extraordinarily disordered, with some even protruding outwards from the aggregate. Furthermore, during certain irregular and small periods of the simulation, both hydrogenated surfactants have a small number of molecules which can be seen leaving the aggregate and being isolated from the rest of the domain, in a gaseous phase, just for them to return to the aggregate later. This phenomenon occurs more regularly for the H14OH than for the H18OH, presumably due to the weaker attractive inter-molecular forces of the shorter chain alcohol producing a less stable aggregate.

These simulation results further confirm the polygonal shape and well-defined and sharp height-profile of the fluorinated surfactants seen experimentally. Although these domains have a much larger scale, isolated hexagonal domains can be observed in Teixeira's AFM measurements [25] of transferred F18OH monolayers onto a silicon substrate, and in AFM measurements of Spin-coated F18OH (fig.19). The circular periphery of the hydrogenated simulations also agrees with what is seen experimentally on Teixeira's AFM measurements of mixed monolayers of F18OH and H18OH, seen in fig. (20).

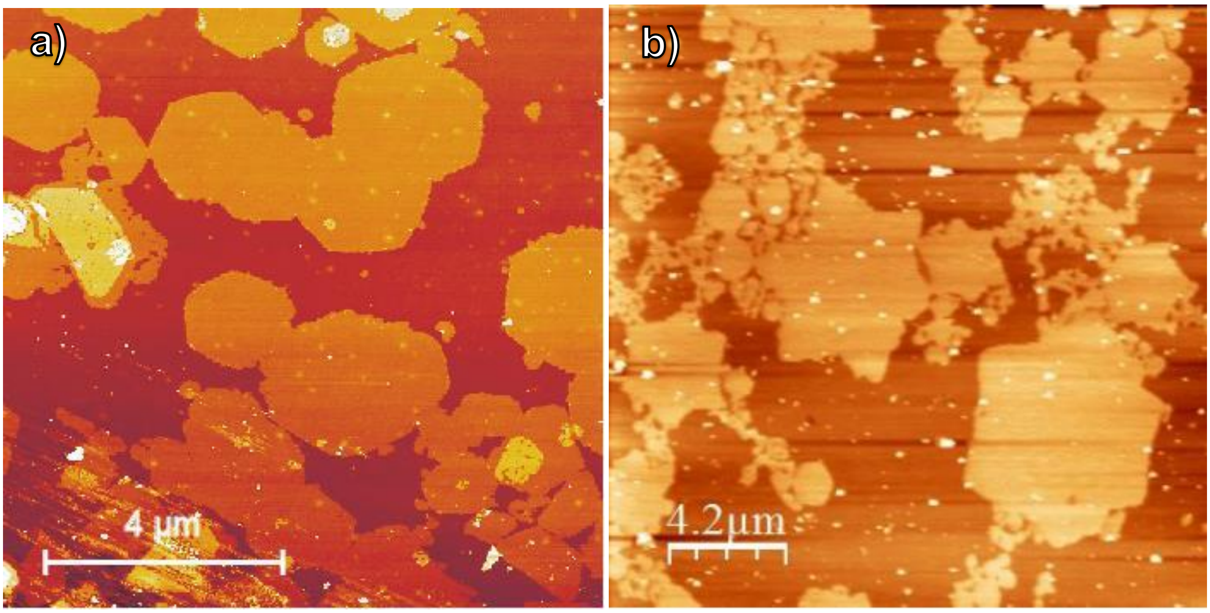

Figure 19 –a) Spin-coated F18OH monolayer on silicon substrate; b) Langmuir-Blodgett transferred F18OH monolayer onto a silicon substrate.

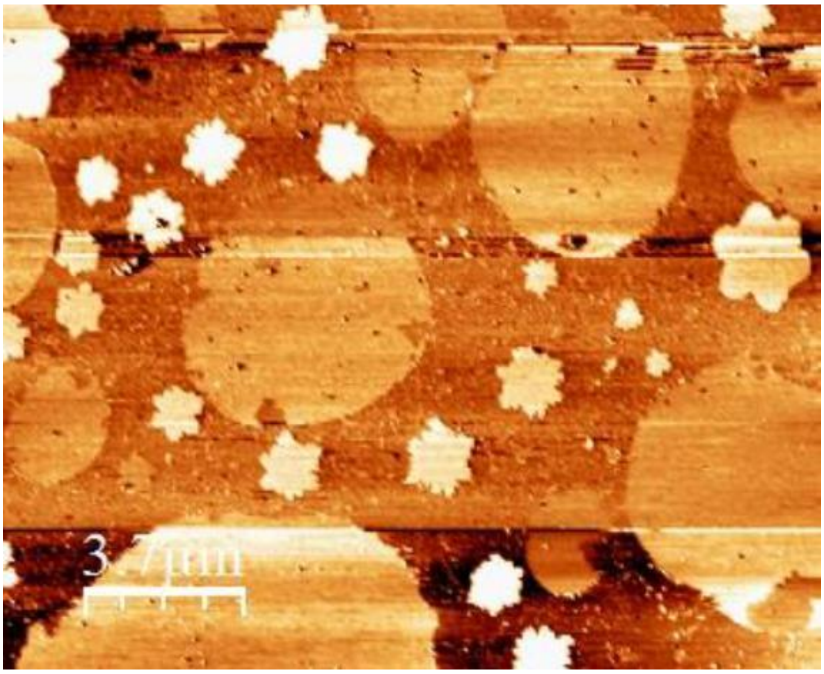

Figure 20 – Langmuir-Blodgett transfer of mixed monolayer of F18OH and H18OH showing the star (hexagonal) and circular domains.

In conclusion, the simulations provide evidence of the fluorinated films to spontaneously assemble in a very ordered crystal-like aggregate while the hydrogenated films exhibit a more amorphous and disordered structure. Due to their rigidity, the fluorinated molecules visibly display two possible orientations: lying flat at the surface of water; or standing vertically parallel to the other molecules in the aggregate. As a result, the fluorinated aggregates display “clear cut” periphery due to their higher line tension. Whereas the conformational freedom and flexibility of the hydrogenated surfactants allows for a gradual orientation of the molecules at the periphery of the aggregate, which makes the domain more circular and with a less well-defined periphery. The stability, formation and size of monolayer domains has been correlated with line tension in other works [26].

For further conclusions a more quantitative analysis of the monolayers must be made. An orientational order parameter was calculated by defining a unit vector for every molecule, which points from the head group of the molecule to its terminal carbon (Terminal carbon to terminal carbon for the F20). The scalar product of every unit vector pair is summed and averaged for each frame of the simulation. The order parameter value ranges from 0 to 1, with 1 representing a very ordered monolayer with all molecules pointing in the same direction.

This parameter was calculated for each frame of the simulation for the first eight nanoseconds of the five simulated monolayers for the aggregates 400 molecules. The value of the order parameter for the first frame is very close to 1 due to the vertically aligned initial configuration used and decreases as the monolayer reaches an equilibrium showing the true order parameter of the monolayer.

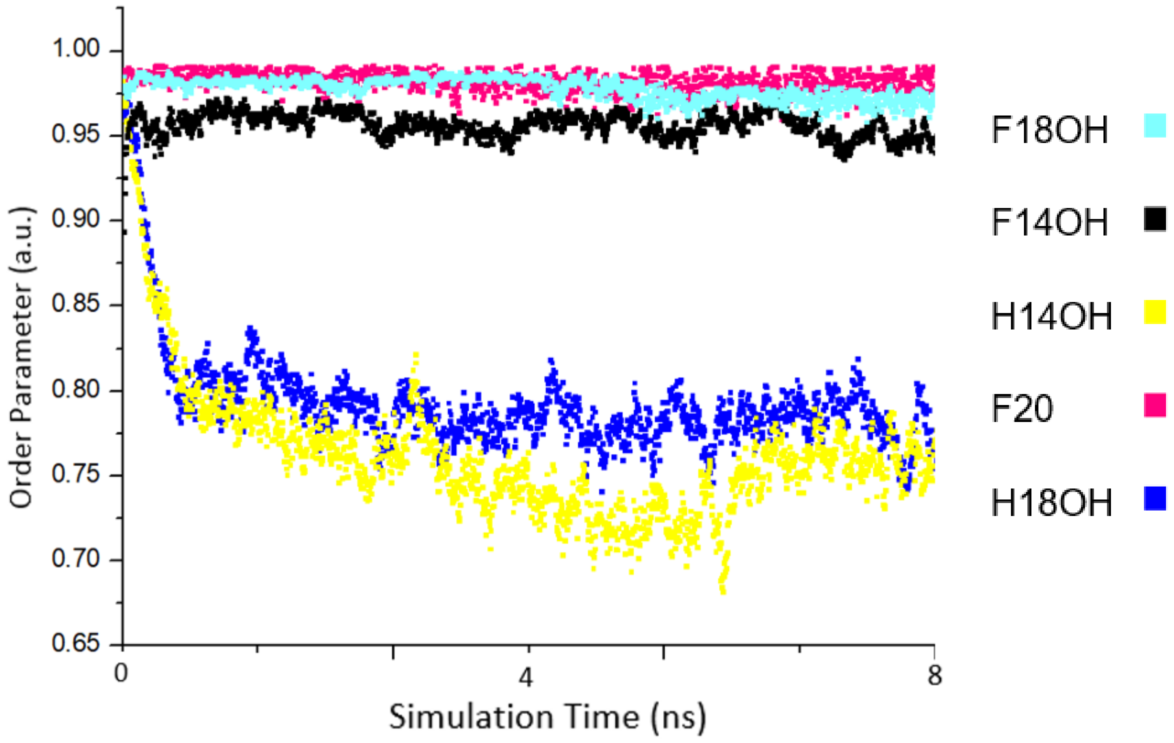

Figure 21– Orientational order parameter for the aggregates of 400 molecules as a function of simulation time.

The order parameter confirms that the films formed by fluorinated chains are considerably more ordered than those formed by hydrogenated chains. For both the fluorinated and hydrogenated chains it can also be seen that the longer the chain the higher the ordering.

3.1.1 F20 Simulation Results

Simulations of F20 were also carried out in order to evaluate the effect of the lack of hydrophilic head group on the organization of the molecules. The 400 molecule F20 simulation snapshots are shown in fig. (22)

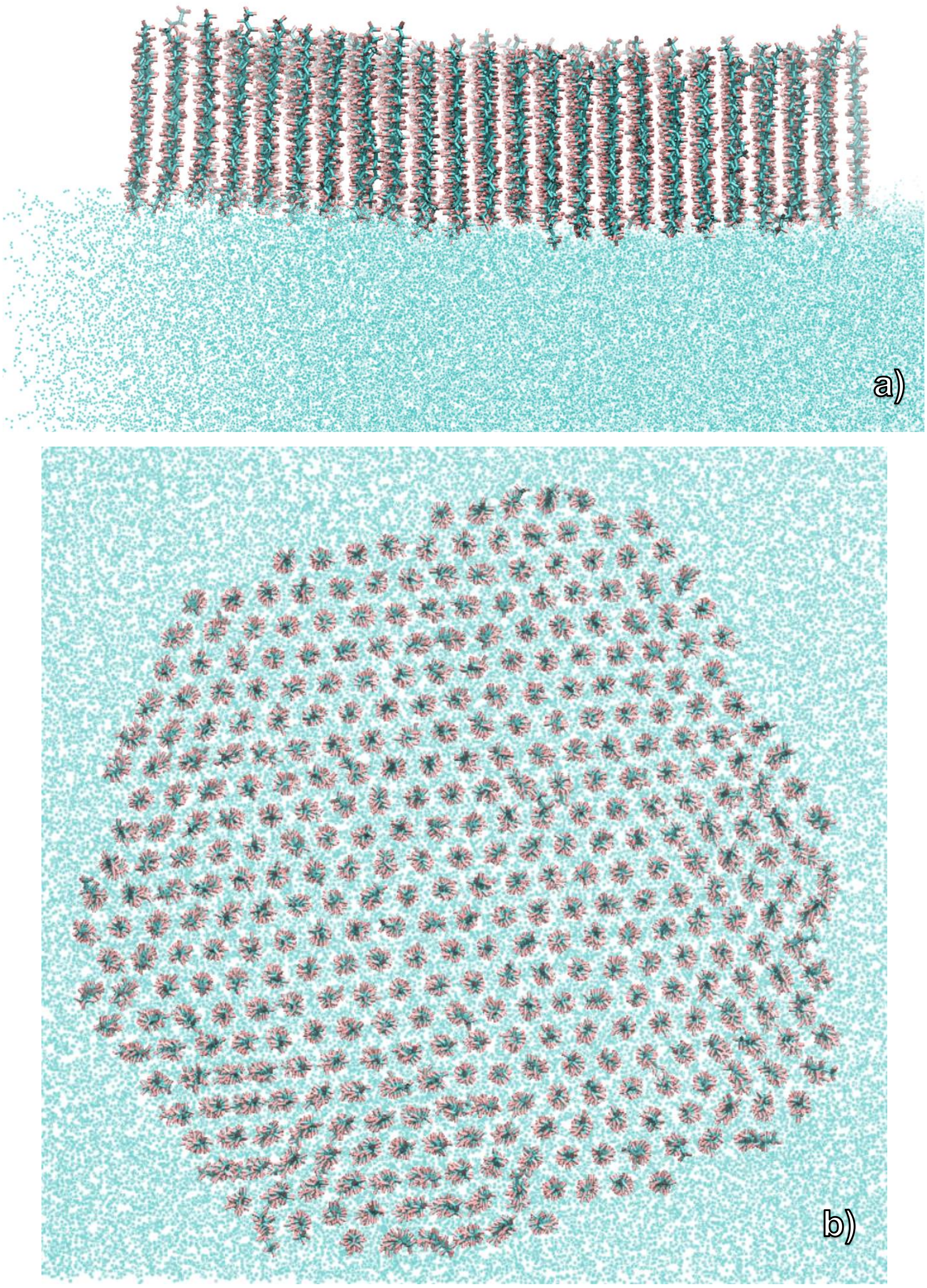

Figure 22 – a) Side and b) top view of 400 molecule F20 aggregate at 10 ns simulation time.

The 400-molecule aggregate exhibits a hexagonal domain with all molecules standing vertically in a hexagonal packing, similar to the fluorinated alcohols already studied above. Surprisingly, even though the F20 has no polar head group for added stability, no molecules are seen lying down during the entire simulation trajectory.

The values of the order parameter were already shown in fig (21) where the F20 presents a higher order parameter than the F18OH and F14OH for the simulations of 400 molecules, due to having no molecules lying down in the rim of the aggregate contrary to the fluorinated alcohols.

However, for F20 aggregates with smaller numbers of molecules, a molecular tilt angle to the water surface is present on the entire crystal. To provide an explanation, simulation snapshots of the 100 and 200 molecules aggregates of F20 are shown in fig. (23) and fig. (24) and compared with the snapshots of the F18OH aggregates in fig. (25) and fig. (26).

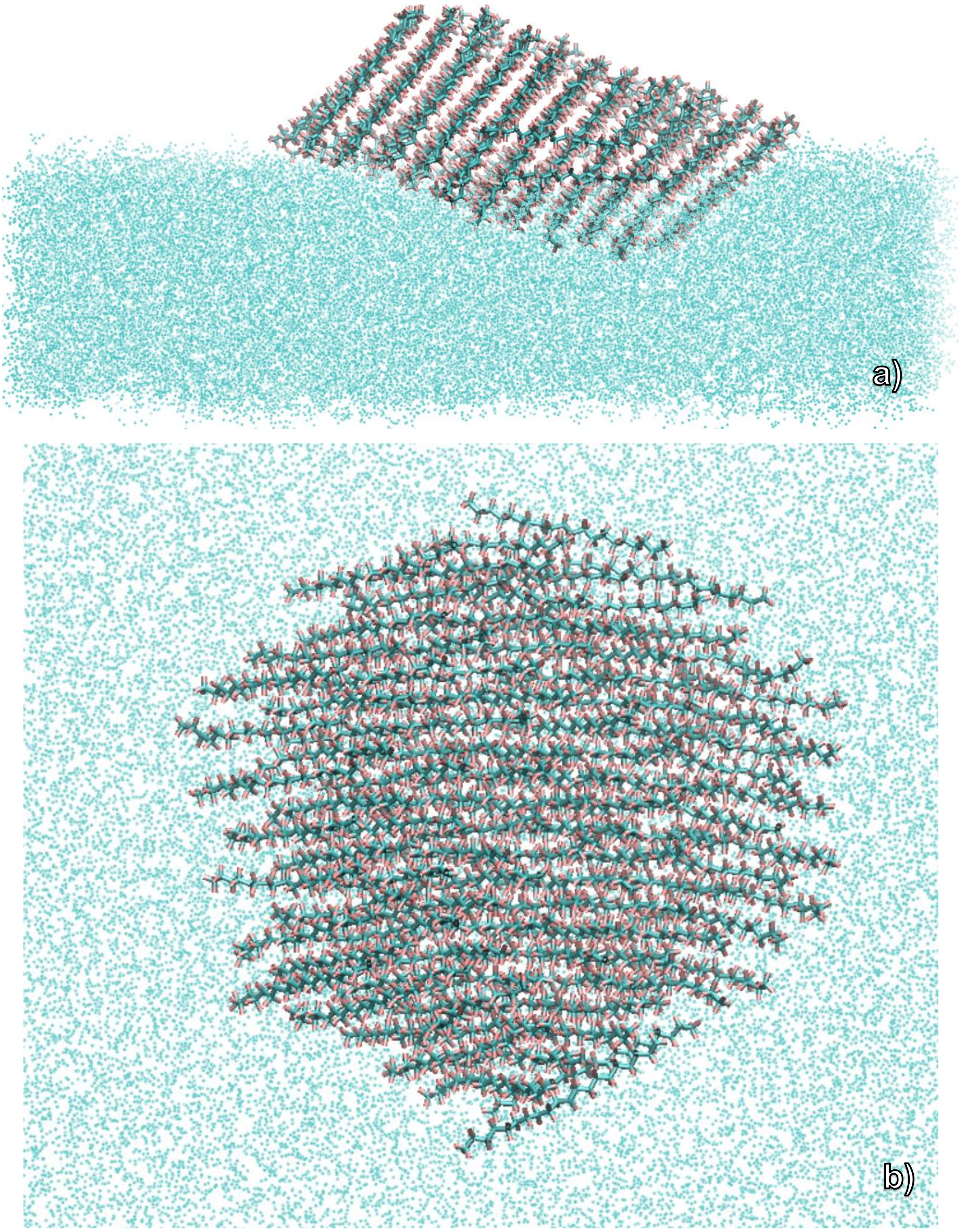

Figure 23 – a) Side and b) top view of 100 molecule F20 aggregate at 5 ns simulation time.

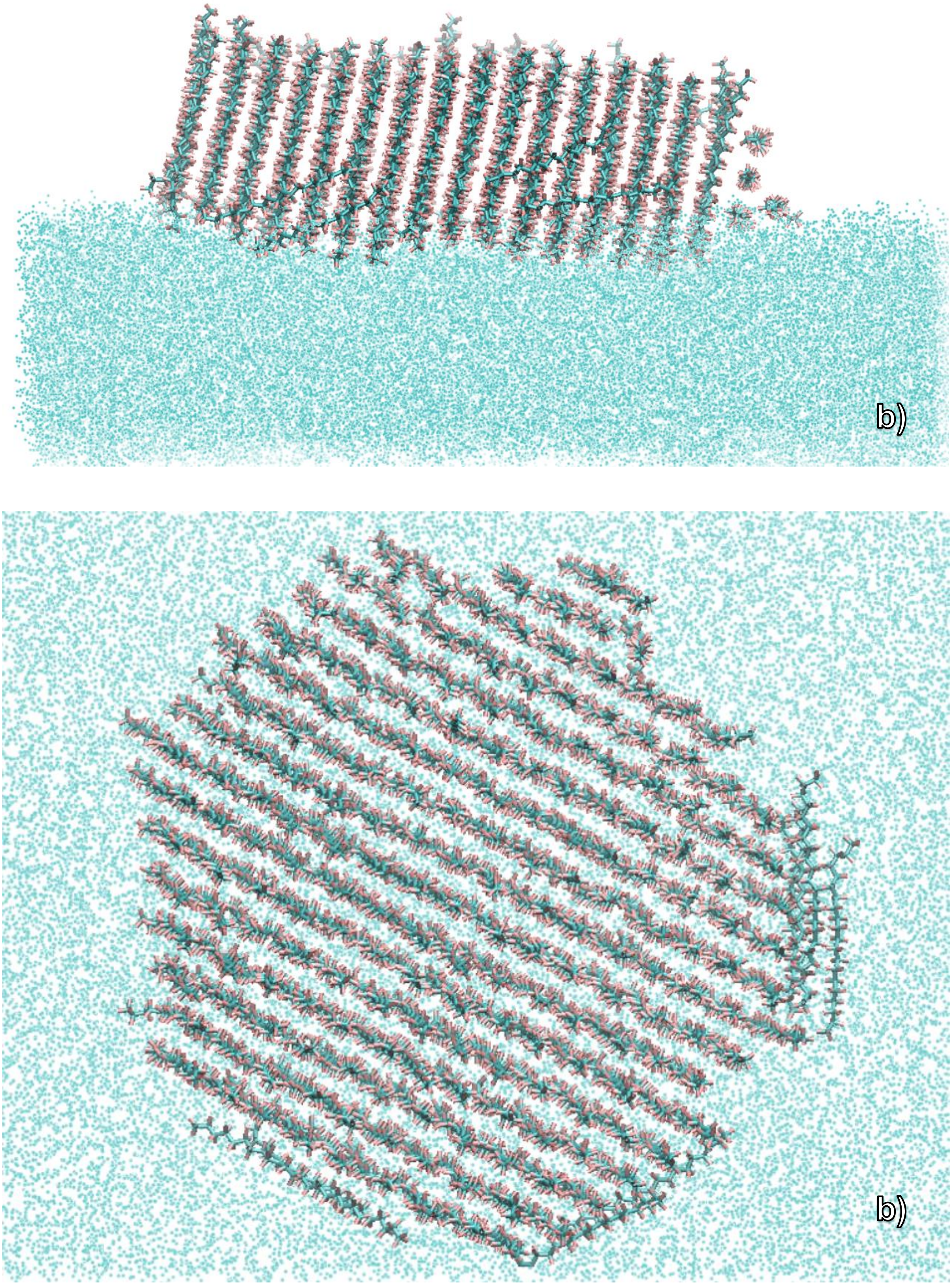

Figure 24- a) Side and b) top view of 200 molecule aggregate of F20 at 10 ns simulation time.

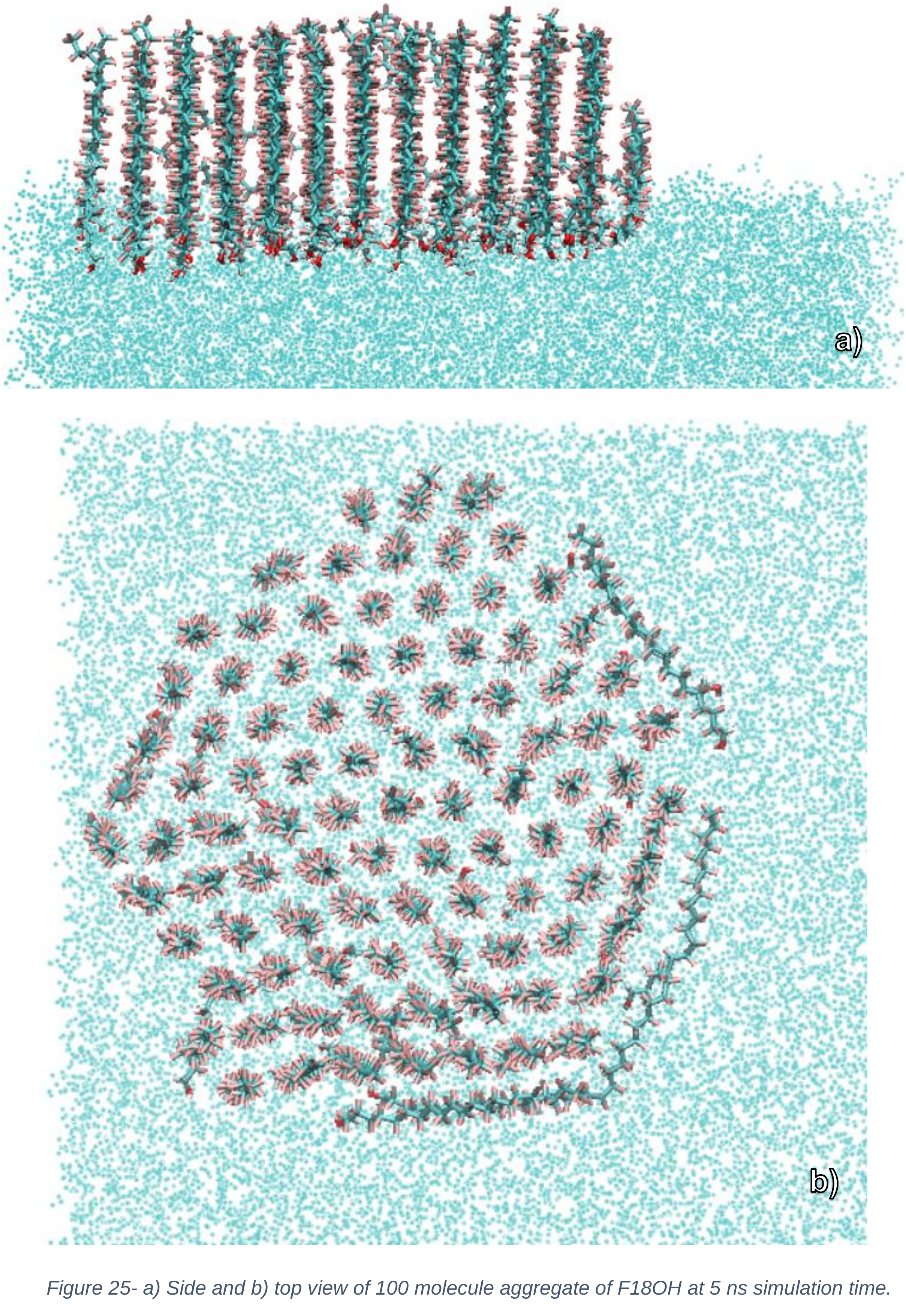

Figure 25- a) Side and b) top view of 100 molecule aggregate of F18OH at 5 ns simulation time.

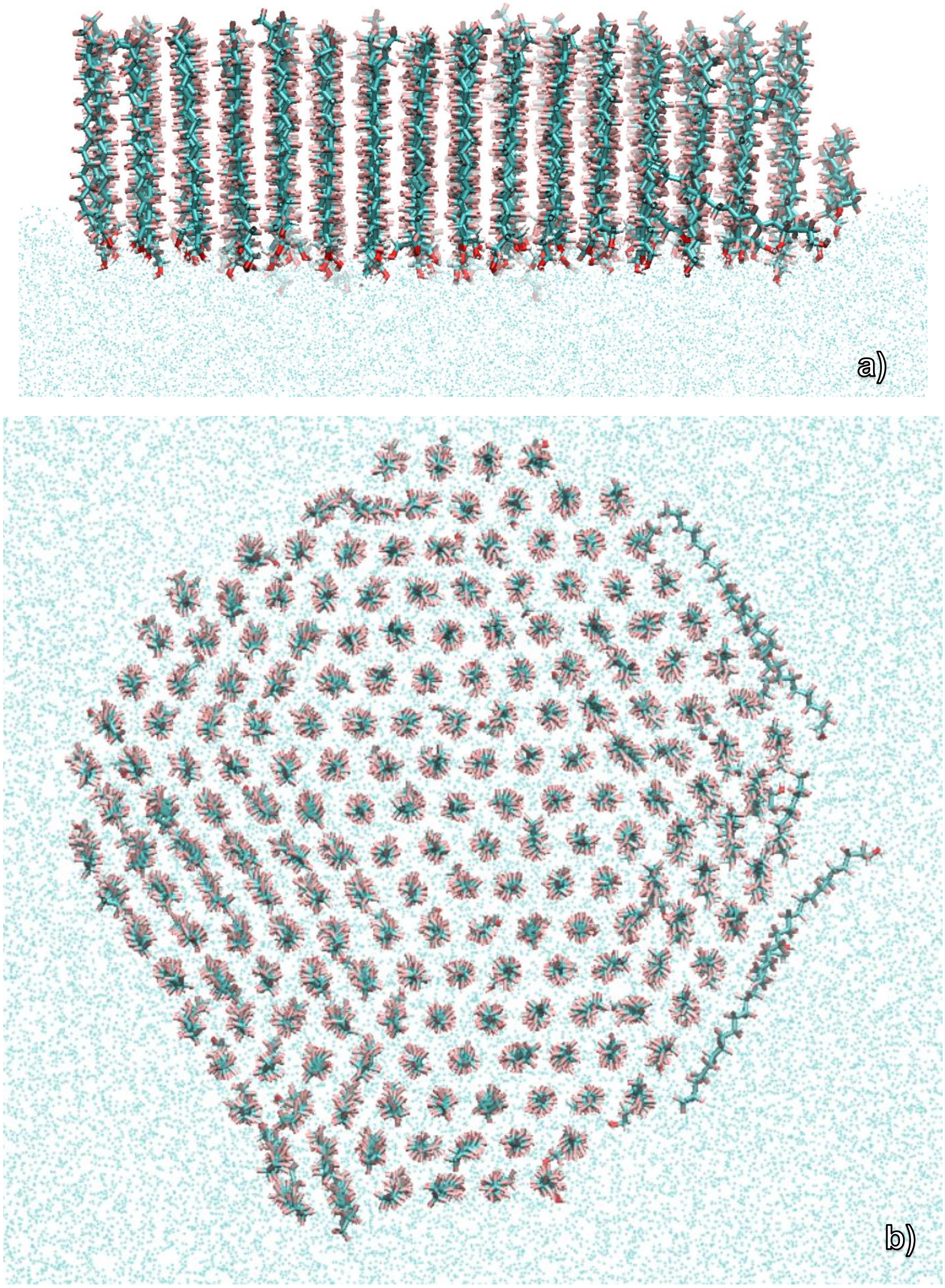

Figure 26 - Side and top view of 200 molecule aggregate of F18OH at 10 ns simulation time.

Contrary to the 400-molecule aggregate, the F20 100-molecule and 200-molecule monolayers present a molecular tilt as well as some molecules lying parallel to the water surface. The F18OH on the other hand, is notably more stable at smaller aggregate sizes. In conclusion, the MD simulations and the order parameter suggest that that the van der Waals forces alone of the F20 are enough to stabilize the monolayer with all molecules perpendicular to the water surface, however this is only true after a minimum number of molecules in the aggregate has been reached, whereas the amphiphilic character of the fluorinated alcohols presents stable untilted domains at all aggregate sizes.

3.2. Simulated Diffraction Results

3.2.1. Characteristics of Simulated Spectra

For further validation of the MD results, the diffraction spectra for the simulated monolayers was calculated using the developed diffraction program. However, before diving deeper into the results, the key differences between simulated and experimental diffraction peaks must be addressed.

To assess such differences, the in-plane simulated diffraction spectra for 400 molecules of F18OH is displayed in figure (27a) along with the experimental F18OH spectra measured at the SOLEIL synchrotron in fig(27b); A Gaussian fit was used for both.

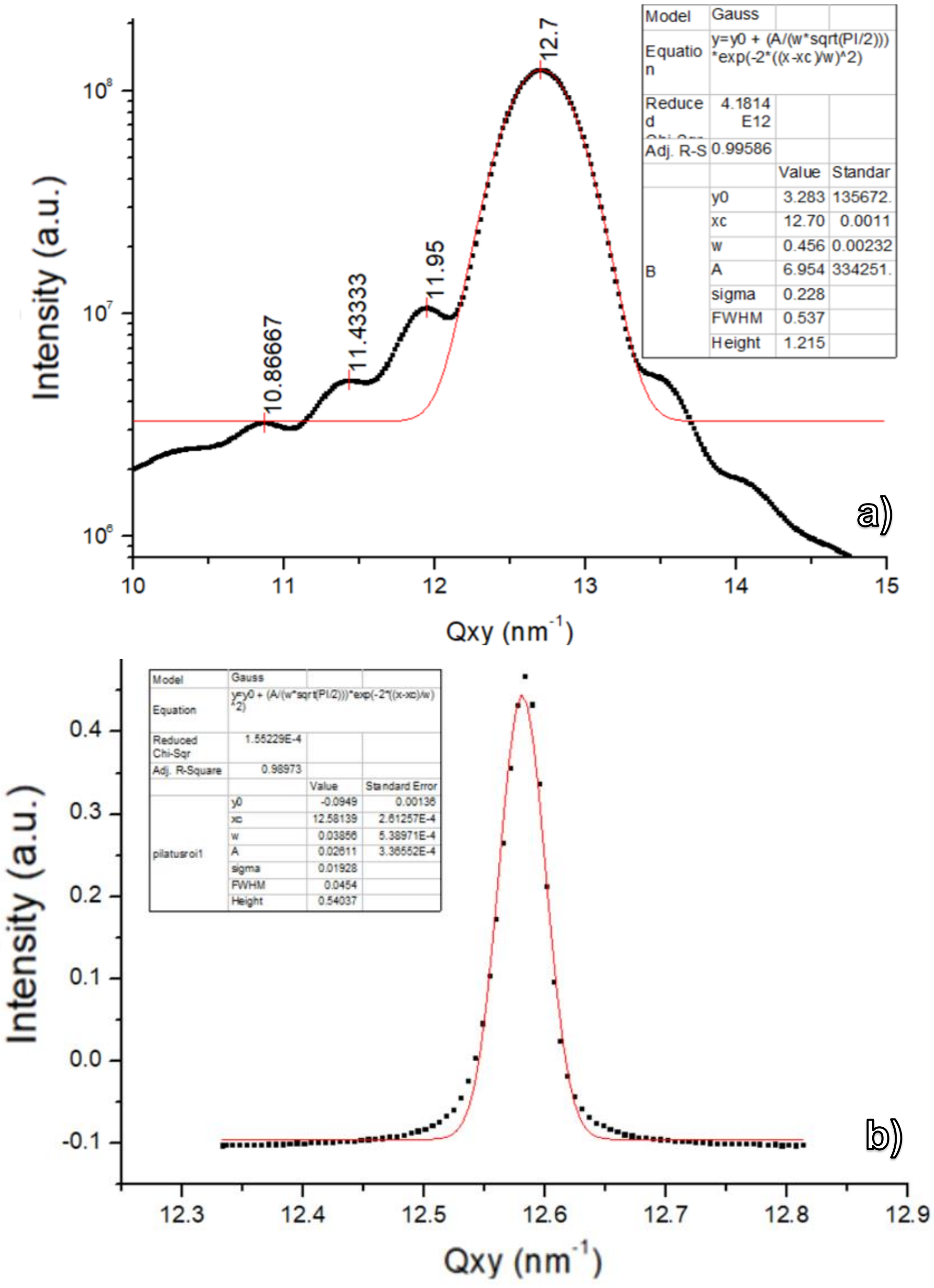

Model	Gauss		
Equation	y=y0 + (A/(w*sqrt(PI/2)))*exp(-2*((x-xc)/w)^2)		
Reduced	4.1814 E12		
Adj. R-S	0.99586		
		Value	Standar
B	y0	3.283	135672.
	xc	12.70	0.0011
	w	0.456	0.00232
	A	6.954	334251.
	sigma	0.228	
	FWHM	0.537	
	Height	1.215	

Model	Gauss		
Equation	y=y0 + (A/(w*sqrt(PI/2)))*exp(-2*((x-xc)/w)^2)		
Reduced Chi-Sqr	1.55229E-4		
Adj. R-Square	0.98973		
		Value	Standard Error
pilatusroi1	y0	-0.0949	0.00136
	xc	12.58139	2.61257E-4
	w	0.03856	5.38971E-4
	A	0.02611	3.36552E-4
	sigma	0.01928	
	FWHM	0.0454	
	Height	0.54037	

Figure 27 – a) Simulated F18OH diffraction spectra. b) Experimental diffraction spectra.

As expected, the simulated in-plane diffraction scan presents relative maxima around the main Bragg peak, something which is not seen experimentally. As explained in section (2.2.1), the Qxy difference between relative maxima was calculated to investigate if these are in-fact just diffraction satellites due to the finite and single simulated crystal. To achieve this, the simulated spectra was fitted with a Gaussian curve and the relative maxima were found numerically with Origin software.

The simulated peak's FWHM is $\approx 0.54\, nm^{-1}$ and the distance from the 1st relative maxima to the 2nd and from the 2nd relative maxima to the 3rd is $\Delta q_{1,2} = 11.95 - 11.43 = 0.52\, nm^{-1}$ and $\Delta q_{2,3} = 11.43 - 10.87 = 0.56\, nm^{-1}$, respectively. And thus, the relative maxima observed in the simulated spectra, are in fact, diffraction satellites as the distance between satellites is equal to the width of the main peak. The exact same is observed for the diffraction spectra of the 100 and 200 molecules aggregates.

Another thing that is different in the simulated spectra is the large width of the peak. The experimental peak's FWHM for the F18OH is 0.0454 nm-1 corresponding to a coherence length of approximately 138 nm, while the simulated peak's FWHM corresponds to a coherence length of 11.7 nm. This is expected as the simulated crystal's diameter is also in the 11/12 nanometer range and thus the coherence length in the simulations is limited by the crystal's small dimensions. For this reason, in this work, experimental coherence lengths are not reproducible in the simulations as it would require simulation boxes too big to be computationally feasible.

Diffraction satellites are not usually observed in GIXD experiments because the monolayers diffracting at the synchrotron are most often in fact just composed of multiple crystals with different dimensions and orientations, called a 2D powder. When the x-rays strike the 2D powder, the position and intensity of the satellites is different for each crystal length, and thus the effect of the satellites is averaged leaving us with a cleaner diffraction peak. To better visualize this effect, the diffraction spectra of the three simulated F18OH monolayers with 100, 200 and 400 molecules are shown below, along with the sum of the three spectra as to be analogous to the diffraction of a monolayer composed of three different domains.

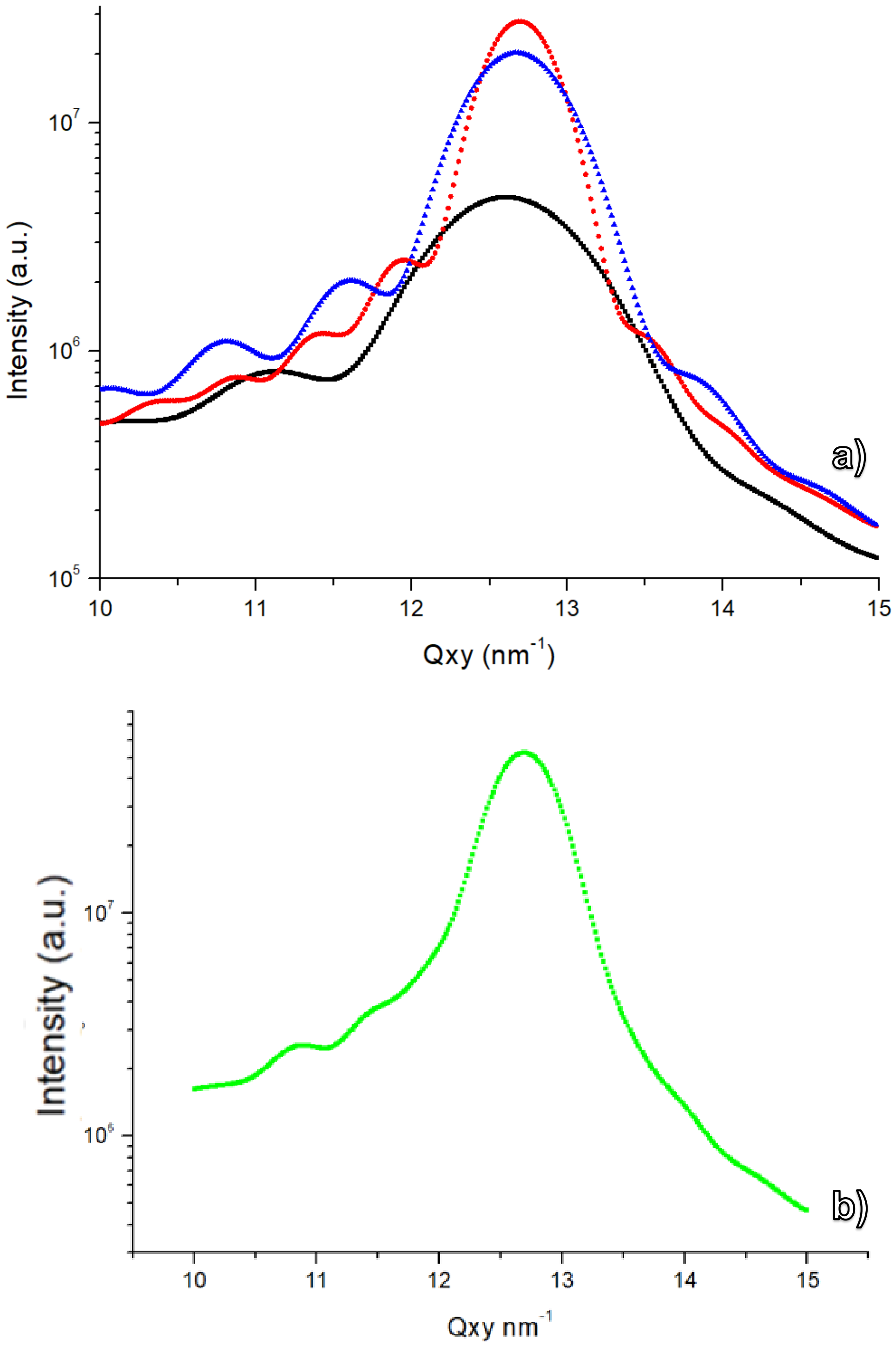

Figure 28 – a) Normalized diffraction spectra for 100 (black), 200 (blue) and 400 (red) molecules of F18OH. b) Sum and average of the three diffraction spectra.

The larger the domain, the closer the satellites are to the main peak. The width of the peak decreases with the increase of the crystal’s length and the intensity increases with the increase of the total number of molecules, as expected. The sum of the three diffraction spectra improves the smoothness of the peak greatly. In conclusion, the simulated structure factor program works as expected and allows for straightforward comparisons with the experimental diffraction patterns.

3.2.2. Simulated Diffraction Spectra of F18OH, F14OH and F20.

To analyse if the structures formed by the F18OH, F14OH and F20 simulated films are plausible, the diffraction spectra was obtained by running the diffraction program on 50 frames of the trajectory data after 7 nanoseconds of simulation time.

The in-plane diffraction spectra, for the F18OH, F14OH and F20 correspondent to the nearest neighbour (the [10] family of planes), $q_{||10}$, are shown below, along with the out-of-plane profile integration at the centre of the in-plane peak. The true fit is neither Gaussian nor Lorentzian and thus a Gaussian fit for all spectra was used rather than a Lorentzian as the fitting to the width and centre of the peaks is much better.

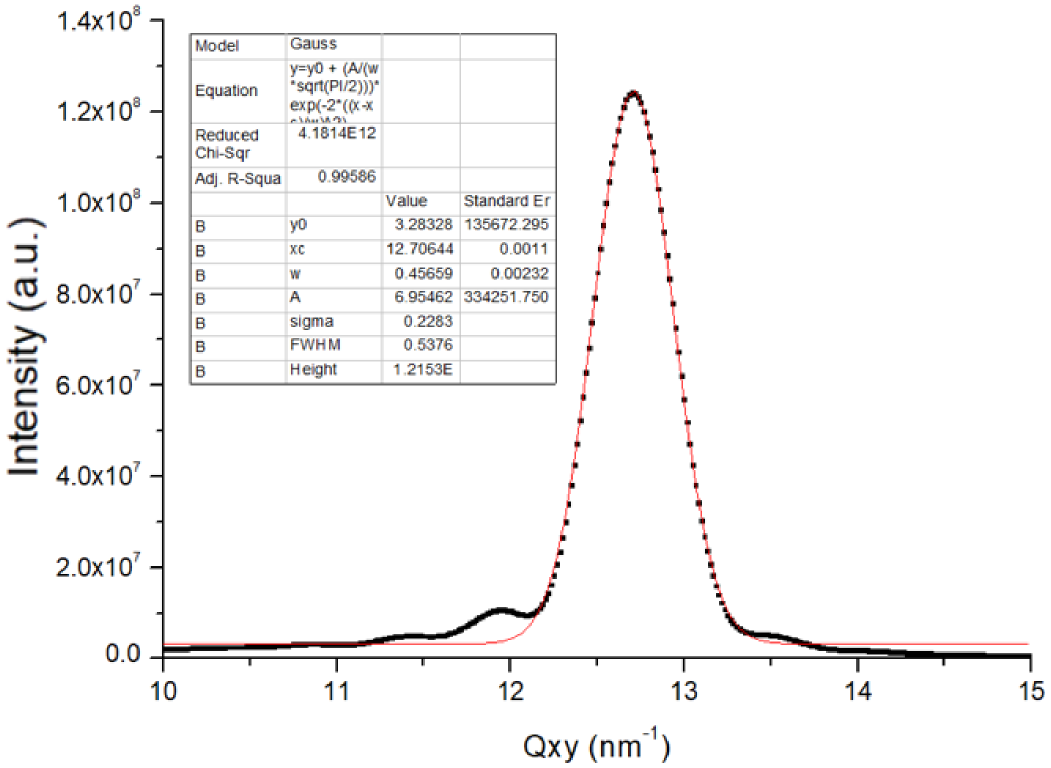

Model	Gauss		
Equation	y=y0 + (A/(w *sqrt(PI/2)))* exp(-2*((x-x		
Reduced Chi-Sqr	4.1814E12		
Adj. R-Squa	0.99586		
		Value	Standard Er
B	y0	3.28328	135672.295
B	xc	12.70644	0.0011
B	w	0.45659	0.00232
B	A	6.95462	334251.750
B	sigma	0.2283	
B	FWHM	0.5376	
B	Height	1.2153E	

Figure 29- In-plane [10] simulated diffraction spectra of 400 F18OH molecules.

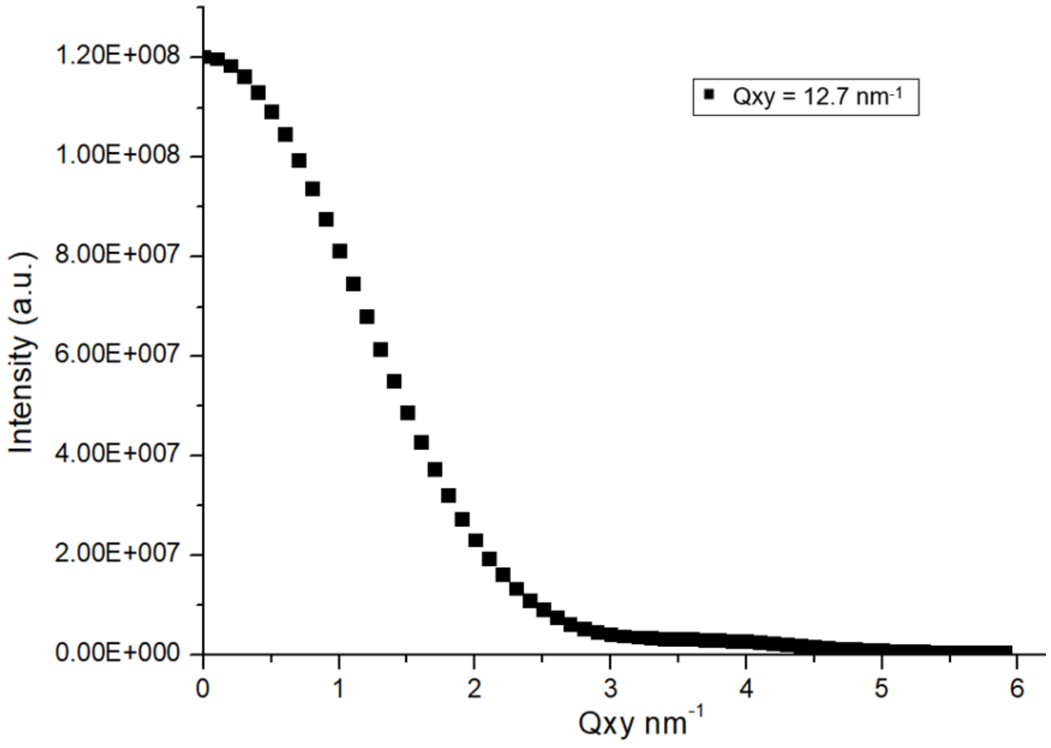

Figure 30 – Simulated F18OH out-of-plane integration with Qxy=12.7 nm^{-1}

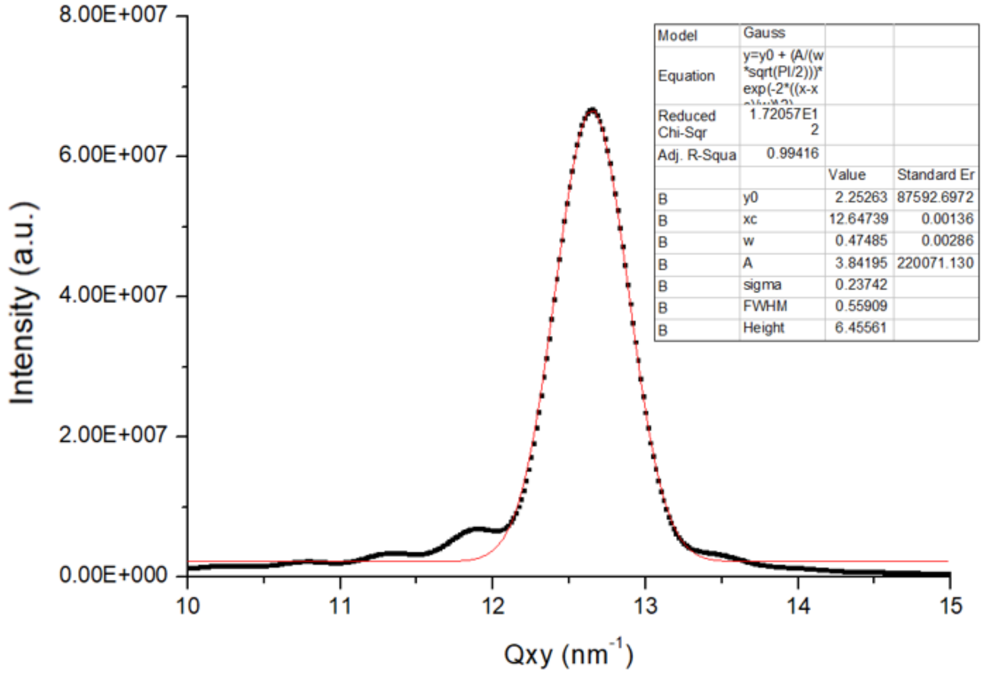

Model	Gauss		
Equation	y=y0 + (A/(w *sqrt(PI/2)))* exp(-2*((x-x		
Reduced Chi-Sqr	1.72057E12		
Adj. R-Squa	0.99416		
		Value	Standard Er
B	y0	2.25263	87592.6972
B	xc	12.64739	0.00136
B	w	0.47485	0.00286
B	A	3.84195	220071.130
B	sigma	0.23742	
B	FWHM	0.55909	
B	Height	6.45561	

Figure 31 – [10] In-plane simulated diffraction spectra of 400 F14OH molecules

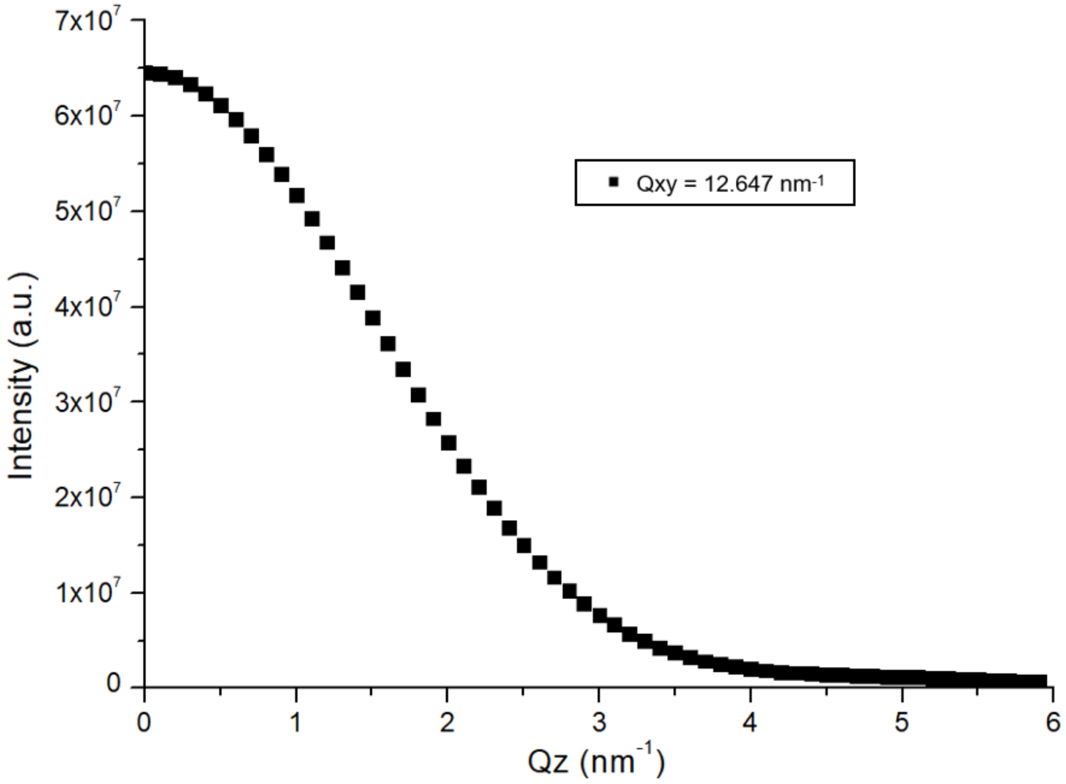

Figure 32 - Simulated F14OH out-of-plane integration with Qxy=12.647 nm^{-1}

The diffraction spectra evidently shows clear in-plane peaks at Qxy $= 12.7\, nm^{-1}$, Qxy $= 12.65\, nm^{-1}$ for the F18OH and the F14OH, respectively. There is a slight shift to higher Qxy (0.05 nm^{-1} increase in value for both the F18OH and F14OH) when compared to the experimental spectra, however the in-plane Qxy difference between the F18OH and F14OH peaks is of $0.05\, nm^{-1}$, which agrees with the experimental $0.05\, nm^{-1}$, meaning that the effect of the chain length on the lattice length is well modelled. The out-of-plane scans are characteristic of aggregates of untilted molecules as the spectrum's maxima, q_{z01} is located at Qz= $0\, nm^{-1}$, which agrees with the experimental spectra.

The F20 simulation presents an in-plane peak at lower Qxy (0.07 nm^{-1} decrease) than the experimental[7]. The F20 diffraction spectrum is shown below in (fig .31) and (fig. 32)

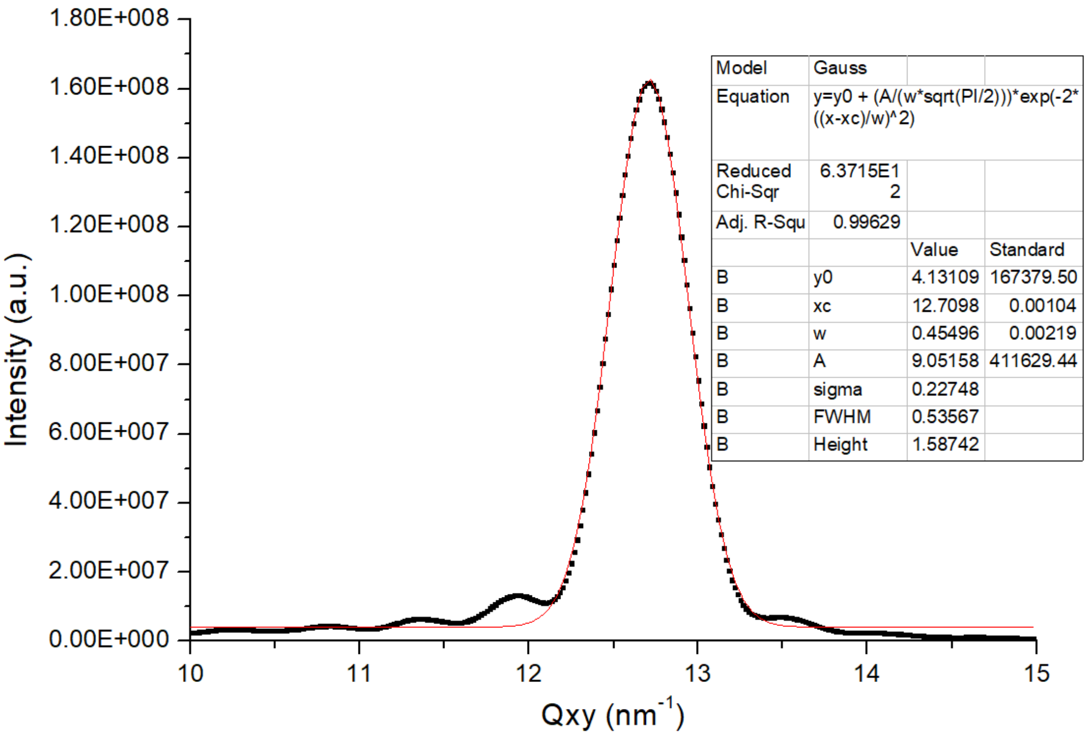

Figure 31 – [10] In-plane simulated diffraction spectra of 400 F20 molecules.

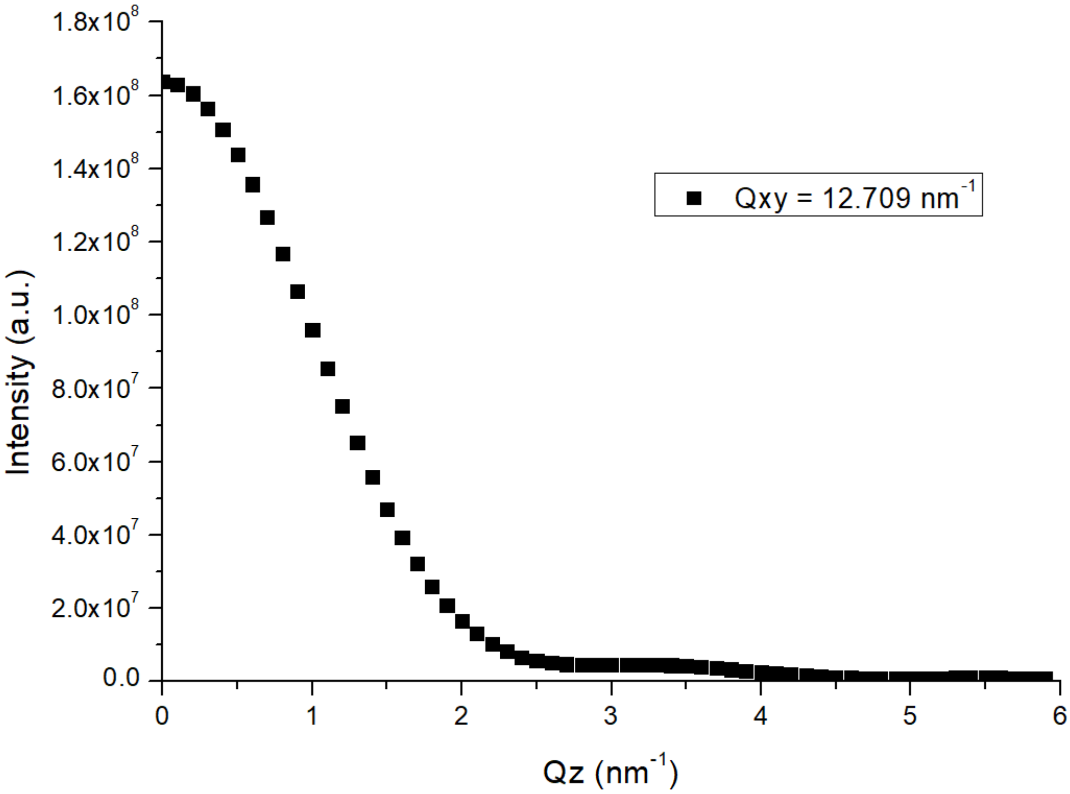

Figure 32 - Simulated F20 out-of-plane integration with Qxy=12.709 nm^{-1}

The approximate aggregate diameter was measured using the VMD software and is presented in fig. (33) along with the diffracted coherence length (extracted from the FWHM of the fitted peaks) as a function of number of molecules in the aggregate.

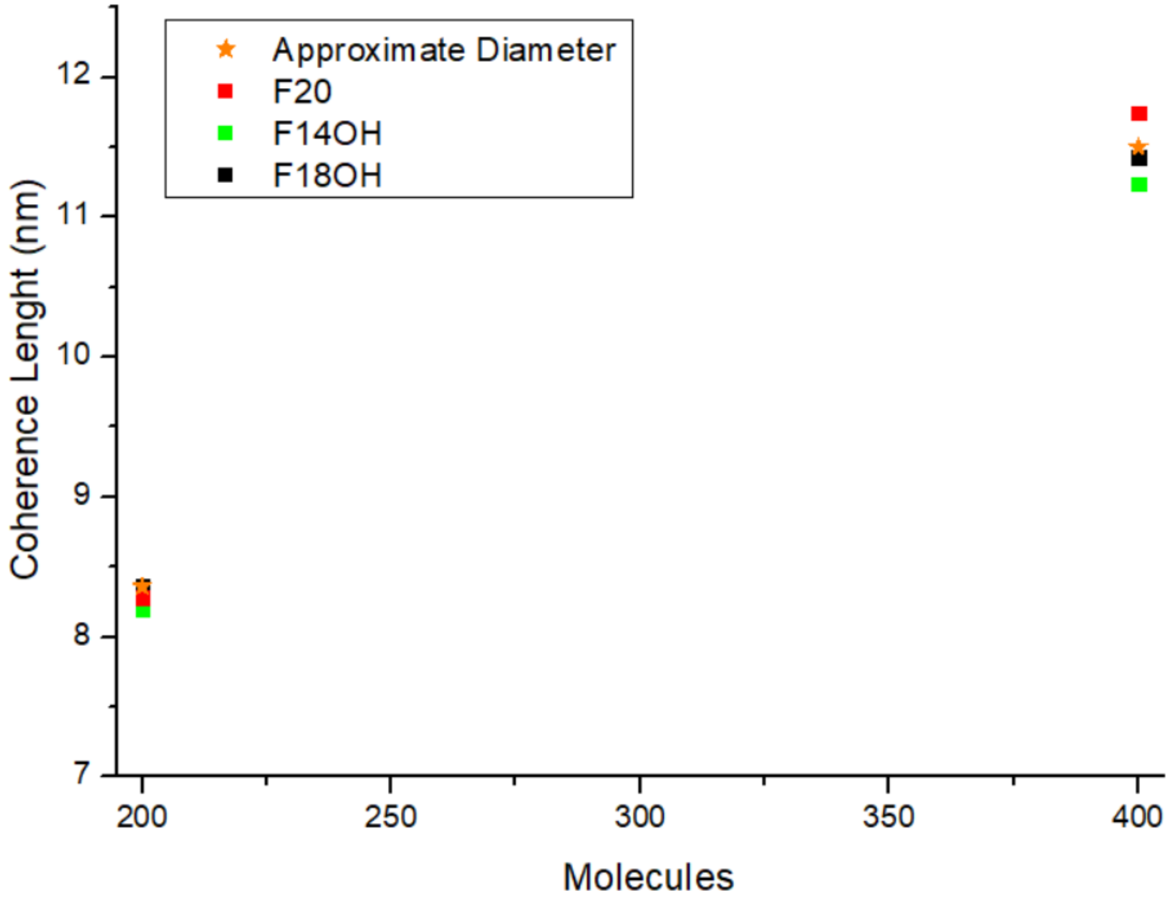

Figure 33 – Aggregate diameter and coherence length as a function of number of molecules.

And thus, it is confirmed by means of diffraction that the fluorinated films exhibit molecular ordering on the entire dimension of the aggregate. The observed difference in coherence lengths between different molecules is not significant as it was taken from the width of Gaussian fit to the spectra, which is far from perfect. In this case, one can merely say that the diffracted coherence length is always limited by the size of the simulations and that It would not be computationally feasible to check if the forcefields are able to reproduce the experimental coherence lengths (ranging in the hundreds of nanometers) as simulations with hundreds of thousands of surfactant molecules would be needed.

With the simulated diffraction peaks, the unit cell of the simulated films was calculated using the following equations: [27]

$$\cos(\gamma) = \frac{q_{||11}^2 - q_{||10}^2 - q_{||01}^2}{2q_{||10}q_{||01}} \quad (16)$$

$$a = \frac{2\pi}{q_{||10}\sin(\gamma)} \quad (17)$$

$$b = \frac{2\pi}{q_{||01}\sin(\gamma)} \quad (18)$$

$$\cot \emptyset = \frac{1}{\sin \gamma}\left[\cos \gamma + \frac{q_{z10}/q_{||10}}{q_{z01}\,/q_{||01}}\right] \quad (19)$$

$$\tan t = -\frac{1}{\sin \emptyset}\frac{q_{z01}}{q_{||01}} \quad (20)$$

Unit cell lattice parameters $\vec{a}$ and $\vec{b}$ must have the same length as there appears to be a single diffraction peak corresponding to the [10] index, and so $q_{||10} = q_{||01}$. Such single peak suggests a perfect hexagonal organization, however, to fully characterize and confirm the unit cell one needs to find the angle γ between lattice vectors, and thus the $q_{||11}$ spectra is also needed. For a perfect hexagonal lattice, the [11] peak can be expected at $q_{||11} = \sqrt{3}q_{||10}$ and the [20] peak can be expected at $q_{||20} = 2q_{||10}$.

The simulated diffraction $q_{||11}$ and $q_{||20}$ peaks and corresponding out-of-plane profile integration are shown below in fig. (34) to fig. (39).

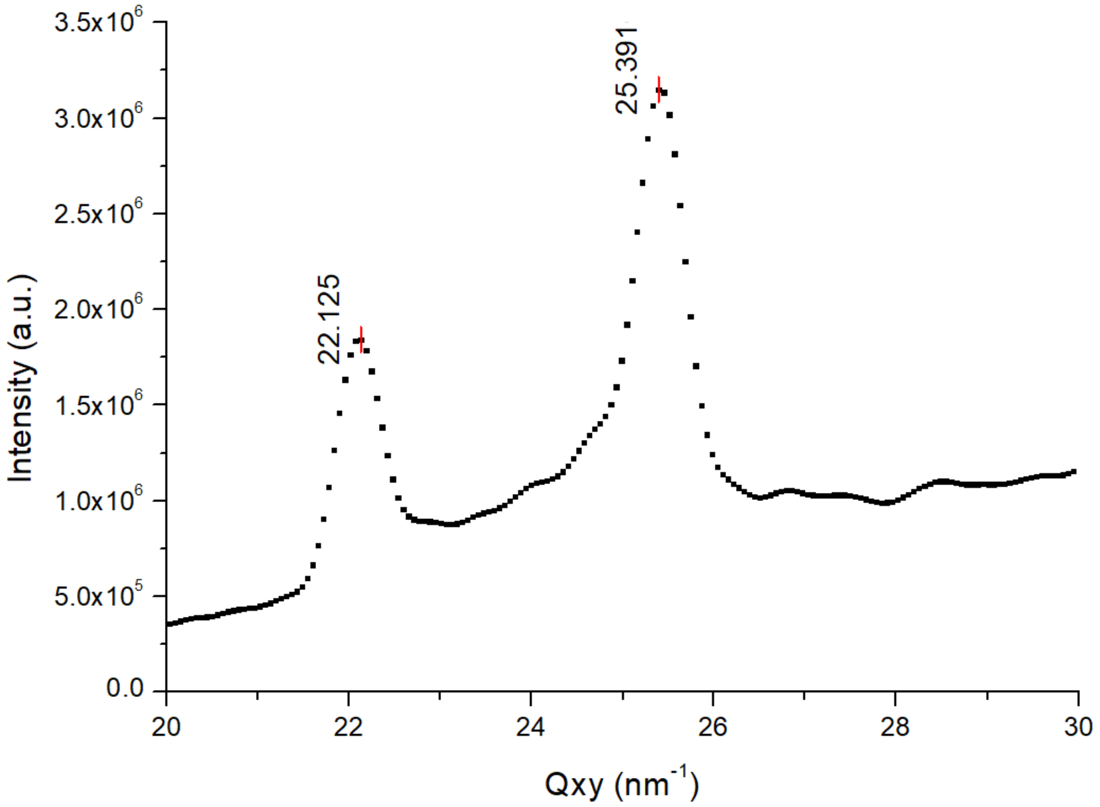

Figure 34 – [11] and [20] simulated diffraction peaks for 400 molecules of F18OH.

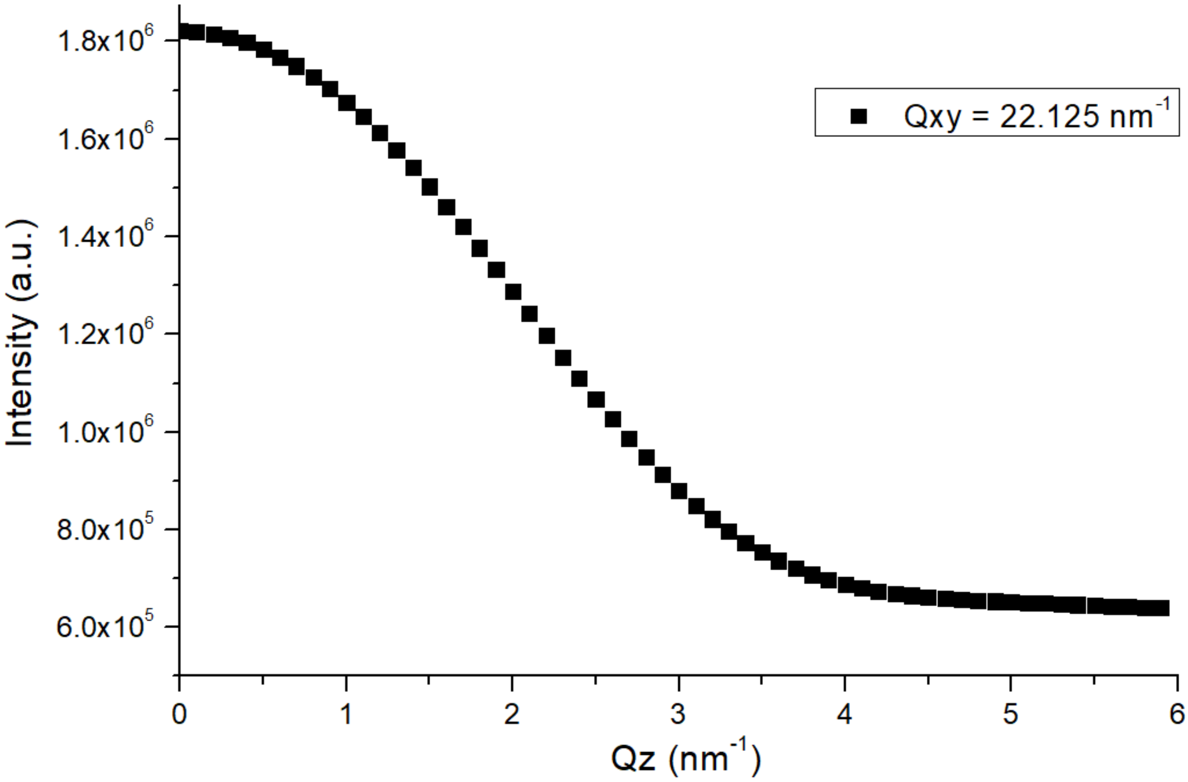

Figure 35 - Simulated F18OH out-of-plane integration with Qxy = 22.125 nm^{-1}

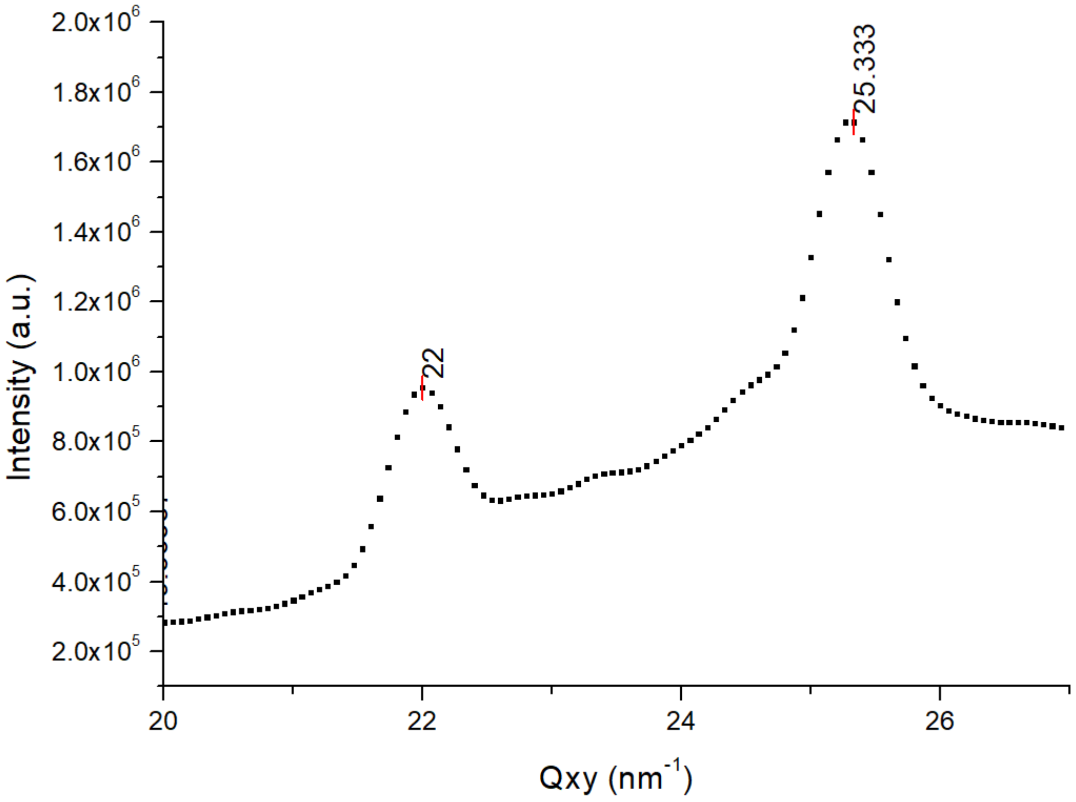

Figure 36 - [11] and [20] simulated diffraction peaks for 400 molecules of F14OH.

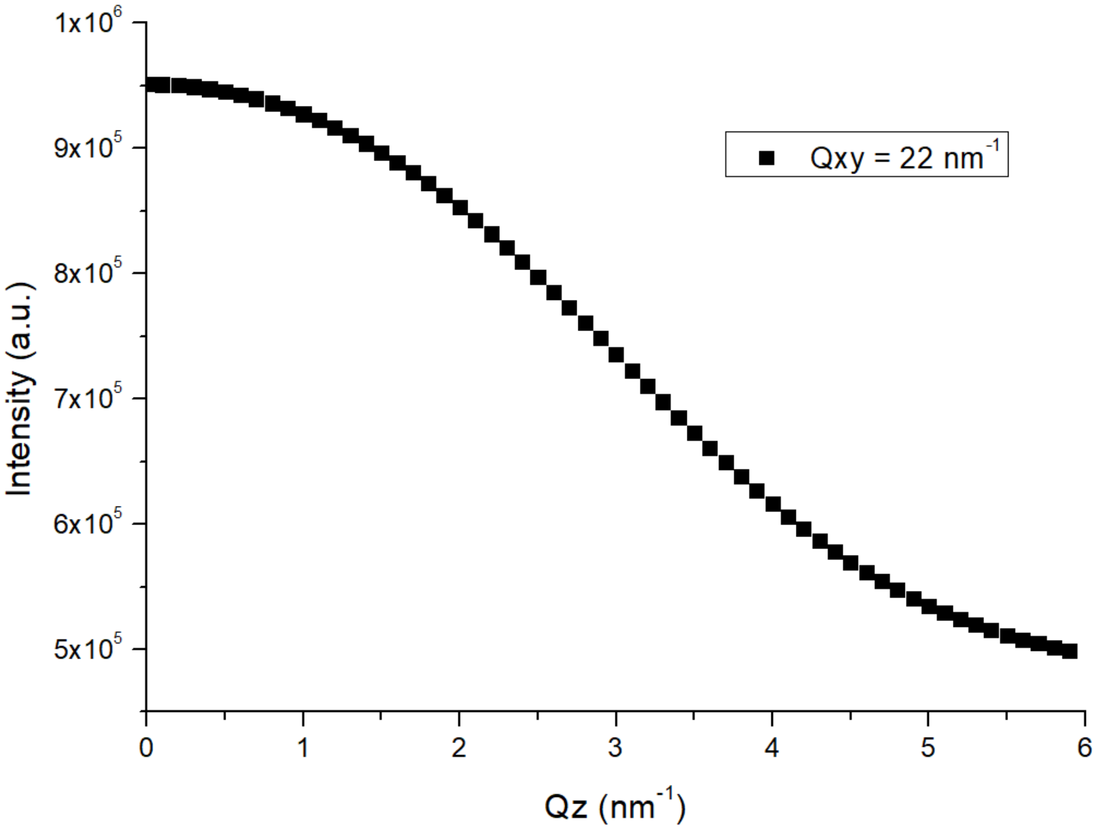

Figure 37 - Simulated F14OH out-of-plane integration with Qxy = 22 nm^{-1}.

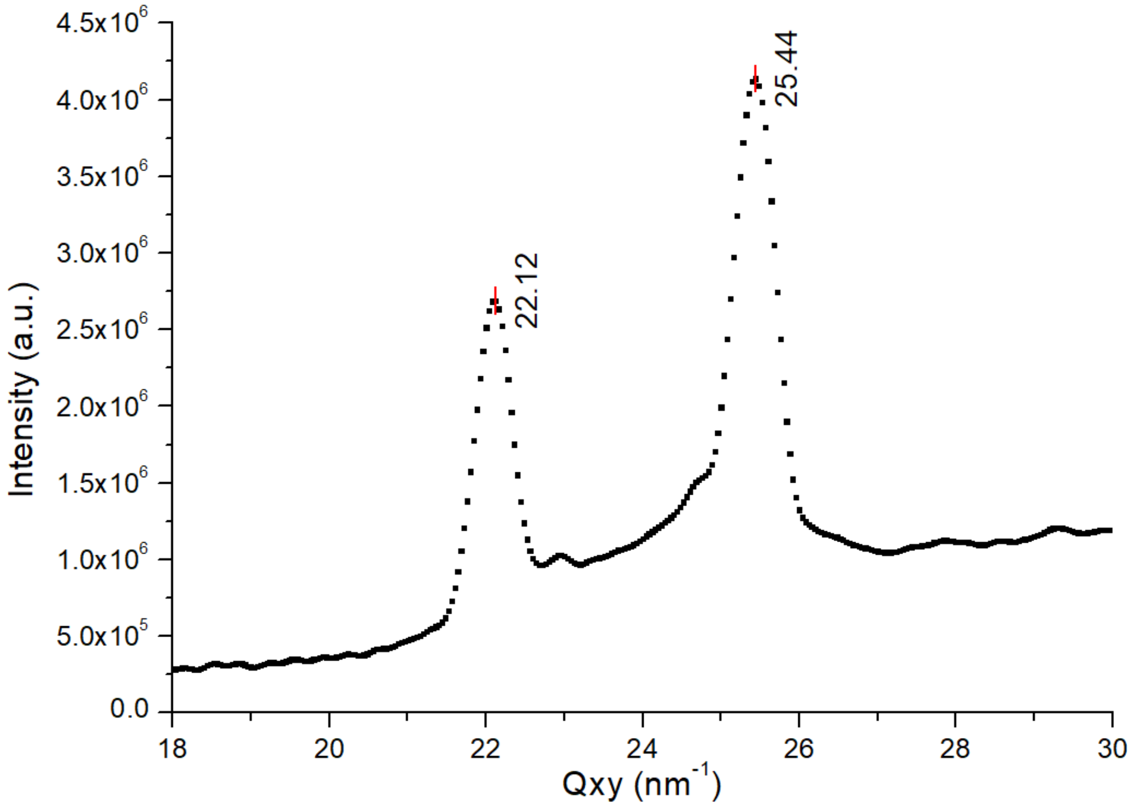

Figure 38 - [11] and [20] simulated diffraction peaks for 400 molecules of F20.

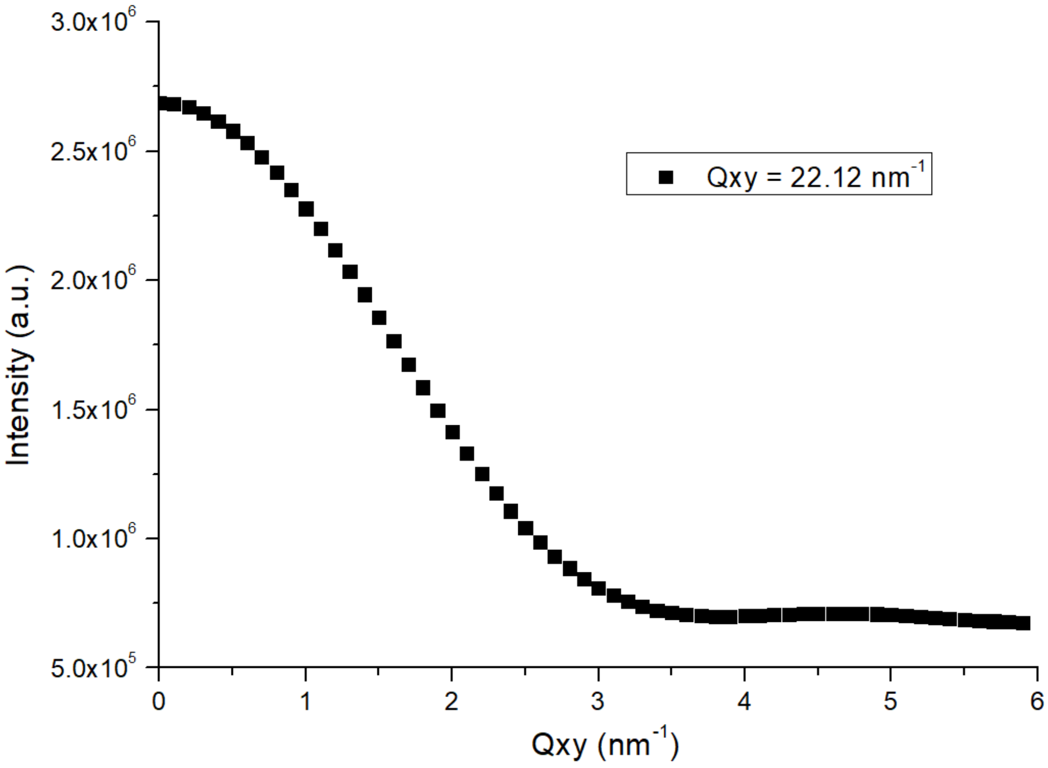

Figure 39 - Simulated F20OH out-of-plane integration with Qxy=22.12 nm^{-1}.

The simulated aggregates present [11] and [20] diffraction peaks at the expected values, confirming that the unit cell is the hexagonal type.

The experimental F18OH and F14OH unit cells were calculated using the data from Carolina[28] of monolayers at a surface pressure of virtually 0 mN/m. The experimental F20 unit cell was calculated by hypothesizing (hip.) a unit cell angle of 60º, azimuth and tilt angles of 0º, and using the data from [7].

Table 1 – Simulated and Experimental Unit Cells.

	Simulated Unit Cell			Experimental Unit Cell		
	F18OH (25ºC)	F14OH (25ºC)	F20 (25ºC)	F18OH (18ºC)	F14OH (22ºC)	F20
a (nm)	0.577	0.578	0.576	0.574	0.576	0.567
b (nm)	0.577	0.578	0.576	0.574	0.576	0.567
γ(degrees)	58.9	59.12	59.01	60	60	60 (hip.)
Azimuth (degrees)	0	0	0	0	0	0 (hip.)
Tilt (degrees)	0	0	0	0	0	0 (hip.)
Unit Cell Area (nm^2)	0.285	0.286	0.284	0.285	0.287	0.278

The simulated unit cell area is in very good agreement with the experimental and it's γ angle is very close to the 60º of a perfect hexagonal lattice (-1.6% less than 60º). Even if visually the films might appear to have a very slight tilt, it is not seen in the diffraction spectrum, as the out-of-plane scans show maxima at Qz=0 which agrees with the experimental spectra. In conclusion, the simulated structure of the fluorinated aggregates is fully confirmed by the diffraction spectra.

3.2.3. Simulated Diffraction Spectra of H18OH and H14OH.

To analyse if the structures formed by the hydrogenated films in the simulation are plausible, the diffraction spectra was obtained by running the diffraction program on 50 frames of the trajectory data after 7 nanoseconds of running. The in-plane $(q_{||10})$ scans are shown below in fig. (40) and fig. (41).

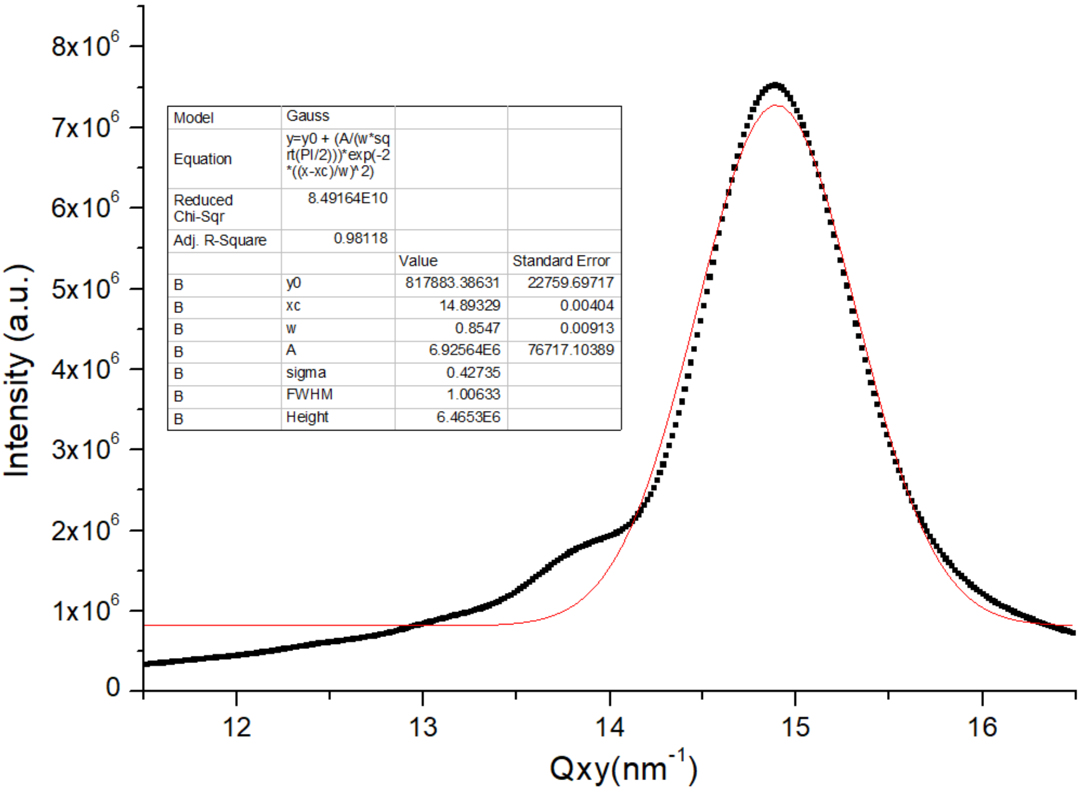

Model	Gauss		
Equation	y=y0 + (A/(w*sqrt(PI/2)))*exp(-2*((x-xc)/w)^2)		
Reduced Chi-Sqr	8.49164E10		
Adj. R-Square	0.98118		
		Value	Standard Error
B	y0	817883.38631	22759.69717
B	xc	14.89329	0.00404
B	w	0.8547	0.00913
B	A	6.92564E6	76717.10389
B	sigma	0.42735	
B	FWHM	1.00633	
B	Height	6.4653E6	

Figure 40 - [10] In-plane simulated diffraction spectra of 400 H14OH molecules.

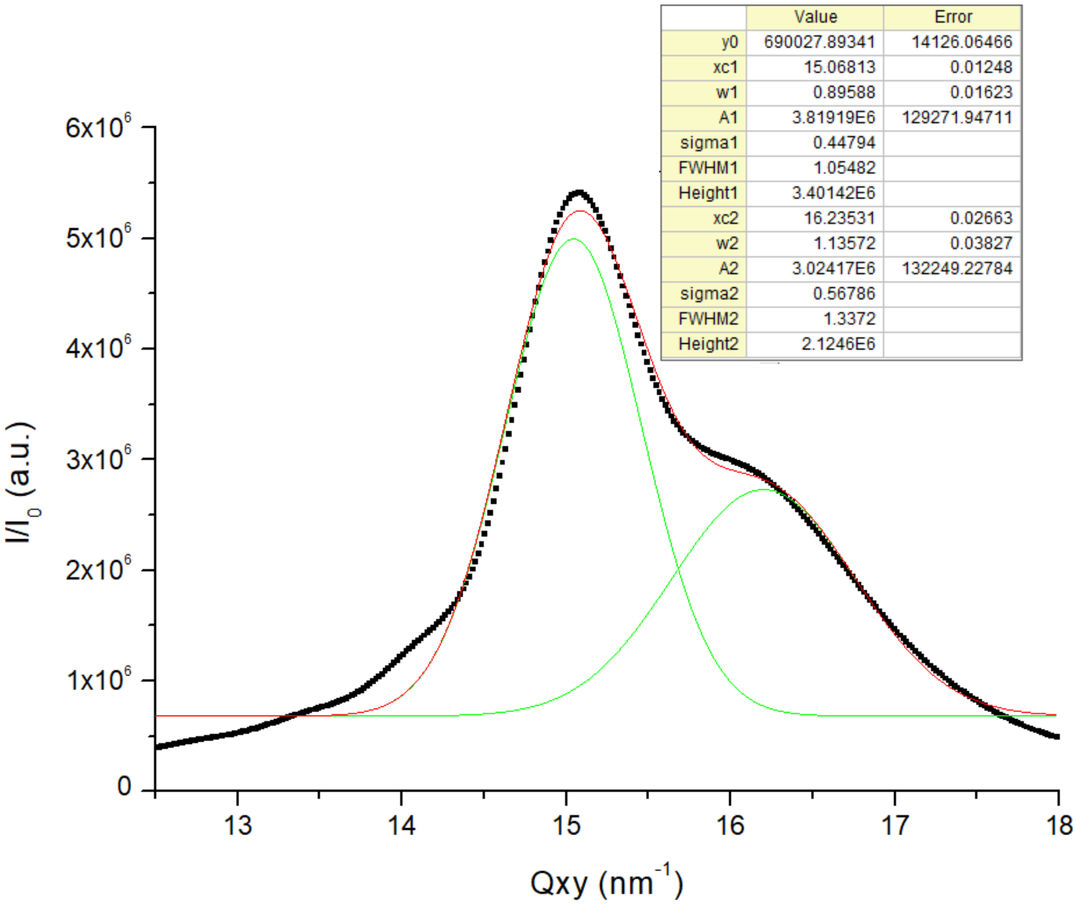

	Value	Error
y0	690027.89341	14126.06466
xc1	15.06813	0.01248
w1	0.89588	0.01623
A1	3.81919E6	129271.94711
sigma1	0.44794	
FWHM1	1.05482	
Height1	3.40142E6	
xc2	16.23531	0.02663
w2	1.13572	0.03827
A2	3.02417E6	132249.22784
sigma2	0.56786	
FWHM2	1.3372	
Height2	2.1246E6	

Figure 41 - [10] In-plane simulated diffraction spectra of 400 H18OH molecules

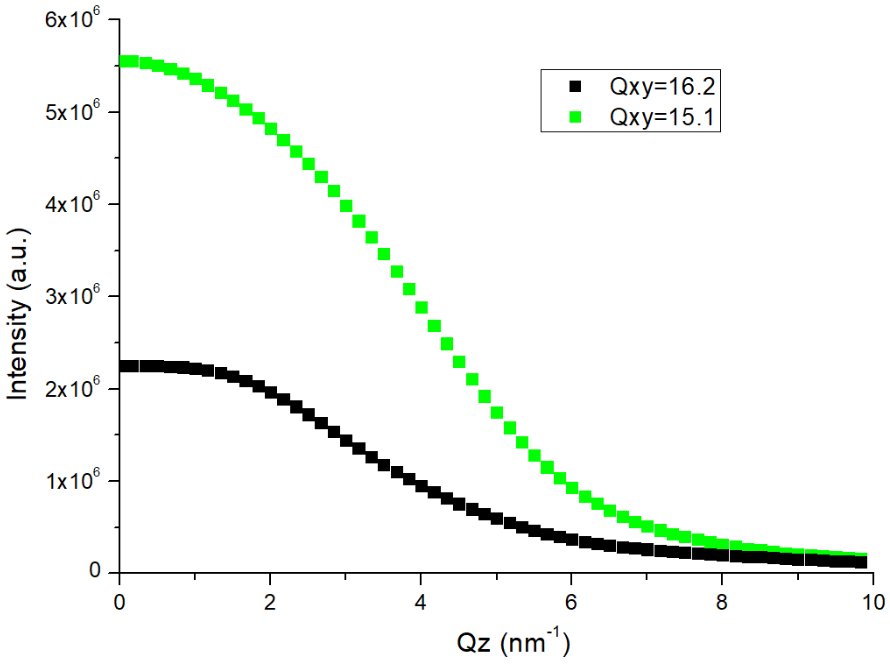

Figure 42 - H18OH Out-of-plane analysis at Qxy=16.2 nm^{-1} (green squares) and at Qxy=15.1 nm^{-1} (black squares)

Experimentally, for H18OH monolayers at virtually zero surface pressure and 25ºC, a single [10] peak is expected. [29] However, the simulated diffraction spectra in fig.(41) clearly shows a double in-plane peak, one peak located at xc = 15 nm and another peak located at xc= 16.23 nm, which is representative of distorted hexagonal/tetragonal unit cell. The single-peak Gaussian fit for the H14OH is insufficient, also suggesting the presence of a double peak. This peak splitting for the hydrogenated alcohols disagrees with the experiments as the Qxy splitting of the peaks is observed only for the H18OH at lower temperatures and higher pressures [29] [30]. The out-of-plane analysis fig. (42) of both H18OH diffraction peaks is typical of a monolayer of untilted molecules as the maximum is found at Qz=0. Yet, it is also known from the experiments that H18OH monolayers at zero surface pressure should present a molecular tilt. [29] These deviations provide evidence that the force field parameters used in the simulations produce an unexpected structured phase of H18OH which is obtained experimentally at lower temperatures. If the intermolecular forces are too strongly modelled by the force fields, then the free rotation of the molecules around their axes (high temperature rotator phase, characteristic of the hexagonal lattice) will not occur and a tetragonal lattice is obtained instead.

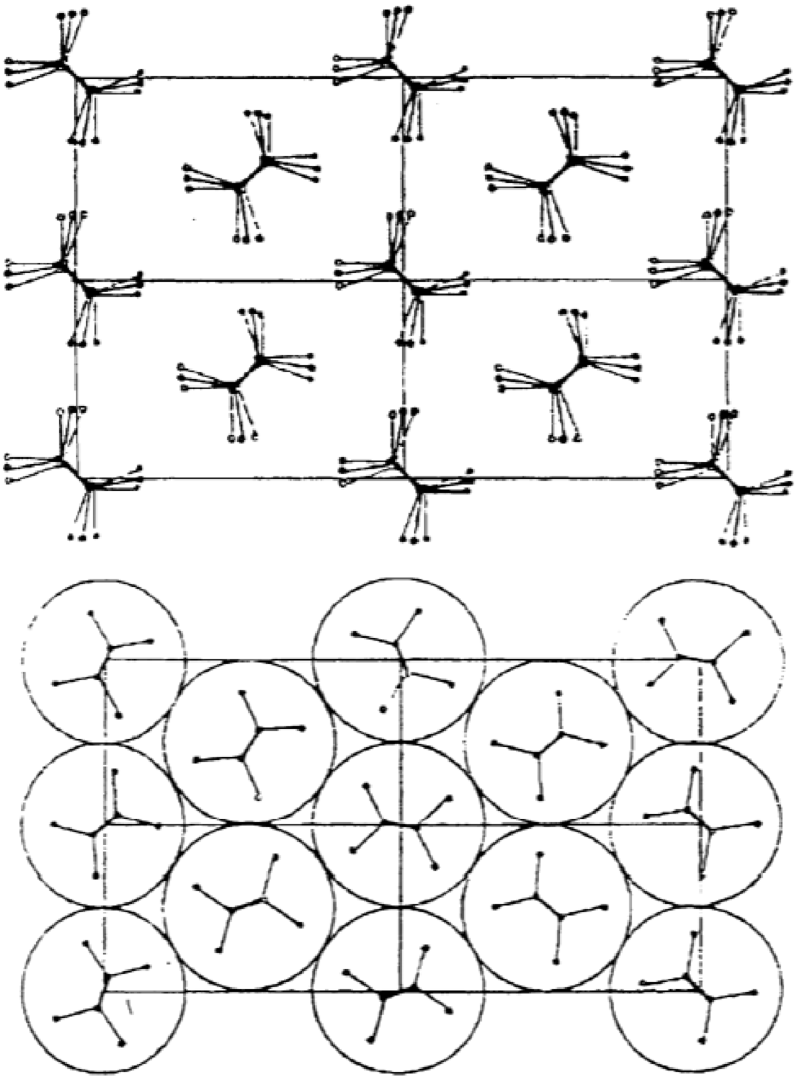

Figure 43 – a) Crystalline state with the molecules packed in a herringbone type structure. b) High temperature rotator phase characterized by the free rotation of the molecules (circles) which pack into a hexagonal lattice. [31]

For comparison with the fluorinated surfactants, the approximate aggregate diameter of the hydrogenated alcohols was also measured using VMD and is presented along with the diffracted coherence length as a function of number of molecules in the aggregate.

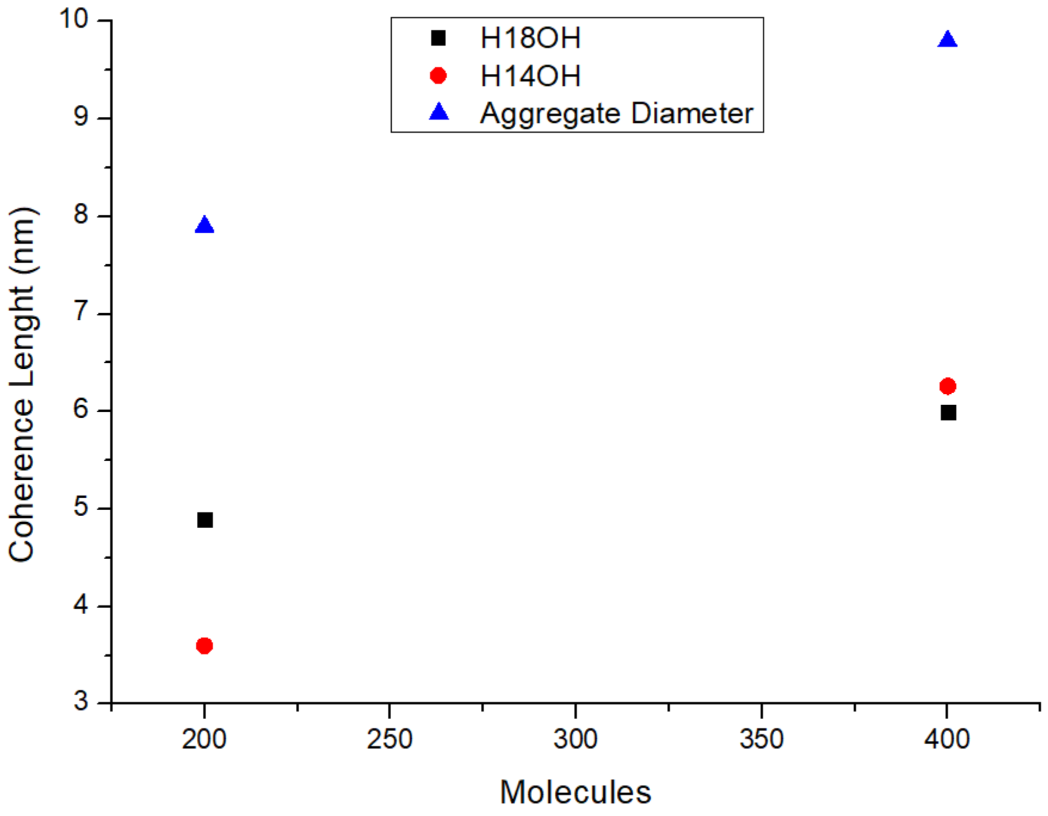

Figure 44 - *Aggregate diameter and coherence length as a function of number of molecules*

And thus, contrary to their fluorinated counterparts, the diffracted coherence length is systematically smaller than the diameter of the aggregate for both the H18OH and the H14OH. The hydrogenated films do not exhibit ordering on the entire dimension of the aggregate providing yet another evidence that the hydrogenated surfactant aggregates are not completely crystalline.

In conclusion, the hydrogenated surfactants present less long-range ordering than the fluorinated molecules. The internal structure of the H18OH film appears to disagree with the hexagonal lattice structure experimentally seen from GIXD. This result might suggest that some special reparameterization of the forcefields might be needed for thin-film simulations, as the molecular interactions in Langmuir monolayers are known to significantly differ from the molecular interactions in the bulk [32], however, for a more definite conclusion boxes with a higher number of H18OH molecules should be simulated in the future.

3.2.4. Simulated Diffraction Spectra of Perfluoroalkylalkane Hemimicelles

When unexpected molecular structures arise from MD simulations, there is a debate on whether such complex, non-periodic structures could produce a diffraction spectrum compatible with the experimental one.

Such is the case for the perfluoroalkylalkane monolayers, where experimentally they were thought to be formed by upright molecules in the centre being slightly more tilted towards the rim of the aggregate. However, recently in our group, the F8H16 simulations by Gonçalo Silva showed that the hemi-micelles have in fact an almost 90º degree tilt at the rim of the aggregate and that the hydrogenated chains are partially submerged giving the hemi-micelles a non-periodic structure. [33]

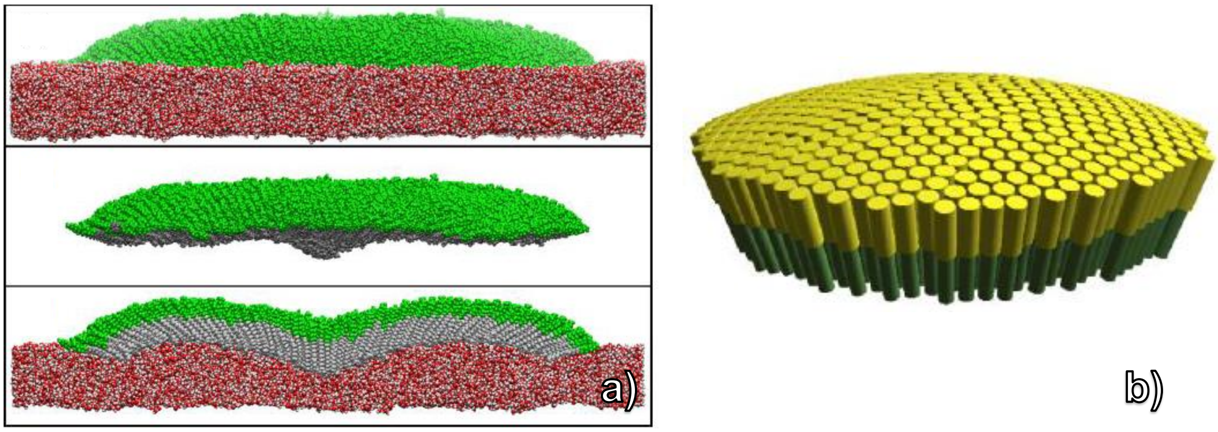

Figure 45 - a) Final configuration of the simulated hemimicelle (with water, without water and crosssection); b) Previous model of the hemimicelles.

A definite validation of these simulation results was obtained by comparing the experimental GIXD spectrum of the system with that calculated from the simulated trajectories. The results are presented in fig. (49).

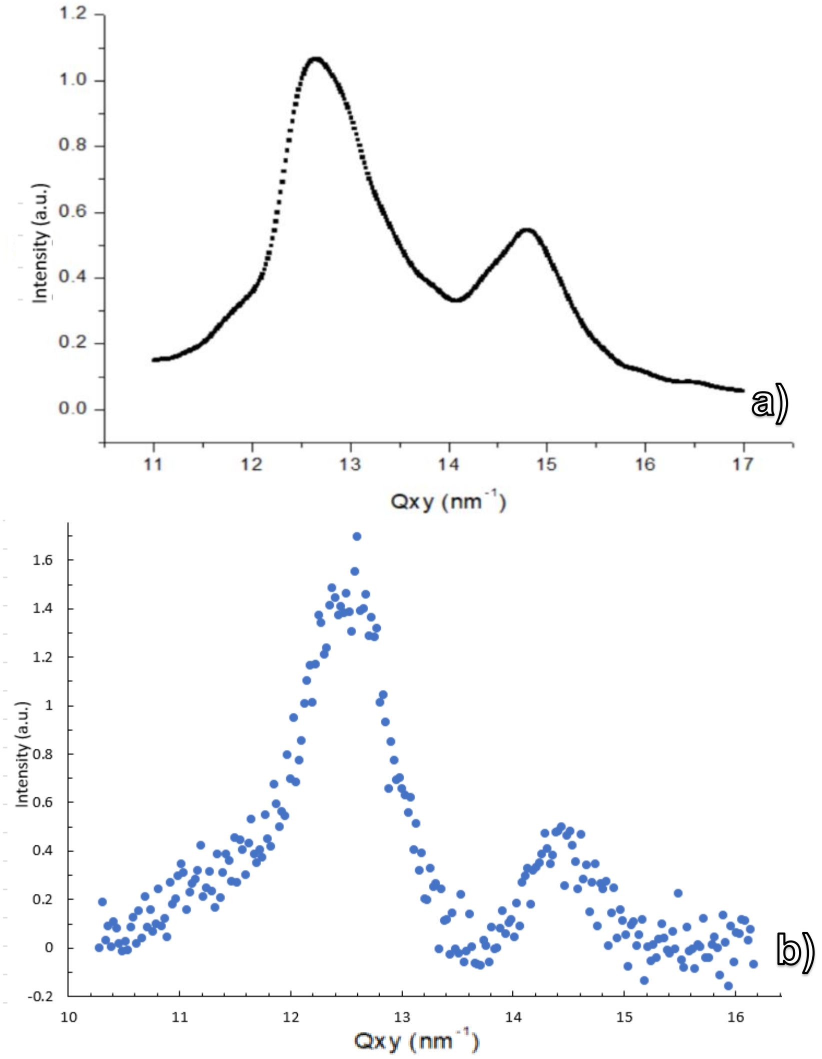

Figure 46 - a) Simulated and b) GIXD diffraction spectra of the F8H16 hemimicelles.

In the spectrum obtained from the simulated system one can clearly observe an in-plane peak at Qxy = 12.63 nm-1, which corresponds to the stacking of the fluorinated segments and a second one at Qxy = 14.77 nm-1 associated with the diffraction of the hydrogenated blocks. This is in very good agreement with the experimental diffraction spectra presented in figure 44b which shows a peak at Qxy = 12.45 nm-1 and second one at Qxy = 14.44 nm-1.

The relative intensity of the peaks, Ifluo/Ihydro, is larger in the simulated spectra than in the experimental (Ifluo/Ihydo is 1.9 and 3 for the simulation and experiment, respectively). In fact, if one assumes that all electrons from the fluorinated block are very organized with all molecules fully diffracting, then the simulated ratio gives that all hydrogenated blocks are also fully diffracting, something which could be explained by the forcefields used which might make the hydrogenated part interact too strongly. However, one can still conclude that the complex and non-periodic molecular organization proposed by the MD simulations for the internal structure of the hemimicelles is fully confirmed by the simulated and experimental diffraction results. And thus, it has been demonstrated that complex quasi-crystal structures can also produce diffraction spectra.

3.3. Conclusions

In this work, the atomistic MD simulations performed were able to highlight some key differences between perfluorinated chains and hydrogenated chains. Due to their rigidity, the perfluorinated chains evidently tend to assemble into very ordered polygonal aggregates independently of the molecule’s head group (including the inexistence of a head-group, like the F20), while the hydrogenated chains, due to their higher flexibility, formed less ordered aggregates with a circular-like profile. These results are in agreement with the morphologies observed by AFM measurements of the respective Langmuir-Blodgett films from previous works.

Furthermore, the structure factor program developed was crucial to validate (or invalidate) the MD simulation results. The structural organization of the fluorinated aggregates obtained from MD simulations agrees with that experimentally found from GIXD experiments as the experimental and simulated diffraction peaks coincide. The simulated H18OH on the other hand exhibits an untilted distorted hexagonal/tetragonal unit cell, in disagreement with the tilted hexagonal lattice from the experiments, suggesting that some future reparameterization of the force fields might be needed. Such discrepancy might be caused by too strong non-bonded potential energies.

The molecular organization of the simulated F8H16 hemi-micelle was found to produce a diffraction spectrum compatible with the experimental one, fully confirming the simulated structure. The F8H16 micelle diffraction results also demonstrated that non-periodic and amorphous structures without a translational unit cell (quasi-crystals), produce clear diffraction peaks similar to those which are considered crystals with well-defined unit cells.

Traditionally, the parameterization and development of forcefields for computer simulations is done by fitting the simulation results of the pure condensed in-bulk compounds with its corresponding experimental data. However, the interactions of molecules in Langmuir monolayers significantly differ from the interactions of the same molecules in the bulk. As it was demonstrated in this work, calculating the diffraction spectra from MD monolayers produces good quantitative data for comparison with the monolayer experiments, which could be used for fitting and parametrization of new forcefields.

4. Future Work

For a better understanding of the dynamics and the structural organization of fluorinated and hydrogenated monolayers some further research work must be performed. This includes:

- Re-running monolayer simulations of H18OH at higher temperatures or with different non-bonded parameters to evaluate which part of the force field might be overparameterized.
- Optimizing the OPLS-AA and LOPLS-AA forcefields for thin-film and monolayer simulations.
- Re-running the MD simulations done in this work with the newly optimized forcefields and with increased number of molecules.
- Running MD simulations of fluorinated molecules with other headgroups.
- Further develop the diffraction program to account for the diffraction satellites or to account for the charge distribution of each molecule.

5. Bibliography

[1] R.C. Buck, J. Franklin, U. Berger, J.M. Conder, I.T. Cousins, P. de Voogt, A.A. Jensen, K. Kannan, S.A. Mabury, S. van Leeuwen, Perfluoroalkyl and polyfluoroalkyl substances in the environment: terminology, classification, and origins, Integr. Environ. Assess. Manage. 7 (2011) 513–541.

[2] A. Drame', E.T. Givenchy, S.Y. Dieng, S. Amigoni, M. Oumar, A. Diouf, T. Darmanin, F. Guittard, Perfluoroalkyl and polyfluoroalkyl substances in the environment: terminology, classification and origins, Langmuir 29 (2013) 14815–14822.

[3] J.G. Riess, Oxygen carriers (blood substitutes)—Raison d'Etre, chemistry, and some physiology, Chem. Rev. 101 (2001) 2797–2919.

[4] H.M. Courrier, T.F. Vandamme, M.P. Krafft, Reverse water-in-fluorocarbon emulsions and microemulsions obtained with a fluorinated surfactant, Colloids Surf. A: Physicochem. Eng. Aspects 244 (2004) 141–148.

[5] S. Rossi, C. Szíjjártó, F. Gerber, G. Waton, M.P. Krafft, Fluorous materials in microbubble engineering science and technology—design and development of new bubble preparation and sizing technologies, J. Fluor. Chem. 132 (2011) 1102–1109.

[6] M. P. Krafft, M. Goldmann, Monolayers made from fluorinated amphiphiles, Current opinion in Colloid & Interface Science 8 (2003) 243-250

[7] M. Li, A. A. Acero, Z. Huang, S. A. Rice, Formation of an ordered Langmuir monolayer by a non-polar chain molecule, Nature 367 (1994) 151-153

[8] S. S. Jang, M. Blanco, W. A. Goddard III, G. Caldwell, R. B. Ross, The source of helicity in perfluorinated N-alkanes Macromolecules 36 (2003) 5531-5341

[9] W. L. Jorgensen, J. Tirado-Rives, The OPLS Potential Functions for Proteins. Energy Minimizations for Crystals of Cyclic Peptides and Crambin. J. of American Chem. Soc. 6, 110 (1988)

[10] G. S. Girolami, X-ray Crystallography. University Science Books, California (2016)

[11] S. L. Prunty, A primer on the theory of Thomson scattering for high-temperature fusion plasmas, Phys. Scr. 89 2014 128001

[12] W. G. J. Langeveld, Effective Atomic Number, Mass Attenuation Coefficient Parametrization, and Implications for High-Energy X-ray Cargo Inspection Systems, Phys. Proc. 90 (2017) 291-304

[13] S. W. Barton, A. Goudot, O. Bouloussa, F. Rondelez, B. Lin, F. Novak, A. Acero, S. A. Rice, Structural transitions in a monolayer of fluorinated amphiphile molecules,The Journal of Chemical Physics 96, (1992), 1343

[14] He, B. B. *Two-dimensional X-ray diffraction*. John Wiley & Sons (2011)

[15] P. Fontaine, M. Goldmann, M. Bordessoule, A. Jucha, Fast and adjustable resolution grazing incidence x-ray liquid surfaces diffraction achieved through 2D detector.

[16] Van Der Spoel, D.; Lindahl, E.; Hess, B.; Groenhof, G.; Mark, A. E.; Berendsen, H. J. C. GROMACS: Fast, Flexible and Free. J. Comput. Chem. 26, (2005), 1701−1718.

[17] Pronk, S.; Páll, S.; Schulz, R.; Larsson, P.; Bjelkmar, P.; Apostolov, R.; Shirts, M. R.; Smith, J. C.; Kasson, P. M.; van der Spoel, D.; Hess, B.; Lindahl, E. GROMACS 4.5: a High-Throughput and Highly Parallel Open Source Molecular Simulation Toolkit. Bioinformatics, 29, (2013) 845−854.

[18] Jorgensen, W. L.; Maxwell, D. S.; Tirado-Rives, J. Development and Testing of the OPLS All-Atom Force Field on Conformational Energetics and Properties of Organic Liquids. J. Am. Chem. Soc. 118, (1996) 11225−11236.

[19] E. K. Watkins, W. L. Jorgensen, Perfluoroalkanes: Conformational Analysis and Liquid-State Properties from ab Initio and Monte Carlo Calculations, *J. Phys. Chem. A, 105 (*2001) 4118-4125

[20] K. Pluhackova, H. MOrhenn, L. Lautner, W. Lohstroh, K. S. Nemkovski, T. Unruh, R. A. Bockmann, Extension of the LOPLS-AA Force Field for Alcohols, Ester and Monoolein Bilayers and its Validation by Neutron Scattering Experiments, *J. Phys. Chem. B (*2015) 119, 49, 15287-15299

[21] Martínez, L.; Andrade, R.; Birgin, E. G.; Martínez, J. M. Packmol: A Package for Building Initial Configurations for Molecular Dynamics Simulations. *J. Comput. Chem.* 2009, *30*, 2157–2164.

[22] J. D., The Use of Fourier Transforms in Protein Crystal Analysis J. D. Biological Sciences, Vol. 141 No.902 (1953) 71-85

[23] L- Largeau I. Camara, J.-Y. Duquesne, C. Gourdon, P. Rovillain, L. Thevenard and B. CrosetLaboratory X-ray characterization of a surface acoustic wave on GaAs: the critical role of instrumental convolution, *J. Appl. Cryst.* (2016). 49, 2073-2081

[24] Andrew M. Bruckner, Judith B. Bruckner, Brian S. Thomson: *Real Analysis*. (1996)

[25] M. Teixeira, Complex Interfacial Behaviour of Mixtures of Fluorinated and Hydrogenated Alcohols (2014)

[26] A. J. García-Sáez, S. Chlantla, P. Schwille, Effect of line tension of the lateral organization of lipid membranes, The Journal Of Bio. Chem. 282, 46 (2007) 33537–33544

[27] P. Fontaine, Grazing Incidence X-Ray Diffraction on Langmuir Monolayers, (2014)

[28] A. C. M. Pedrosa, Nanostructure fluorinated molecular films (2017)

[29] C. Lautz, Th. M. Fischer, M. Weygand, M. Losche, P.B. Howes, K. Kjaer, Determination of alkyl chain tilt angles in Langmuir monolayers: A comparison of
Brewster angle autocorrelation spectroscopy and x-ray diffraction The Journal of Chemical Physics 108, (1998) 4640.

[30] G. Brezesinski, V. M. Kaganer, H. MOhwalkd, P. B. Howes Structure of octadecanol monolayers: An x-ray diffraction study The Journal of Chemical Physics 109, 2006 (1998);

[31] S.Y. Chazhegina, E.N. Kotelnikova, I.V. Filippova, S.K. Filatov, Phase transitions of n-alkanes as rotator crystals. J. of Mol. Structure 647, (2003), 243-257,

[32] D. Murakami, U. Langer, Z. Khattari, Th. M. Fischer, Fluorinated Langmir Monolayers Are More Viscous than Non-Fluorinated Monolayers *J. Phys. Chem. B (*2010), *114,* 5376–5379

[33] G. M. C. Silva, P. Mogado, P. Lourenço, M. Goldmann, E. J. M. Filipe, Self-assembled hemimicelles of perfluoroalkylalkane “primitive” surfactants: Spontaneous formation and structure by molecular dynamics simulations (2018)

6. Supplementary Information

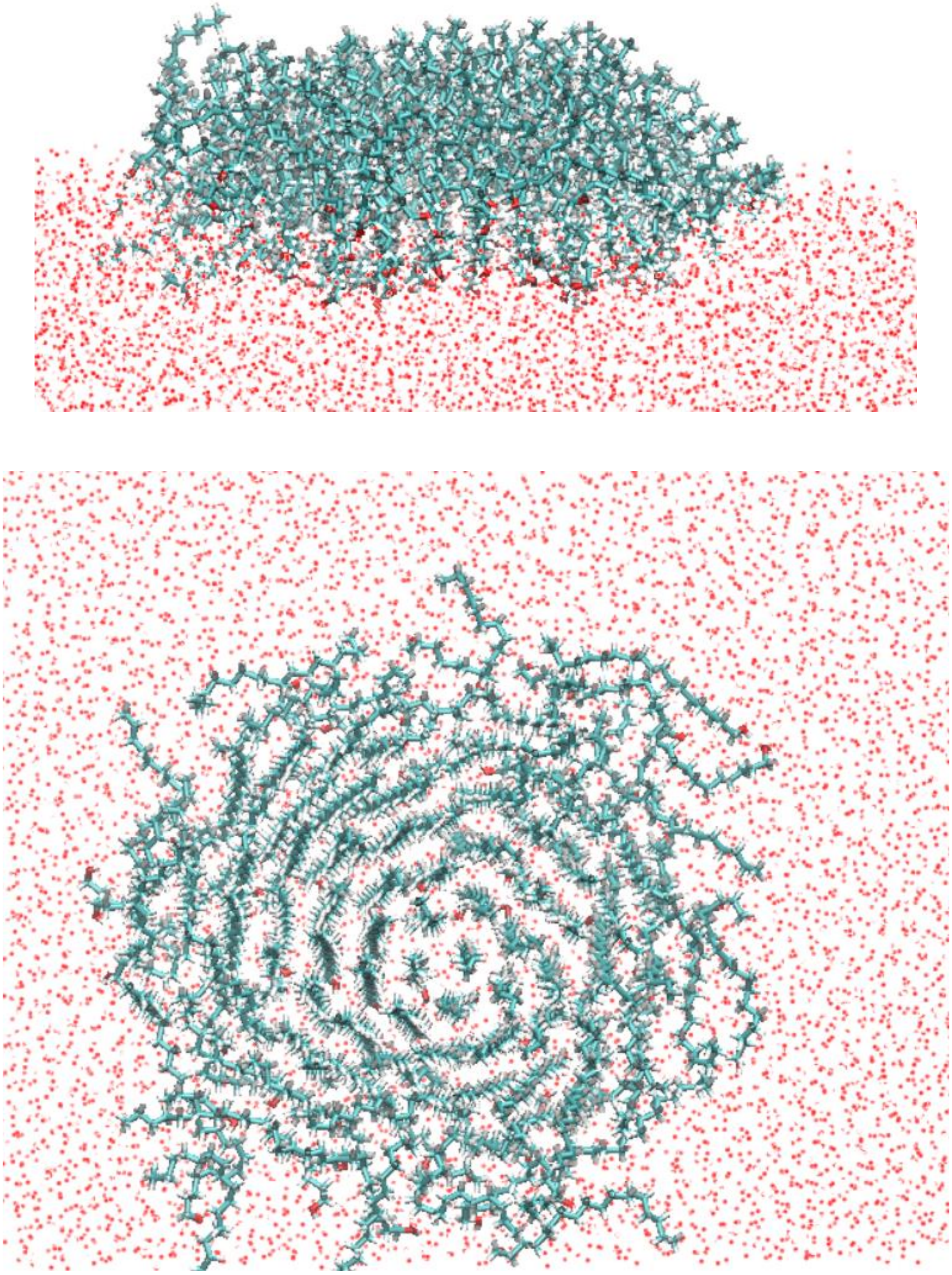

Figure 47 - Side and top view of 100 molecule aggregate of H18OH at 5 ns simulation time.

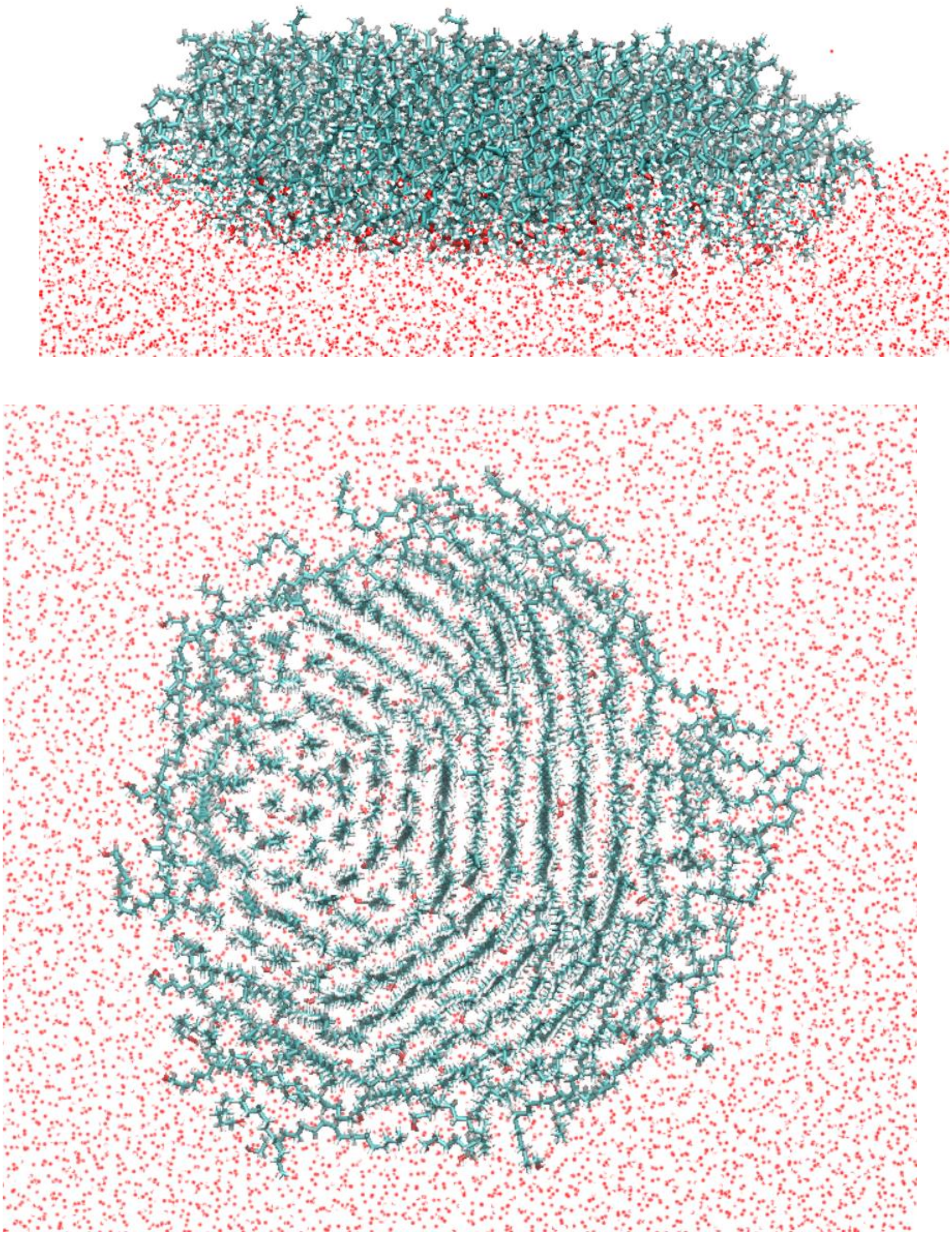

Figure 48 - Side and top view of 200 molecule aggregate of H18OH at 10 ns simulation time.

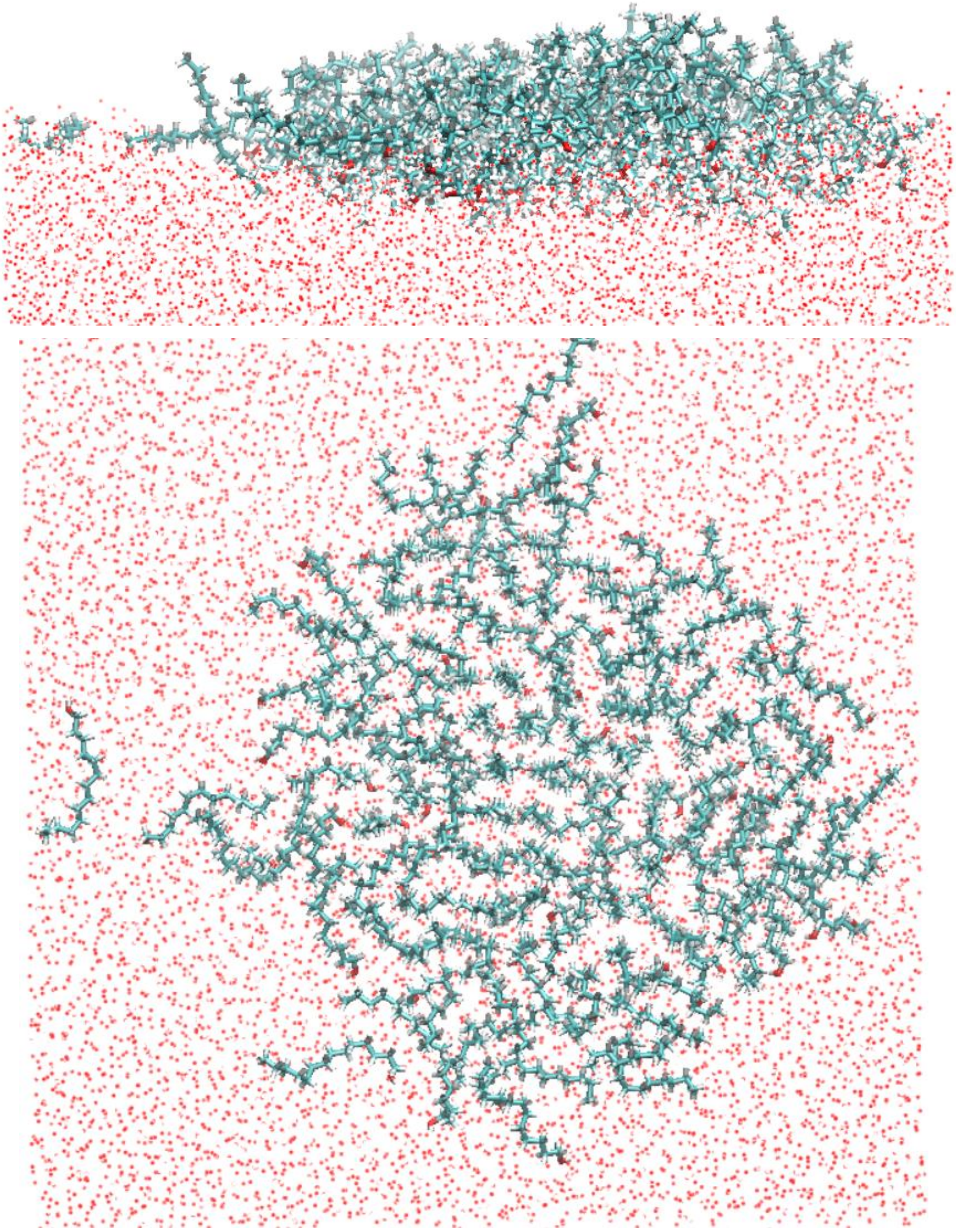

Figure 49 - Side and top view of 100 molecule aggregate of H14OH at 5 ns simulation time

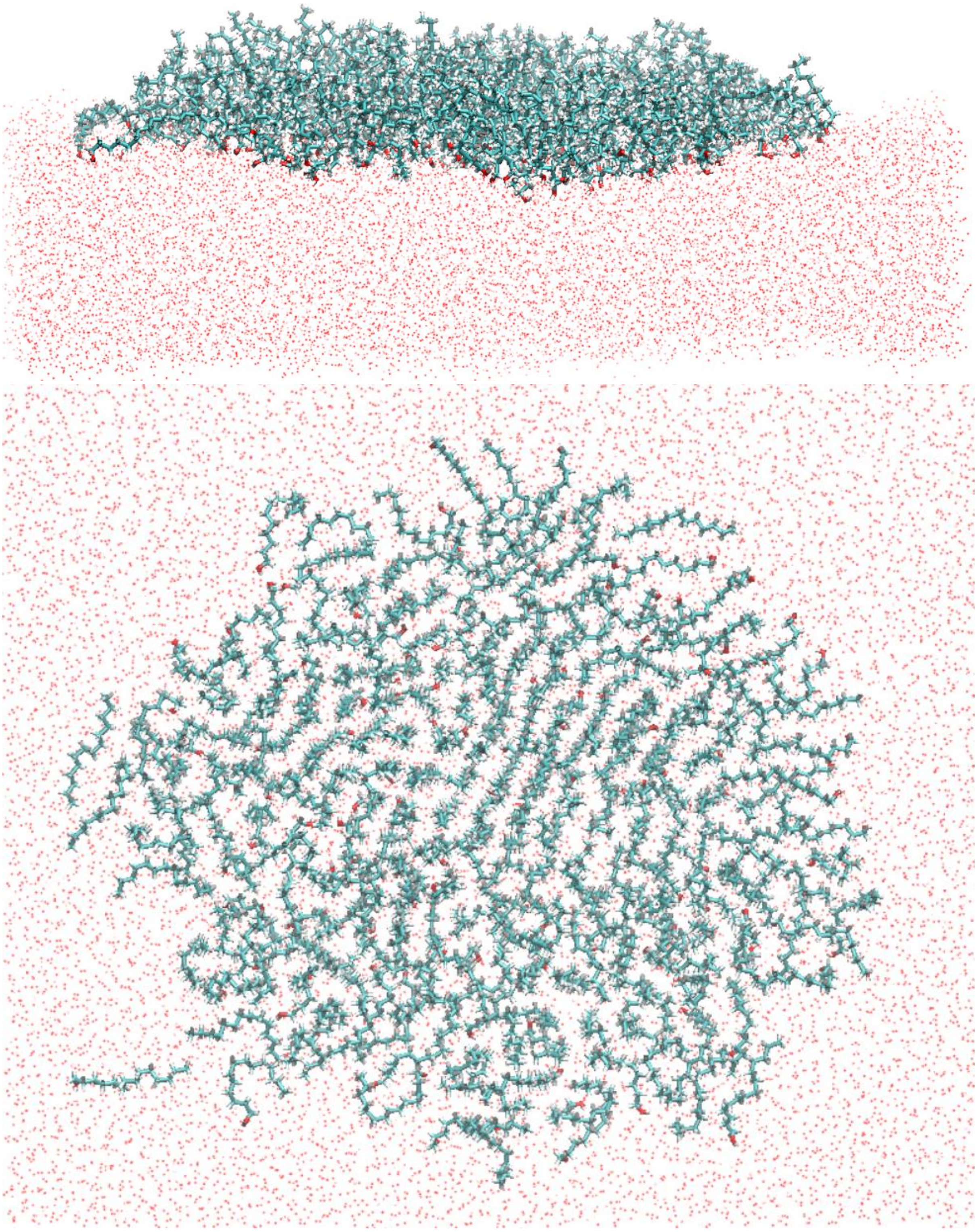

Figure 50 - Side and top view of 200 molecule aggregate of H14OH at 10 ns simulation time

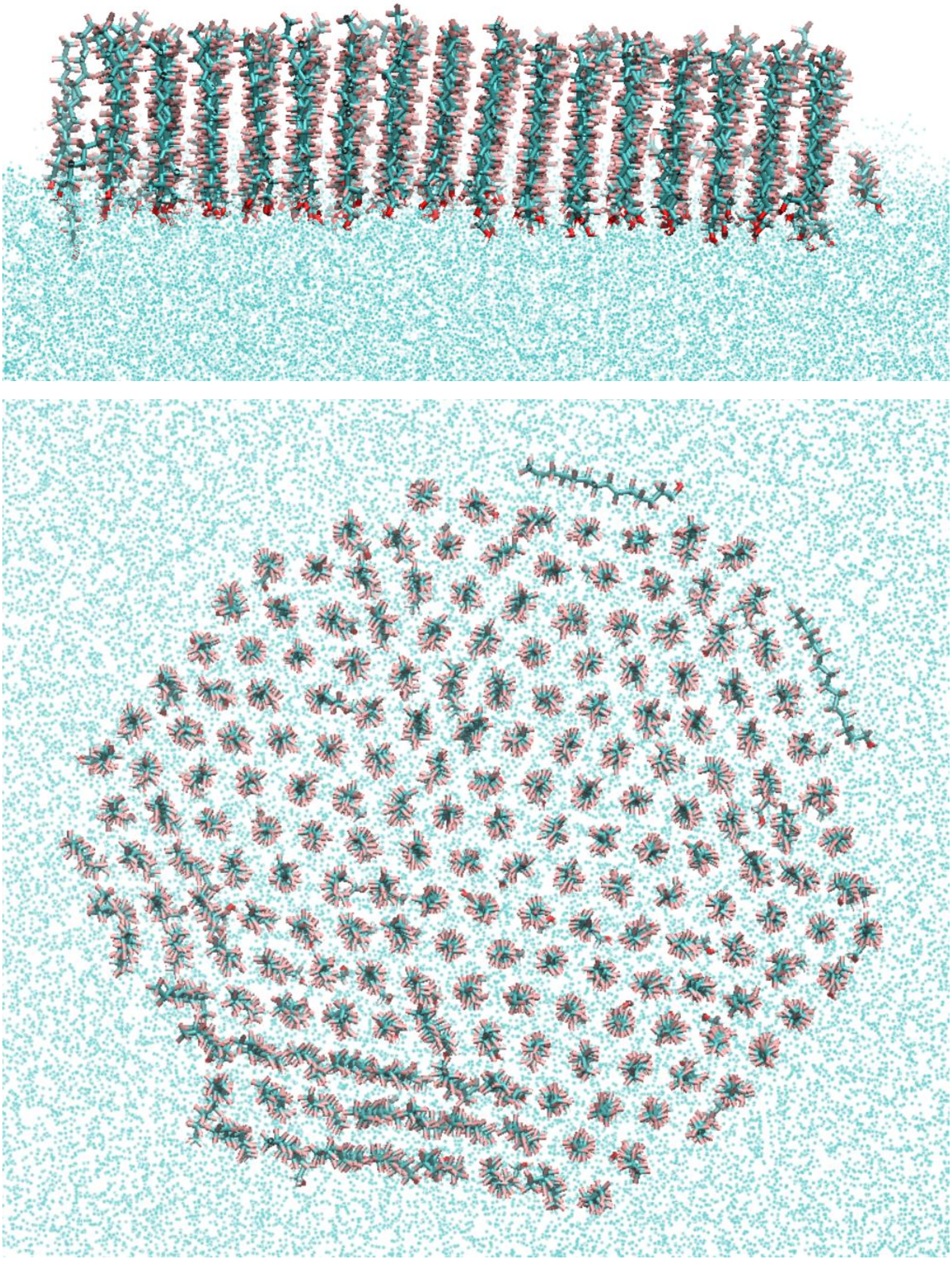

Figure 51 - Side and top view of 200 molecule aggregate of F14OH at 10 ns simulation time

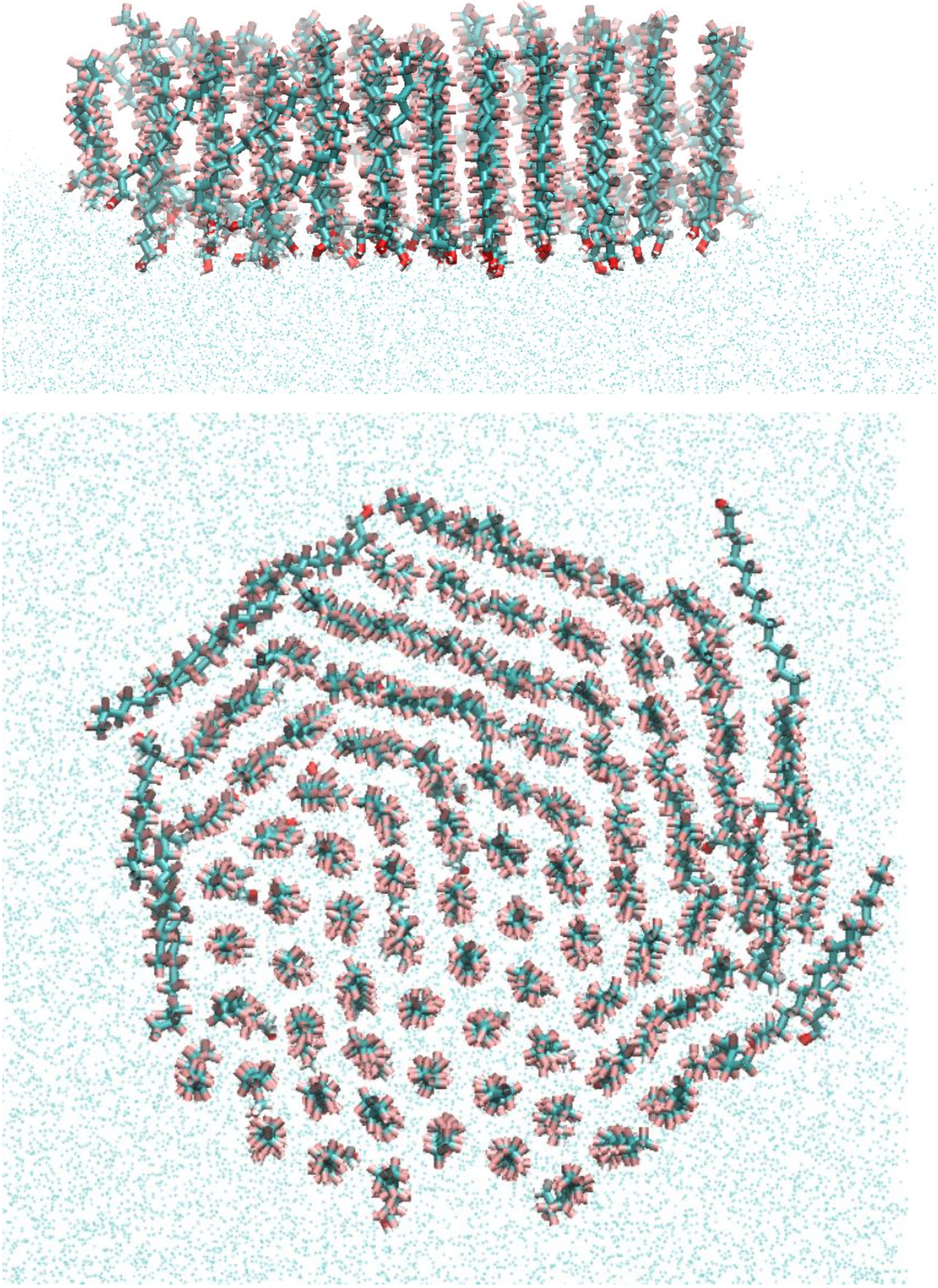

Figure 52 - - Side and top view of 100 molecule aggregate of H14OH at 5 ns simulation time

```fortran
program structure

implicit none

INTEGER, PARAMETER :: DP = SELECTED_REAL_KIND(14)
real(KIND = DP)::x,y,z,Qxs,Qys,Qzs,Qx,Qy,Qz,Fq,Qxy,lim,dQ,dQxy,PI,Qxys,ang,limZ
integer::io,natomos,i,j,frames,nrPontos,angIterator,nrPontosXY,nrPontosz,xyi,zi
character(8) :: molecule,filename
character(7) :: atom
real (KIND = DP),allocatable :: vx(:),vy(:),vz(:),N(:),sumar(:),sumai(:),arrayQZ(:),arrayQxy(:)

j=1
!!//number of residue atoms
natomos=22800
!!//number of frames to calculate the spectra
frames=50
!!//Qxy starting value
Qxys=12.5
!!//lim = Qxy final value
lim=30
i=0
!!//number of points for reciprocal space circle division
nrPontos=60*4
PI=3.1415
!!//number of points to calculate structure factor
nrPontosXY=60*5
!!// step size
dQxy=(lim-Qxys)/(nrPontosXY)

allocate(vx(natomos))
allocate(vy(natomos))
allocate(vz(natomos))
allocate(N(natomos))
allocate(sumar(natomos))
allocate(sumai(natomos))
allocate(arrayQz(nrPontosz))
allocate(arrayQxy(nrPontosXY))
arrayQz = 0
arrayQxy = 0
i=0

!!//open the trajectory file with only the residue molecules
open(unit=10,file='traj400molF18OH.gro')
READ(10,*)
READ(10,*)

!!//this do cycle appends the number of electrons of each atom into N(i)
do while (i<natomos)

        READ(10,'(A8,5x,A7,3(2x,F6.0))',iostat=io) molecule, atom, x, y, z

        IF (atom(2:2)=='C') THEN
            N(i)=6
        ELSEIF (atom(2:2)=='F') THEN
            N(i)=9
        ELSEIF (atom(2:2)=='O') THEN
            N(i)=8
        ELSEIF (atom(2:2)=='H') THEN
            N(i)=1
        ENDIF
        i=i+1
end do

READ(10,*)
do while (j <= frames)
    i=0
    READ(10,*)
    READ(10,*)
    !!// this do cycle appends the atoms positions into vx(i) and vy(i)
    do while (i<natomos)
        READ(10,'(A8,5x,A7,3(2x,F6.0))',iostat=io) molecule, atom, x, y, z
        IF (io/=0) EXIT
```

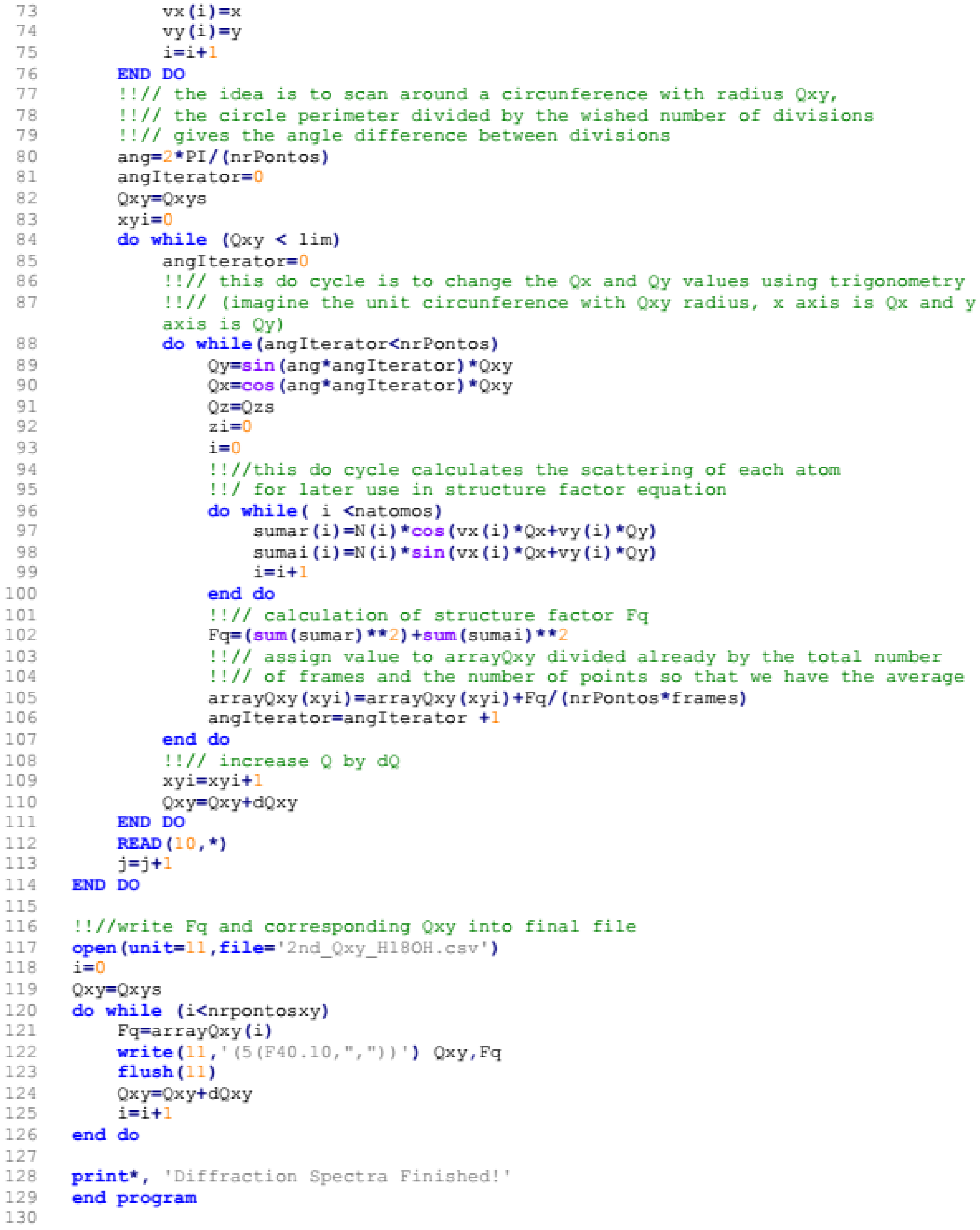

```
        vx(i)=x
        vy(i)=y
        i=i+1
    END DO
    !!// the idea is to scan around a circunference with radius Qxy,
    !!// the circle perimeter divided by the wished number of divisions
    !!// gives the angle difference between divisions
    ang=2*PI/(nrPontos)
    angIterator=0
    Qxy=Qxys
    xyi=0
    do while (Qxy < lim)
        angIterator=0
        !!// this do cycle is to change the Qx and Qy values using trigonometry
        !!// (imagine the unit circunference with Qxy radius, x axis is Qx and y axis is Qy)
        do while(angIterator<nrPontos)
            Qy=sin(ang*angIterator)*Qxy
            Qx=cos(ang*angIterator)*Qxy
            Qz=Qzs
            zi=0
            i=0
            !!//this do cycle calculates the scattering of each atom
            !!/ for later use in structure factor equation
            do while( i <natomos)
                sumar(i)=N(i)*cos(vx(i)*Qx+vy(i)*Qy)
                sumai(i)=N(i)*sin(vx(i)*Qx+vy(i)*Qy)
                i=i+1
            end do
            !!// calculation of structure factor Fq
            Fq=(sum(sumar)**2)+sum(sumai)**2
            !!// assign value to arrayQxy divided already by the total number
            !!// of frames and the number of points so that we have the average
            arrayQxy(xyi)=arrayQxy(xyi)+Fq/(nrPontos*frames)
            angIterator=angIterator +1
        end do
        !!// increase Q by dQ
        xyi=xyi+1
        Qxy=Qxy+dQxy
    END DO
    READ(10,*)
    j=j+1
END DO

!!//write Fq and corresponding Qxy into final file
open(unit=11,file='2nd_Qxy_H18OH.csv')
i=0
Qxy=Qxys
do while (i<nrpontosxy)
    Fq=arrayQxy(i)
    write(11,'(5(F40.10,","))') Qxy,Fq
    flush(11)
    Qxy=Qxy+dQxy
    i=i+1
end do

print*, 'Diffraction Spectra Finished!'
end program
```

Figure 53 – Fortran Code for In-plane Diffraction Spectrum Calculations.

Instructions:

To use the in-plane program, the number of atoms (natomos) in the monolayer must be defined. The initial Qxy value is set up in variable name “Qxys” iterating until the Qxy limit “lim” with a step size which is defined by the number of points that the user wishes to have in the diffraction spectrum (variable name nrPontosXY). A good number of points for a good spectrum is 60 points per unit of Qxy calculated. The number of simulation frames that will be used for the diffraction calculations is defined in variable name “frames”.

The “nrPontos” variable defines the number of points to calculate the intensity of the spectra at a fixed Qxy. (Recommended is 240 points or higher).

Another very similar program calculates the out-of-plane diffraction spectrum. The code is shown below.

To use the out-of-plane program, the number atoms (natomos) in the monolayer must be defined. The initial Qz value is set up in variable name “Qzs” (most often this value starts at zero) iterating until the final Qz value defined in “limZ”, with a step-size defined by the number of points (“nrpontosz”) that the user wishes to have in the diffraction spectra (recommended 60 points per unit of Qz). The Qxy value at which the calculation will occur is defined in “Qxys”.

```

program structure

implicit none

INTEGER, PARAMETER :: DP = SELECTED_REAL_KIND(14)
real(KIND = DP)::x,y,z,Qxs,Qys,Qzs,Qx,Qy,Qz,Fq,Qxy,lim,dQ,dQxy,PI,Qxys,ang,limZ
integer::nlines,io,natomos,i,j,frames,nrPontos,angIterator,nrPontosXY,nrPontosz,xyi,zi
character(8) :: molecule,filename
character(7) :: atom
real (KIND = DP),allocatable :: vx(:),vy(:),vz(:),N(:),sumar(:),sumai(:),arrayQZ(:),arrayQxy(:)

j=1
natomos=22800
frames=50
!!// Qxy value where the rod scan will occur
Qxys=22.11
!!// Qz starting value
Qzs=0
i=0
!!// Qz final value
limZ=6
nrPontos=60*4
PI=3.1415

nrPontosz=60
dQ=(limz-Qzs)/(nrPontosz)
nlines=0


allocate(vx(natomos))
allocate(vy(natomos))
allocate(vz(natomos))
allocate(N(natomos))
allocate(sumar(natomos))
allocate(sumai(natomos))
allocate(arrayQz(nrPontosz))
allocate(arrayQxy(nrPontosXY))
arrayQz = 0
arrayQxy = 0
i=0

open(unit=10,file='traj400molF18OH.gro')
READ(10,*)
READ(10,*)
do while (i<natomos)

        READ(10,'(A8,5x,A7,3(2x,F6.0))',iostat=io) molecule, atom, x, y, z

        IF (atom(2:2)=='C') THEN
            N(i)=6
        ELSEIF (atom(2:2)=='F') THEN
            N(i)=9
        ELSEIF (atom(2:2)=='O') THEN
            N(i)=8
        ELSEIF (atom(2:2)=='H') THEN
            N(i)=1
        ENDIF
        i=i+1
end do

READ(10,*)
do while (j <= frames)
    i=0
    READ(10,*)
    READ(10,*)
    do while (i<natomos)
        READ(10,'(A8,5x,A7,3(2x,F6.0))',iostat=io) molecule, atom, x, y, z
        IF (io/=0) EXIT
        !!// three coordinates instead of two
        vx(i)=x
        vy(i)=y
```

```
        vx(i)=x
        vy(i)=y
        vz(i)=z
        i=i+1
    END DO

    ang=2*PI/(nrPontos)
    angIterator=0
    Qxy=Qxys
    xyi=0
    angIterator=0
    do while(angIterator<nrPontos)
        Qy=sin(ang*angIterator)*Qxy
        Qx=cos(ang*angIterator)*Qxy
        Qz=Qzs
        zi=0
        do while ( Qz < limZ)
            i=0
            do while( i <natomos)
                sumar(i)=N(i)*cos(vx(i)*Qx+vy(i)*Qy+vz(i)*Qz)
                sumai(i)=N(i)*sin(vx(i)*Qx+vy(i)*Qy+vz(i)*Qz)
                i=i+1
            end do
            Fq=(sum(sumar)**2)+sum(sumai)**2
            arrayQZ(zi)=arrayQz(zi)+Fq/(nrPontos*frames)
            Qz=Qz+dQ
            zi=zi+1
        end do
        angIterator=angIterator +1
    end do
    READ(10,*)
    j=j+1
END DO


!!// write everything into file
open(unit=12,file='GraficoQz.csv')
i=0
Qz=Qzs
do while (i<nrpontosz)
    Fq=arrayQz(i)
    write(12,'(5(F40.10,","))') Qz,Fq
    flush(12)
    Qz=Qz+dQ
    i=i+1
end do
print*, 'Rod scan complete!'
end program

```

Figure 54 – Fortran Code for Out-of-plane Diffraction Calculations.